NASA TECHNICAL NOTE

NASA TN D-6897

NASA TN D-6897

EFFECT OF JET CONVERGENCE ANGLE ON THE PERFORMANCE OF ANNULAR NOZZLES WITH SEMITOROIDAL CONCAVE PLUGS AT MACH NUMBERS UP TO 1.82

by Charles E. Mercer

Langley Research Center
Hampton, Va. 23365

NATIONAL AERONAUTICS AND SPACE ADMINISTRATION • WASHINGTON, D. C. • OCTOBER 1972

1. Report No.	2. Government Accession No.	3. Recipient's Catalog No.
NASA TN D-6897		

4. Title and Subtitle	5. Report Date
EFFECT OF JET CONVERGENCE ANGLE ON THE PERFORMANCE OF ANNULAR NOZZLES WITH SEMITOROIDAL CONCAVE PLUGS AT MACH NUMBERS UP TO 1.82	6. Performing Organization Code: October 1972

7. Author(s)	8. Performing Organization Report No.
Charles E. Mercer	L-8440
	10. Work Unit No. 501-24-06-01
9. Performing Organization Name and Address: NASA Langley Research Center, Hampton, Va. 23365	11. Contract or Grant No.
	13. Type of Report and Period Covered: Technical Note
12. Sponsoring Agency Name and Address: National Aeronautics and Space Administration, Washington, D.C. 20546	14. Sponsoring Agency Code

15. Supplementary Notes

16. Abstract

Results of an investigation at static conditions and at Mach numbers up to 1.82 are presented for 12 nozzle configurations which have jet convergence angle and jet throat area as geometric parameters. The variation of jet convergence angle from 15^{o} to 40^{o} had little effect on the performance of the nozzles having the larger value of primary throat area; however, increasing jet convergence angle generally had an adverse effect on performance of the nozzles having the smaller value of primary throat area. The performance of the nozzle configurations with the larger primary throat area is competitive with nozzles designed for operation over the Mach number range.

17. Key Words (Suggested by Author(s))	18. Distribution Statement
Plug nozzles Performance	Unclassified – Unlimited

19. Security Classif. (of this report)	20. Security Classif. (of this page)	21. No. of Pages	22. Price*
Unclassified	Unclassified	103	$3.00

*For sale by the National Technical Information Service, Springfield, Virginia 22151

EFFECT OF JET CONVERGENCE ANGLE ON THE PERFORMANCE OF ANNULAR NOZZLES WITH SEMITOROIDAL CONCAVE PLUGS AT MACH NUMBERS UP TO 1.82

By Charles E. Mercer
Langley Research Center

SUMMARY

The performance characteristics of 12 configurations of an annular nozzle with a semitoroidal concave axisymmetric plug have been investigated at static conditions and at Mach numbers up to 1.82. The nozzle configurations were varied with six afterbodies or boattails which differ in inner surface convergence angle and with two sizes of plugs which determined the throat area of the jet. The jet total-pressure ratio was varied from 1.0 to approximately 23, depending on the Mach number.

The results indicate that increasing jet convergence angle from 15° to 40° caused little change in the internal performance and thrust-minus-drag performance for the nozzle configurations that simulate the afterburning mode; however, a loss in the performance occurred for the nozzle configurations that simulate the nonafterburning mode. The performance of the nozzle configurations with the larger primary throat area is competitive with nozzles designed for operation over the Mach number range and at a given typical turbojet total-pressure ratio schedule.

INTRODUCTION

Nozzles capable of producing near-optimum thrust at all operating conditions have long been desired; however, such nozzles generally are mechanically complex and heavy. Variable-geometry convergent-divergent nozzles designed to have good internal performance at higher subsonic, transonic, and supersonic speeds generally have boattail drag penalties at the lower speeds where the low internal-expansion ratios are required, due either to a large base or to high boattail angles (refs. 1, 2, and 3). As maximum flight speed increases, the magnitude of change in afterbody geometry increases significantly. Isentropic plug nozzles have exhibited good internal performance in quiescent air (refs. 4 and 5) and at design pressure ratios; however, the short, steep shroud lip, characteristic of isentropic plug nozzles induces a sharp turning of the external flow during flight and, thus, at high subsonic and low supersonic speeds resulting drag offsets some of the good performance obtained at static conditions and at supersonic speeds (refs. 6 and 7). Annu-

lar nozzles with concave central bases have represented an attempt to achieve simplicity, light weight, and low boattail drag in a nozzle design without sacrifice of internal performance at moderately high values of pressure ratio (refs. 8, 9, and 10).

The purpose of the present investigation was to determine from a further parametric study the effects on performance of varying the jet convergence angle in combination with a semitoroidal base plug.

The results reported herein are for 12 configurations of an annular nozzle with a semitoroidal concave plug, investigated under static conditions and in an airstream over a Mach number range from 0.50 to 1.82 at an angle of attack of 0°. Jet total-pressure ratio ranged from 1.0 (jet off) to values at each test Mach number greater than is required by conventional turbojet engines. The investigation was conducted in the Langley 16-foot transonic tunnel and the Langley 4-foot supersonic pressure tunnel.

SYMBOLS

A cross-sectional area, m^2

A_l local area, m^2

A_{max} maximum nacelle cross-sectional area, m^2

A_t nozzle throat area, m^2

$C_{A,\beta}$ boattail pressure drag coefficient, $\sum C_{p,\beta} \frac{A_l}{A_{max}}$

$C_{F,plug}$ plug thrust coefficient, $\frac{F_{plug}}{q_\infty A_{max}}$; for static conditions, $\frac{F_{plug}}{p_a A_{max}}$

$C_{p,plug}$ plug pressure coefficient, $\frac{p_{plug} - p_\infty}{q_\infty}$; for static conditions, $\frac{p_{plug} - p_a}{p_a}$

$C_{p,\beta}$ boattail pressure coefficient, $\frac{p_\beta - p_\infty}{q_\infty}$

d_{max} maximum cross-section diameter, m

$F_{A,\beta}$ axial force on boattail (external drag), N

F_i ideal thrust for complete isentropic expansion of jet flow,

$$\dot{m}\sqrt{2R\frac{\gamma}{\gamma - 1}T_{t,j}\left[1 - \left(\frac{p_\infty}{p_{t,j}}\right)^{\frac{\gamma-1}{\gamma}}\right]}, \text{ N}$$

F_j gross thrust, N

F_{plug} semitoroidal base thrust, $\sum (p_{plug} - p_\infty)A_l$, N

g annulus-gap width, m

l_p overhang of nozzle outer lip, m

l_β distance from start of boattail curvature to exit, m

M free-stream Mach number

$\dot{m}$ measured mass-flow rate, kg/sec

p_a atmospheric pressure, N/m^2

p_{plug} local static pressure on plug, N/m^2

$p_{t,j}$ jet total pressure, N/m^2

p_β local static pressure on boattail, N/m^2

p_∞ free-stream static pressure, N/m^2

q_∞ free-stream dynamic pressure, N/m^2

R gas constant, N-m/kg-K; or radius, m

R_1 radius to outer boundary of boattail, m

R_2 radius to inner boundary of boattail, m

R_3 radius to outer boundary of semitoroidal plug, m

R_4 radius to inner boundary of semitoroidal plug, m

r radial distance from axis of symmetry to pressure orifice, m

$T_{t,j}$ jet total temperature, K

x axial distance from start of boattail, positive downstream, m

β boattail or jet convergence angle, deg

γ ratio of specific heats

ϕ radial angle of pressure orifice rows, deg

APPARATUS AND METHODS

Wind Tunnels

The investigation was conducted in the Langley 16-foot transonic tunnel and the Langley 4-foot supersonic pressure tunnel. The Langley 16-foot transonic tunnel is an atmospheric wind tunnel with a slotted octagonal test section which has a continuously variable speed range from a Mach number of 0.20 to 1.30. The Langley 4-foot supersonic pressure tunnel is a single-return, continuous wind tunnel with a stagnation-pressure range from 27.58 kN/m^2 (0.272 atm) to 206.84 kN/m^2 (2.041 atm) and a stagnation-temperature range from 310.9 K to 322.2 K. By the use of interchangeable nozzle blocks, the tunnel Mach number can be varied from 1.25 to 2.2.

Model and Support System

A sketch of the strut-supported turbojet-engine simulator model used in the investigation is presented in figure 1, and photographs of the model installed in the test section are shown in figure 2. The model was an air-powered cone-cylinder nacelle with a rounded shoulder at the junction of the nose and the cylindrical section to which afterbody-plug combinations were attached. The afterbody-plug combination consisted of a cylindrical section of 15.24-cm diameter, a boattail, and a semitoroidal concave plug. The model was supported from the tunnel floor by a 5-percent-thick strut swept back with respect to the model and having a leading-edge sweep of 45°. A description of the air-powered nacelle and its air introduction and balance arrangements is given in reference 11.

Details of the 12 afterbody-plug configurations investigated are given in figure 3. The configurations are identified by a two-number code. The first number designates the boattail or jet convergence angle. The selected fixed angles β of 15°, 20°, 25°, 30°,

35°, and 40° are represented by the numbers 1 to 6, respectively. Afterbody external geometry was varied only aft of axial station 110.307, with coordinates as given in table 1. The second number of the configuration code designates the simulated engine power setting, nonafterburning mode or unaugmented power $\left(A_t/A_{max} = 0.25\right)$ and afterburning mode or augmented power $\left(A_t/A_{max} = 0.50\right)$. Two semitoroidal concave plugs numbered 1 (nonafterburning) and 2 (afterburning) were tested with each afterbody to simulate the two types of flight operation. Details of the plug geometry are given in figure 3 and table 1.

Instrumentation and Tests

Static pressures were measured on the afterbody and semitoroidal plug with strain-gage pressure transducers remotely located from the model. The locations of the static-pressure orifices are given in figure 3 and table 2. The jet total pressure and stagnation temperature were measured at locations shown in figure 1. Thrust and drag forces on the metric portion of the model were obtained by means of a three-component strain-gage balance. A turbine flowmeter located in the air supply system was used to obtain the mass-flow rate through the nozzle.

Data were obtained at static conditions and at Mach numbers from 0.50 to 1.30 in the Langley 16-foot transonic tunnel and at a Mach number of 1.82 in the Langley 4-foot supersonic pressure tunnel. At all test conditions the model angle of attack was 0°. Primary total-pressure ratio $p_{t,j}/p_\infty$ varied from 1.0 (jet off) to approximately 23, depending on Mach number.

RESULTS AND DISCUSSION

Afterbody Characteristics

Pressure distribution.- Figures 4 and 5 show, respectively, the jet-off and jet-on pressure distributions on the external surface of the six afterbodies for various Mach numbers. Pressures were measured around the boattail at 0°, 45°, 90°, 135°, and 180° locations but only the data from the top row (0°) are presented in figures 4 and 5, to indicate a typical pressure distribution. For the boattail pressure distributions at jet-off operation, increasing the boattail angle caused a reduction in the peak negative pressure and tended to move it upstream, a result indicative of the kind of flow that separates with increase in boattail angle. This separation is typical for afterbodies having large boattail angles, as emphasized by the pressure distributions presented in reference 12.

The pressure distributions in figure 5 show that for all afterbodies the lowest level of boattail pressure coefficient generally occurs for the lower values of jet-on total-pressure ratio $\left(p_{t,j}/p_\infty \approx 3\right)$. This large decrease in pressure coefficient is probably due to the jet either aspirating the separated boattail region or reducing the amount of

separation which occurs on the boattail. Increased values of jet total-pressure ratio generally tend to reduce the negative pressure-coefficient level for most configurations; however, the decrease in pressure coefficient due to jet influence never returns to the jet-off level except for configuration 11 at $M = 1.00$. This beneficial jet effect on the boattail pressures at the higher values of jet total-pressure ratio is probably due to the expansion of the jet plume into the free-stream flow which tends to reduce the aspiration effects caused by the initial operation of the jet $\left(p_{t,j}/p_{\infty} \approx 1.5\right)$.

Boattail drag.- The afterbody pressures were integrated over the axially projected boattail area to obtain boattail pressure drag values which are presented in figures 6 and 7. The variation of boattail drag coefficient with Mach number for jet-off conditions is shown in figure 6. In the speed range from $M = 1.00$ to $M = 1.15$ the data may be affected by disturbances reflected from the tunnel wall; thus, fairing of the curves in that speed range is omitted. The boattail drag level decreased with increased boattail angle up to $\beta = 25^{\circ}$ (configurations 11, 21, and 31 and 12, 22, and 32), whereas, for $\beta > 25^{\circ}$ little additional change in boattail drag is noted. Increase in the primary thrust annulus from nonafterburning to afterburning mode had no effect on external boattail drag with jet not operating.

The effects on the boattail drag due to jet operation are presented in figure 7. The configurations with primary throat areas that simulate the nonafterburning mode $\left(A_t/A_{max} = 0.25\right)$ generally had the greatest drag at all test conditions except for $M = 0.90$ where several of the configurations with the large primary throat (afterburning mode, $A_t/A_{max} = 0.50$) had a higher drag level at the lower pressure ratios (see fig. 7(d)). A reduction in boattail drag of approximately 30 percent occurs at the low subsonic speeds when primary throat area is increased from nonafterburning to afterburning mode; however, at the higher Mach numbers the effect due to power position tends to diminish except for the higher jet total-pressure ratios.

Plug Characteristics

Pressure distributions.- The radial distribution of pressure on the concave plug is presented as pressure coefficient in figure 8, with jet total-pressure ratio as a parameter. Results for configurations 11, 12, 51, and 52 are presented for Mach numbers of 0, 0.80, and 1.30 to represent the type of pressure distribution obtained, respectively, at static conditions and at high subsonic and transonic speeds for two vastly different values of jet convergence angle and two primary throat areas. Note that for static conditions, $C_{p,plug}$ is the plug pressure divided by ambient pressure p_a, rather than by free-stream dynamic pressure q_{∞} as it is for Mach numbers greater than zero. Generally, with jet operation the plug pressures remain above the free-stream static pressure p_{∞}. Increases in jet convergence angle increased the plug pressures for configurations in both the nonafterburning and the afterburning modes. The pressure at the center of the plug ($r/R = 0$)

being greater than the average for the distribution is interpreted as an indication of recirculating or vortex-ring-type flow in the base region similar to that shown in reference 8. This type of flow seems to be more pronounced at the higher jet convergence angles than at the low angles, probably because the exhaust flow for nozzles with the higher convergence angles intersects the center-line axis at a point much closer to the plug than for nozzles with lower convergence angles; thus, a greater flow velocity is caused to be directed toward the concave base.

Thrust.- The pressure distributions on the concave plugs presented in figure 8, along with those obtained at the other test Mach numbers and for the other configurations, were integrated with respect to base area to obtain base thrust. The variation of base thrust coefficient with jet total-pressure ratio is presented in figure 9. At $M = 0$ (fig. 9(a)), results are presented in the form of the static coefficient (divided by ambient pressure p_a) which is not numerically comparable with the dynamic coefficient (divided by free-stream dynamic pressure q_∞) used in figures 9(b) to 9(j). At static conditions and for Mach numbers to 0.90, either zero or positive plug thrust was obtained with increasing jet total-pressure ratio; this indicates that a positive pressure field acted around the base annulus. At Mach numbers greater than 0.90 a negative plug force occurs at the low values of pressure ratio for some configurations; this indicates that the base region was aspirated by the jet. The configurations which show severe aspiration effects generally were in the nonafterburner operating mode and had the lower values of jet convergence angle (for example, configurations 11, 21, or 31). The configurations which had the highest plug thrust at all Mach numbers were those with the large primary throat area (afterburning mode). This higher plug thrust is probably due to the thicker jet exhaust restricting the aspiration effects of the external stream flow which in turn increases the recirculating jet flow in the base and therefore produces a greater thrust force on the plug. Jet convergence angle generally had very little effect on the plug thrust at most Mach numbers, with the trend being a slight increase in plug thrust as convergence angle increased.

Nozzle Performance Characteristics

Basic data.- Presented in figure 10 are the static thrust coefficient and the ideal static thrust coefficient as functions of jet total-pressure ratio for the various configurations tested. These static coefficients are defined as the thrust force divided by ambient pressure p_a and the reference area A_{max}. The boattail drag, although included in the measurement of axial force, is regarded as negligible so that the static thrust coefficient essentially includes only internal nozzle thrust.

Thrust-minus-drag coefficients, thrust coefficients, and ideal thrust coefficients for the configurations are shown as a function of jet total-pressure ratio in figures 11 and 12.

These coefficients are defined as thrust-minus-drag force or thrust force (measured or ideal) divided by free-stream dynamic pressure q_∞ and the reference area A_{max}.

Thrust-minus-drag ratio.- The variation of thrust-minus-drag ratio with jet total-pressure ratio and Mach number is shown in figure 13. Under static conditions the ratio of measured to ideal thrust for the six nozzle configurations with the large primary throat area (afterburning mode) is relatively good when compared with other types of nozzles; however, the performance of the six configurations with the small primary throat area (nonafterburning mode) appears to be as much as 7 percent low at low pressure ratios when compared with other nozzles having similar throat areas. The ratios of measured thrust minus drag to ideal thrust at airstream Mach numbers from 0.50 to 1.82 are presented in figures 13(b) to 13(j). The thrust-minus-drag ratio generally increased with increasing jet total-pressure ratio for most Mach numbers and a maximum value of $\frac{F_j - F_{A,\beta}}{F_i}$ was not obtained for most configurations at $M \geq 0.90$. With increased values of Mach number the thrust-minus-drag performance decreased for all configurations when compared at a constant jet total-pressure ratio.

Internal performance.- The variation of internal performance F_j/F_i with jet total-pressure ratio and Mach number is presented in figure 14. As was observed for static conditions (fig. 13) the internal performance of the configurations with the large primary throat area was again higher than that of the configurations with the small primary throat area for all Mach numbers. At the higher Mach numbers the internal performance was lower than that measured at static conditions.

Performance at a scheduled pressure ratio.- A schedule of the variation of jet total-pressure ratio with Mach number for a typical turbojet engine is given in figure 15. Presented in figure 16 is the variation with Mach number of the thrust-minus-drag ratio, internal performance, and afterbody boattail drag coefficients of the 12 nozzle configurations for the foregoing scheduled operating conditions. For the configurations in the afterburning mode $\left(A_t/A_{max} = 0.50\right)$ the thrust-minus-drag ratio is competitive with the performance of convergent-divergent nozzles and isentropic plug nozzles (refs. 1, 6, and 10). The nozzles in the nonafterburning mode $\left(A_t/A_{max} = 0.25\right)$ revealed a fairly large loss in thrust-minus-drag ratio, approaching 25 percent, at Mach numbers greater than 0.80 when compared with the nozzles in the afterburning mode. At subsonic speeds up to $M = 0.90$, the internal performance of the 12 configurations was equal to or greater than the internal performance observed at static conditions. At the higher speeds ($M > 0.90$), the nozzles with the large primary throat area $\left(A_t/A_{max} = 0.50\right)$ suffered a loss of approximately 3 percent in internal performance from that at static conditions; however, the nozzles with the small primary throat area $\left(A_t/A_{max} = 0.25\right)$ experienced a loss in performance of about 12 percent. The improved internal performance (greater than the performance level at $M = 0$) seen at the subsonic Mach numbers probably results from a

beneficial influence of the jet exhaust mixing with the external stream which thus reduces the drag term in the thrust-minus-drag expression. At most Mach numbers the nozzles configured for nonafterburning operation had the higher afterbody drag coefficients; however, for the configurations whose jet convergence angle was equal to or greater than 25° the afterbody boattail drag decreased with increase in Mach number up to 0.90. At $M = 0.90$ and jet convergence angles greater than 20° the nozzles configured in the afterburning mode had a higher drag level than those operating in the nonafterburning mode.

Presented in figure 17 is the effect of nozzle lip angle or jet convergence angle on the performance of annular nozzles in combination with a semitoroidal concave plug for the Mach number range and at scheduled jet total-pressure ratios. Thrust-minus-drag ratio and internal performance for the nozzles with the large primary throat area (afterburning mode, $A_t/A_{max} = 0.50$) generally experienced a slight decrease in performance (approximately 2 percent) with an increase in convergence angle at all Mach numbers except 1.82. The lowest performance generally occurred at a convergence angle of 30° with a tendency to show a small gain in performance with further increase in the convergence angle. At all Mach numbers the nozzles configured for the afterburning mode exhibited an increase in afterbody boattail drag with increase in jet convergence or boattail angle.

The nozzles with the small primary throat area (nonafterburning mode, $A_t/A_{max} = 0.25$) exhibited an increase in performance at $M = 0.50$, experienced mixed results at $M = 0.70$, and showed a loss of performance up to approximately 6 percent at $M > 0.70$ as the jet convergence angle was increased from 15° to 40°. Afterbody boattail drag coefficient generally increased at convergence angles up to $\beta = 30^{\circ}$ and then either leveled off or decreased slightly at the higher convergence angles for most Mach numbers; however, a large reduction in boattail drag occurs for convergence angles of $\beta > 20^{\circ}$ at $M = 0.80$ and $\beta > 15^{\circ}$ at $M = 0.90$.

CONCLUDING REMARKS

An investigation at static conditions and at Mach numbers up to 1.82 of the thrust and drag characteristics of 12 configurations of an annular nozzle has been made. The configurations consisted of six afterbodies with different jet convergence angles, each used with two semitoroidal concave plugs to vary primary jet exit area. Results of the investigation indicated the following trends:

An increase in the jet convergence angle from 15° to 40° resulted in little change in performance levels for nozzles with primary throat areas simulating afterburner operation; however, a loss in performance resulted for nozzles with primary throat areas simulating nonafterburner operation.

The internal performance and thrust-minus-drag performance of the nozzle configurations with the larger primary throat area (afterburning mode) is competitive with nozzles designed for operation over the Mach number range and at a given typical turbojet total-pressure ratio schedule.

The internal performance and thrust-minus-drag performance of the nozzle configurations with the small primary throat area (nonafterburning mode) gave relatively poor performance at the higher subsonic and transonic speeds and would probably be marginal at a typical subsonic cruise flight condition (Mach 0.80).

Langley Research Center,
National Aeronautics and Space Administration,
Hampton, Va., August 17, 1972.

REFERENCES

1. Runckel, Jack F.: Review of NASA Exhaust Nozzle Research. Proceedings of NASA Conference on Supersonic-Transport Feasibility Studies and Supporting Research – September 17-19, 1963, NASA TM X-905, 1963, pp. 315-332.

2. Beheim, Milton A.: Off-Design Performance of Divergent Ejectors. NACA RM E58G10a, 1958.

3. Klann, John L.; and Huff, Ronald G.: Characteristics of Five Ejector Configurations at Free-Stream Mach Numbers From 0 to 2.0. NASA TM X-23, 1959.

4. Krull, H. George; and Beale, William T.: Effect of Plug Design on Performance Characteristics of Convergent-Plug Exhaust Nozzles. NACA RM E54H05, 1954.

5. Krull, H. George; Beale, William T.; and Schmiedlin, Ralph F.: Effect of Several Design Variables on Internal Performance of Convergent-Plug Exhaust Nozzles. NACA RM E56G20, 1956.

6. Salmi, R. J.; and Cortright, E. M., Jr.: Effects of External Stream Flow and Afterbody Variations on the Performance of a Plug Nozzle at High Subsonic Speeds. NACA RM E56F11a, 1956.

7. Valerino, Alfred S.; Zappa, Robert F.; and Abdalla, Kaleel L.: Effects of External Stream on the Performance of Isentropic Plug-Type Nozzles at Mach Numbers of 2.0, 1.8, and 1.5. NASA MEMO 2-17-59E, 1959.

8. Corson, Blake W., Jr.; and Mercer, Charles E.: Static Thrust of an Annular Nozzle With a Concave Central Base. NASA TN D-418, 1960.

9. Mercer, Charles E.; and Simonson, Albert J.: Effect of Geometric Parameters on the Static Performance of an Annular Nozzle With a Concave Central Base. NASA TN D-1006, 1962.

10. Corson, Blake W., Jr.; and Mercer, Charles E.: Transonic Thrust and Drag Characteristics of an Annular Nozzle Having a Semitoroidal Concave Plug. NASA TM X-958, 1964.

11. Compton, William B., III; and Runckel, Jack F.: Jet Effects on the Boattail Axial Force on Conical Afterbodies at Subsonic and Transonic Speeds. NASA TM X-1960, 1970.

12. Henry, Beverly Z., Jr.; and Cahn, Maurice S.: Pressure Distributions Over a Series of Related Afterbody Shapes as Affected by a Propulsive Jet at Transonic Speeds. NACA RM L56K05, 1957.

TABLE 1.- SEMITOROIDAL-PLUG-NOZZLE COORDINATES

Afterbody				Plug			
Conf.	x, cm	R_1, cm	R_2, cm	Conf.	x, cm	R_3, cm	R_4, cm
1	-7.437	7.620	6.431	1	-5.080	1.923	----------
	-2.540	7.620	7.315		-2.540	4.656	----------
	0	7.620	7.315		-2.286	4.930	----------
	.254	7.605	7.310		-2.032	5.217	3.175
	.284	7.592	7.308		-1.778	5.486	4.478, 2.118
	.508	7.569	7.269		-1.524	5.715	4.928, 1.643
	.625	7.554	7.259		-1.270	5.890	5.268, 1.273
	.762	7.518	7.226		-1.016	6.020	5.542, .970
	1.016	7.447	7.163		-.762	6.116	5.761, .699
	1.270	7.371	7.102		-.508	6.190	5.913, .437
	1.524	7.300	7.028		-.254	6.233	5.994, .203
	1.778	7.216	6.960		0	6.246	6.060, 0
	2.032	7.315	6.899		.254	6.238	6.096
	2.286	7.059	6.820		.284	6.226	6.096
	2.540	6.975	6.759		.508	6.195	6.096
	2.794	6.901	6.695		.624	6.157	6.096
	3.048	6.807	6.622				
	3.302	6.716	6.553				
	3.574	6.629	6.477				
				2	-5.080	1.918	----------
					-2.540	3.518	----------
					-2.286	3.678	----------
					-2.032	3.835	----------
					-1.778	4.003	----------
					-1.524	4.163	----------
					-1.270	4.318	2.540
					-1.016	4.481	3.861, 1.176
					-.762	4.641	4.277, .742
					-.508	4.798	4.542, .445
					-.254	4.887	4.714, .203
					0	4.915	4.790, 0
					.254	4.879	4.823
					.284	4.872	4.826

Afterbody				Plug			
Conf.	x, cm	R_1, cm	R_2, cm	Conf.	x, cm	R_3, cm	R_4, cm
2	-7.437	7.620	6.431	1	-5.080	1.905	----------
	-2.540	7.620	7.315		-2.540	4.633	----------
	0	7.620	7.315		-2.286	4.912	----------
	.254	7.610	7.308		-2.032	5.182	3.302
	.366	7.595	7.303		-1.778	5.456	4.511, 2.121
	.508	7.574	7.277		-1.524	5.690	4.963, 1.661
	.762	7.529	7.229		-1.270	5.865	5.296, 1.288
	.823	7.516	7.216		-1.016	5.997	5.558, .998
	1.016	7.460	7.165		-.762	6.099	5.740, .714
	1.270	7.366	7.074		-.508	6.167	5.880, .470
	1.524	7.267	6.982		-.254	6.205	5.979, .226
	1.778	7.163	6.896		0	6.220	6.033, 0
	2.032	7.049	6.800		.254	6.205	6.050
	2.286	6.924	6.706		.366	6.195	6.053
	2.540	6.810	6.614		.508	6.167	6.050
	2.794	6.693	6.518		.762	6.096	6.035
	2.916	6.629	6.477		.823	6.086	6.033
				2	-5.080	1.905	----------
					-2.540	3.500	----------
					-2.286	3.658	----------
					-2.032	3.818	----------
					-1.778	3.975	----------
					-1.524	4.138	----------
					-1.270	4.305	2.540
					-1.016	4.460	3.851, 1.191
					-.762	4.623	4.227, .762
					-.508	4.773	4.481, .467
					-.254	4.869	4.641, .229
					0	4.884	4.729, 0
					.254	4.867	4.775
					.366	4.829	4.775

Afterbody				Plug			
Conf.	x, cm	R_1, cm	R_2, cm	Conf.	x, cm	R_3, cm	R_4, cm
3	-7.437	7.620	6.431	1	-5.080	1.902	----------
	-2.540	7.620	7.315		-2.540	4.585	----------
	0	7.620	7.315		-2.540	4.585	----------
	.254	7.607	7.313		-2.032	5.121	3.429
	.432	7.579	7.292		-1.778	5.387	4.469, 2.131
	.508	7.569	7.280		-1.524	5.636	4.864, 1.641
	.762	7.516	7.234		-1.270	5.819	5.171, 1.280
	1.003	7.442	7.173		-1.016	5.956	5.415, .975
	1.016	7.435	7.168		-.762	6.058	5.624, .709
	1.270	7.341	7.084		-.508	6.132	5.781, .457
	1.524	7.229	6.975		-.254	6.167	5.870, .226
	1.778	7.102	6.855		0	6.187	5.931, 0
	2.032	6.957	6.734		.254	6.165	5.949
	2.286	6.805	6.609		.432	6.147	5.959
	2.540	6.642	6.492		.508	6.132	5.946
	2.558	6.629	6.477		.762	6.058	5.936
					1.003	5.964	5.903
				2	-5.080	1.897	----------
					-2.540	3.459	----------
					-2.286	3.612	----------
					-2.032	3.769	----------
					-1.778	3.922	----------
					-1.524	4.079	----------
					-1.270	4.234	2.540
					-1.016	4.389	3.599, 1.224
					-.762	4.544	4.021, .795
					-.508	4.699	4.313, .483
					-.254	4.808	4.519, .224
					0	4.839	4.643, 0
					.254	4.813	4.694
					.432	4.746	4.681

TABLE 1.- SEMITOROIDAL-PLUG-NOZZLE COORDINATES – Concluded

Afterbody				Plug			
Conf.	x, cm	R_1, cm	R_2, cm	Conf.	x, cm	R_3, cm	R_4, cm
4	-7.437	7.620	6.431	1	-5.080	1.905	----------
	-2.540	7.620	7.315		-2.540	4.564	----------
	0	7.620	7.315		-2.286	4.829	----------
	.254	7.607	7.313		-2.032	5.093	3.327
	.480	7.572	7.305		-1.778	5.357	4.442, 2.134
	.508	7.567	7.287		-1.524	5.603	4.829, 1.651
	.762	7.513	7.249		-1.270	5.794	5.108, 1.280
	1.016	7.430	7.176		-1.016	5.941	5.342, .978
	1.181	7.374	7.120		-.762	6.043	5.532, .704
	1.270	7.330	7.097		-.508	6.111	5.679, .455
	1.524	7.203	6.980		-.254	6.152	5.771, .224
	1.778	7.059	6.850		0	6.167	5.789, 0
	2.032	6.891	6.693		.254	6.152	5.857
	2.286	6.703	6.538		.480	6.119	5.870
	2.385	6.629	6.477		.508	6.109	5.870
					.762	6.045	5.857
					1.016	5.941	5.837
					1.181	5.862	5.804
				2	-5.080	1.905	----------
					-2.540	3.409	----------
					-2.286	3.561	----------
					-2.032	3.711	----------
					-1.778	3.863	----------
					-1.524	4.016	----------
					-1.270	4.168	2.515
					-1.016	4.315	3.630, 1.217
					-.762	4.470	4.034, .787
					-.508	4.623	4.282, .475
					-.254	4.724	4.450, .224
					0	4.760	4.536, 0
					.254	4.727	4.572
					.480	4.638	4.580

Afterbody				Plug			
Conf.	x, cm	R_1, cm	R_2, cm	Conf.	x, cm	R_3, cm	R_4, cm
5	-7.437	7.620	6.431	1	-5.080	1.905	----------
	-2.540	7.620	7.315		-2.540	4.536	----------
	0	7.620	7.315		-2.286	4.798	----------
	.254	7.605	7.313		-2.032	5.065	3.302
	.508	7.567	7.285		-1.778	5.324	4.364, 2.144
	.526	7.564	7.282		-1.524	5.580	4.717, 1.648
	.762	7.503	7.244		-1.270	5.763	5.009, 1.283
	1.016	7.430	7.170		-1.016	5.903	5.237, .973
	1.270	7.318	7.087		-.762	6.007	5.431, .706
	1.336	7.295	7.061		-.508	6.081	5.575, .455
	1.524	7.193	6.980		-.254	6.121	5.672, .224
	1.778	7.036	6.843		0	6.139	5.733, 0
	2.032	6.848	6.678		.254	6.119	5.753
	2.286	6.629	6.497		.508	6.076	5.761
	2.294	6.624	6.477		.526	6.071	5.761
					.762	6.005	5.748
					1.016	5.903	5.720
					1.270	5.763	5.682
					1.336	5.725	5.664
				2	-5.080	1.905	----------
					-2.540	3.391	----------
					-2.286	3.536	----------
					-2.032	3.686	----------
					-1.778	3.833	----------
					-1.524	3.983	----------
					-1.270	4.133	2.515
					-1.016	4.282	3.647, 1.212
					-.762	4.427	4.039, .800
					-.508	4.582	4.255, .478
					-.254	4.691	4.404, .224
					0	4.724	4.475, 0
					.254	4.691	4.509
					.580	4.572	4.506
					.526	4.567	4.506

Afterbody				Plug			
Conf.	x, cm	R_1, cm	R_2, cm	Conf.	x, cm	R_3, cm	R_4, cm
6	-7.437	7.620	6.431	1	-5.080	1.905	----------
	-2.540	7.620	7.315		-2.540	4.514	----------
	0	7.620	7.315		-2.286	4.770	----------
	.254	7.607	7.313		-2.032	5.029	3.353
	.508	7.567	7.285		-1.778	5.288	4.440, 2.129
	.559	7.559	7.269		-1.524	5.540	4.801, 1.646
	.762	7.513	7.239		-1.270	5.735	5.093, 1.283
	1.016	7.432	7.173		-1.016	5.885	5.319, .978
	1.270	7.330	7.087		-.762	5.989	5.499, .709
	1.473	7.234	7.005		-.508	6.050	5.608, .452
	1.524	7.206	6.972		-.254	6.096	5.690, .218
	1.778	7.051	6.845		0	6.114	5.735, 0
	2.032	6.855	6.680		.254	6.096	5.740
	2.289	6.624	6.477		.508	6.050	5.735
					.559	6.043	5.730
					.762	5.989	5.700
					1.016	5.885	5.652
					1.270	5.738	5.588
					1.473	5.588	5.532
				2	-5.080	1.905	----------
					-2.540	3.358	----------
					-2.286	3.503	----------
					-2.032	3.653	----------
					-1.778	3.797	----------
					-1.524	3.942	----------
					-1.270	4.087	2.489
					-1.016	4.237	3.599, 1.212
					-.762	4.376	3.942, .782
					-.508	4.519	4.186, .488
					-.254	4.646	4.361, .218
					0	4.676	4.455, 0
					.254	4.648	4.468
					.508	4.524	4.435
					.559	4.486	4.422

TABLE 2.- PRESSURE-ORIFICE LOCATIONS

Afterbody			Plug				Afterbody			Plug				Afterbody			Plug			
Conf.	ϕ, deg	x, cm	Conf.	ϕ, deg	x, cm	R_4, cm	Conf.	ϕ, deg	x, cm	Conf.	ϕ, deg	x, cm	R_4, cm	Conf.	ϕ, deg	x, cm	Conf.	ϕ, deg	x, cm	R_4, cm
1	0 and 90	-3.810	1	0	0.508	6.096	2	0 and 90	-3.810	1	0	0.508	6.050	3	0 and 90	-3.810	1	0	0.762	5.936
	0 and 90	-2.540		0 and 90	-1.270	5.268		0 and 90	-2.540		0 and 90	-1.270	5.296		0 and 90	-2.540		0 and 90	-1.270	5.171
	0 and 90	-1.270		0	-2.032	3.175		0 and 90	-1.270		0	-2.032	3.302		0 and 90	-1.270		0	-2.032	3.429
	0 and 90	0		0 and 90	-1.524	1.643		0 and 90	0		0 and 90	-1.524	1.661		0 and 90	0		0 and 90	-1.524	1.641
	0 and 90	.762		0	-.508	.437		0 and 90	.635		0	-.508	.470		0 and 90	.572		0	-.508	.457
	0 and 90	1.524		0	-.508	-.437		0 and 90	1.270		0	-.508	-.470		0 and 90	1.143		0	-.508	-.457
	0 and 90	2.286		0	-1.524	-1.643		0 and 90	1.905		0	-1.524	-1.661		0 and 90	1.715		0	-1.524	-1.641
	0 and 90	3.048		0	-2.032	-3.175		0 and 90	2.540		0	-2.032	-3.302		0 and 90	2.286		0	-2.032	-3.429
	45, 135, and 180	0		0	-1.270	-5.268		45, 135, and 180	0		0	-1.270	-5.296		45, 135, and 180	0		0	-1.270	-5.171
	45, 135, and 180	.762		0	.508	-6.096		45, 135, and 180	.635		0	.508	-6.050		45, 135, and 180	.572		0	.762	-5.936
	45, 135, and 180	1.524						45, 135, and 180	1.270						45, 135, and 180	1.143				
	45, 135, and 180	2.286						45, 135, and 180	1.905						45, 135, and 180	1.715				
	45, 135, and 180	3.048						45, 135, and 180	2.540						45, 135, and 180	2.286				
			2	0	0	4.790				2	0	0	4.729				2	0	0	4.643
				0 and 90	-1.016	3.861					0 and 90	-1.016	3.851					0 and 90	-1.016	3.599
				0	-1.270	2.540					0	-1.270	2.540					0	-1.270	2.540
				0 and 90	-1.143	1.524					0 and 90	-1.143	1.524					0 and 90	-1.232	1.524
				0	-.508	.445					0	-.508	.467					0	-.508	.483
				0	-.508	-.445					0	-.508	-.467					0	-.508	-.483
				0	-1.143	-1.524					0	-1.143	-1.524					0	-1.232	-1.524
				0	-1.270	-2.540					0	-1.270	-2.540					0	-1.270	-2.540
				0	-1.016	-3.861					0	-1.016	-3.851					0	-1.016	-3.599
				0	0	-4.790					0	0	-4.729					0	0	-4.643
4	0 and 90	-3.810	1	0	0.762	5.857	5	0 and 90	-3.810	1	0	1.016	5.721	6	0 and 90	-3.810	1	0	1.016	5.652
	0 and 90	-2.540		0 and 90	-1.270	5.108		0 and 90	-2.540		0 and 90	-1.016	5.237		0 and 90	-2.540		0 and 90	-1.016	5.319
	0 and 90	-1.270		0	-2.032	3.327		0 and 90	-1.270		0	-2.032	3.302		0 and 90	-1.270		0	-2.032	3.353
	0 and 90	0		0 and 90	-1.524	1.351		0 and 90	0		0 and 90	-1.524	1.648		0 and 90	0		0 and 90	-1.524	1.646
	0 and 90	.508		0	-.508	.455		0 and 90	.508		0	-.508	.455		0 and 90	.508		0	-.508	.452
	0 and 90	1.016		0	-.508	-.455		0 and 90	1.016		0	-.508	-.455		0 and 90	1.016		0	-.508	-.452
	0 and 90	1.524		0	-1.524	-1.651		0 and 90	1.524		0	-1.524	-1.648		0 and 90	1.524		0	-1.524	-1.646
	0 and 90	2.032		0	-2.032	-3.327		0 and 90	2.032		0	-2.032	-3.302		0 and 90	2.023		0	-2.032	-3.353
	45, 135, and 180	0		0	-1.270	-5.108		45, 135, and 180	0		0	-1.016	-5.237		45, 135, and 180	0		0	-1.016	-5.319
	45, 135, and 180	.508		0	.762	-5.857		45, 135, and 180	.508		0	1.016	-5.720		45, 135, and 180	.508		0	1.016	-5.652
	45, 135, and 180	1.016						45, 135, and 180	1.016						45, 135, and 180	1.016				
	45, 135, and 180	1.524						45, 135, and 180	1.524						45, 135, and 180	1.524				
	45, 135, and 180	2.032						45, 135, and 180	2.032						45, 135, and 180	2.032				
			2	0	.254	4.572				2	0	.254	4.509				2	0	.254	4.468
				0 and 90	-1.016	3.630					0 and 90	-1.016	3.647					0 and 90	-1.016	3.599
				0	-1.270	2.515					0	-1.270	2.515					0	-1.270	2.489
				0 and 90	-1.232	1.524					0 and 90	-1.232	1.524					0 and 90	-1.232	1.524
				0	-.508	.475					0	-.508	.478					0	-.508	.488
				0	-.508	-.475					0	-.508	-.478					0	-.508	-.488
				0	-1.232	-1.524					0	-1.232	-1.524					0	-1.232	-1.524
				0	-1.270	-2.515					0	-1.270	-2.515					0	-1.270	-2.489
				0	-1.016	-3.630					0	-1.016	-3.647					0	-1.016	-3.599
				0	.254	-4.572					0	.254	-4.509					0	.254	-4.468

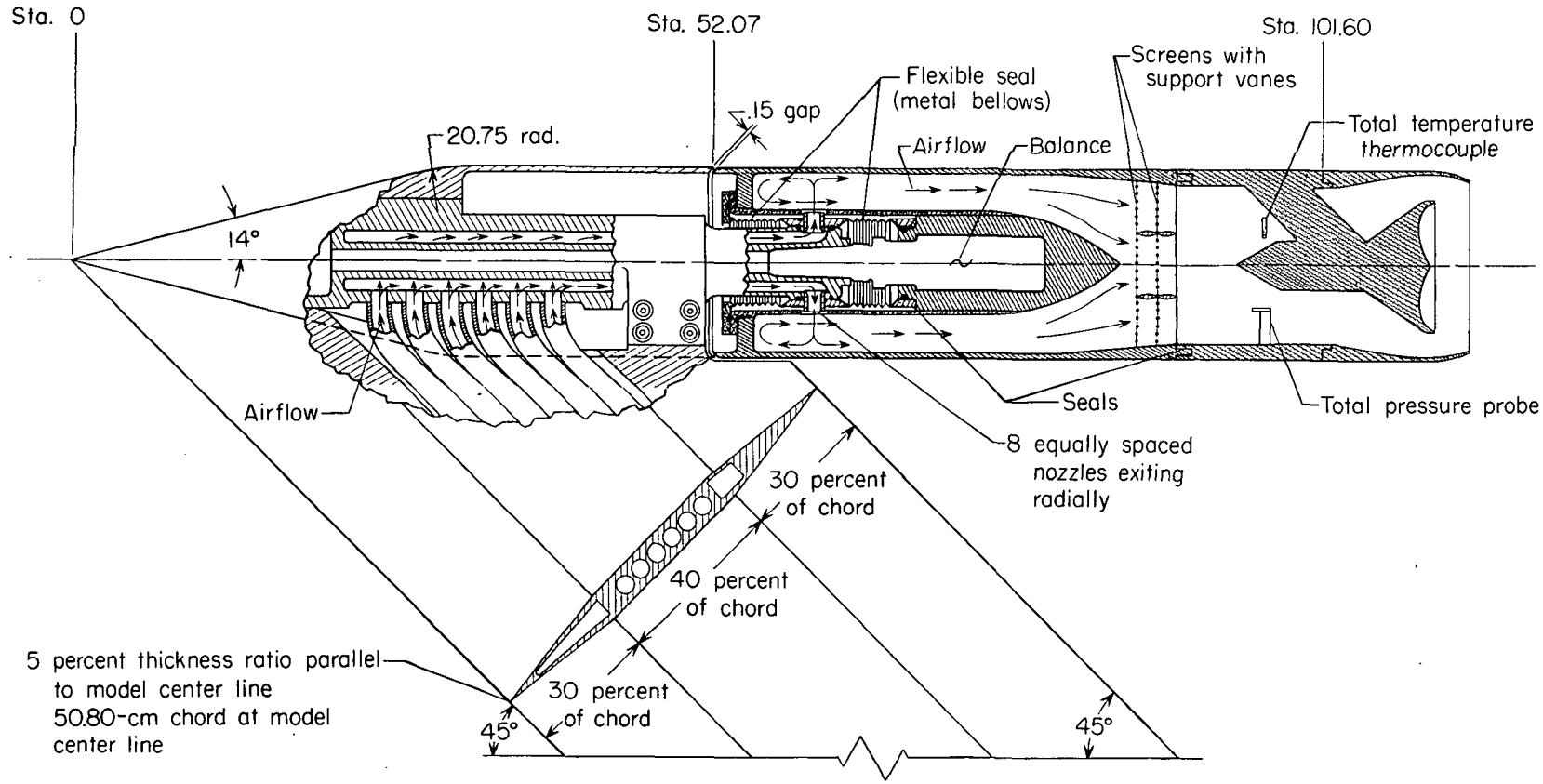

Figure 1.- Sketch of air-powered nacelle model with a circular-arc convergent nozzle installed. All dimensions are in centimeters unless otherwise noted.

L-66-7969

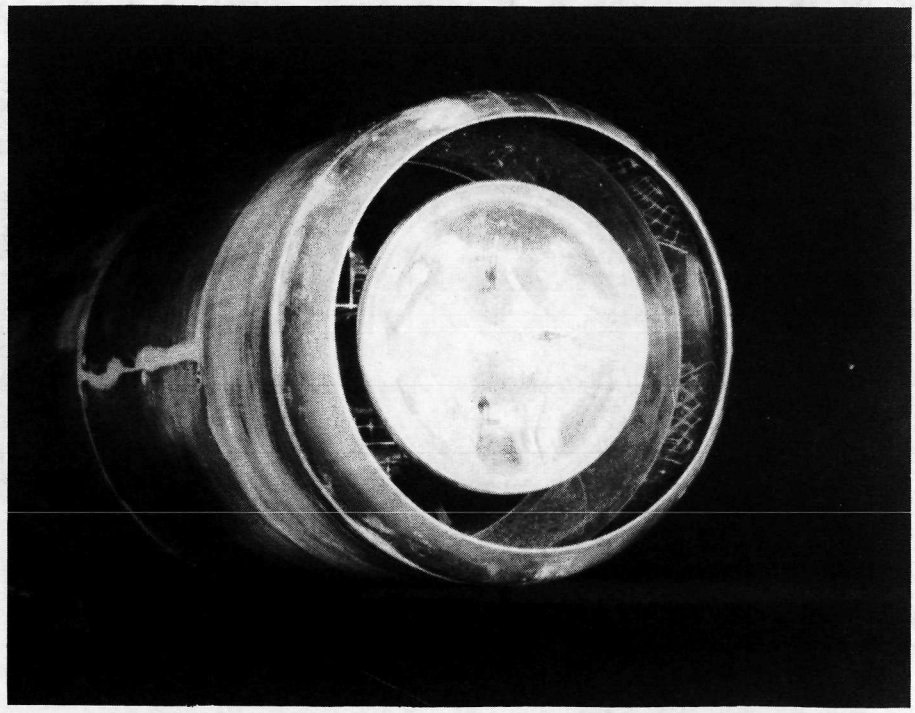

L-66-7971

Figure 2.- Photographs of model installed in test section.

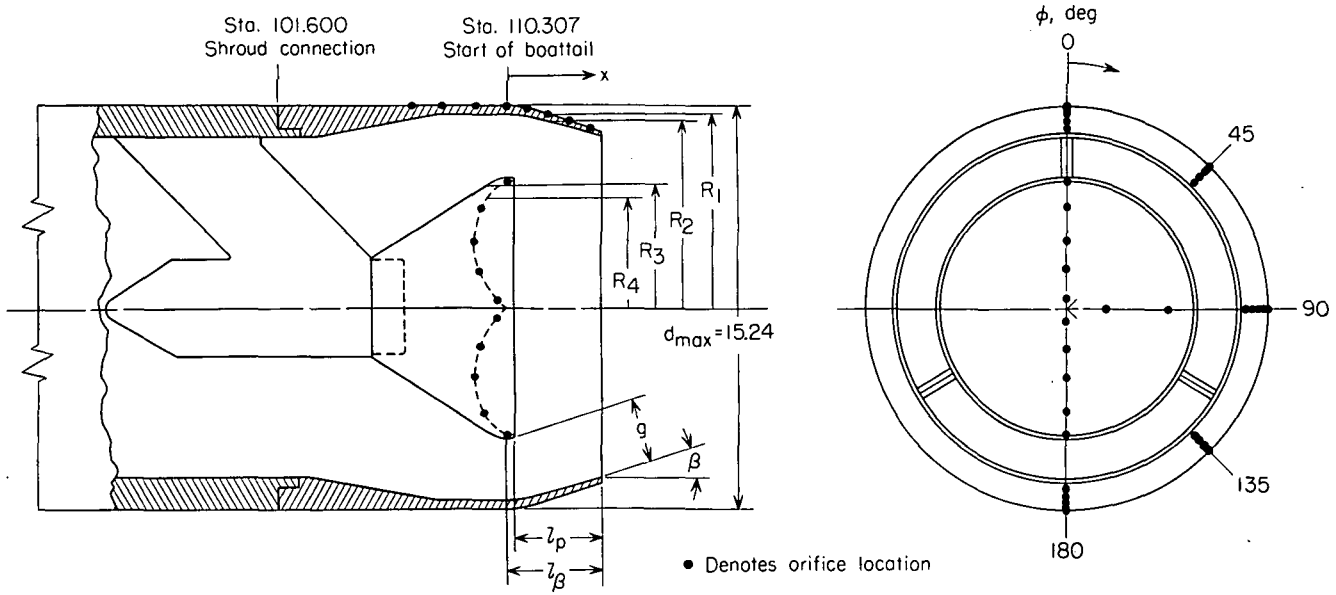

Configuration	Power mode	β, deg	A_t/A_{max}	g	l_β	l_p
11	Nonafterburning	15	0.25	1.069	3.573	2.948
21	↓	20	↓	1.094	2.915	2.092
31	↓	25	↓	1.127	2.557	1.554
41	↓	30	↓	1.148	2.385	1.203
51	↓	35	↓	1.176	2.293	.960
61	↓	40	↓	1.201	2.288	.815
12	Afterburning	15	0.50	2.400	3.573	3.289
22	↓	20	↓	2.430	2.915	2.550
32	↓	25	↓	2.476	2.557	2.125
42	↓	30	↓	2.555	2.385	1.905
52	↓	35	↓	2.590	2.293	1.770
62	↓	40	↓	2.639	2.288	1.729

Figure 3.- Sketch of semitoroidal plug nozzles. All dimensions are in centimeters unless otherwise noted.

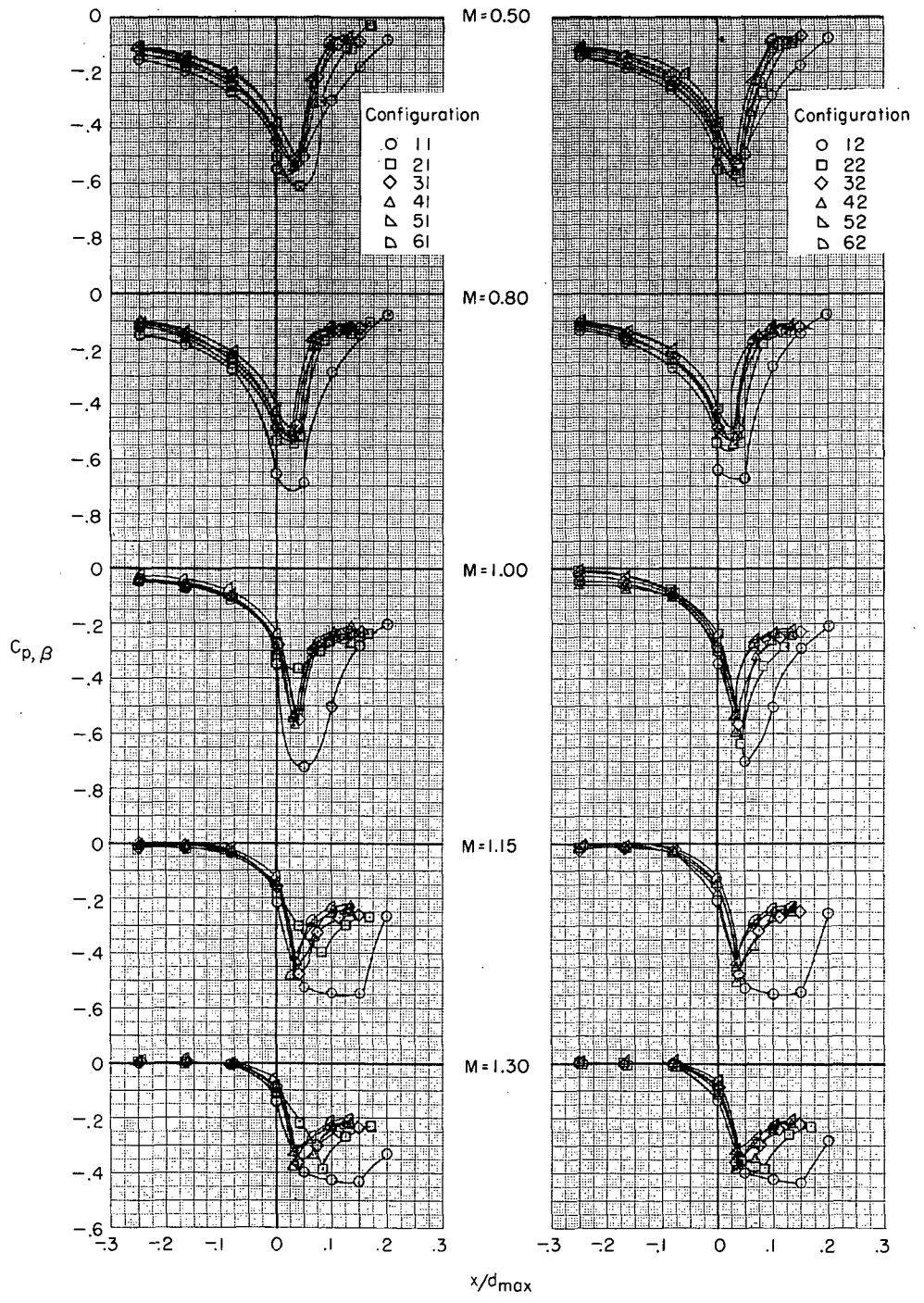

Figure 4.- Effect of boattail angle on boattail pressure distributions. Jet off.

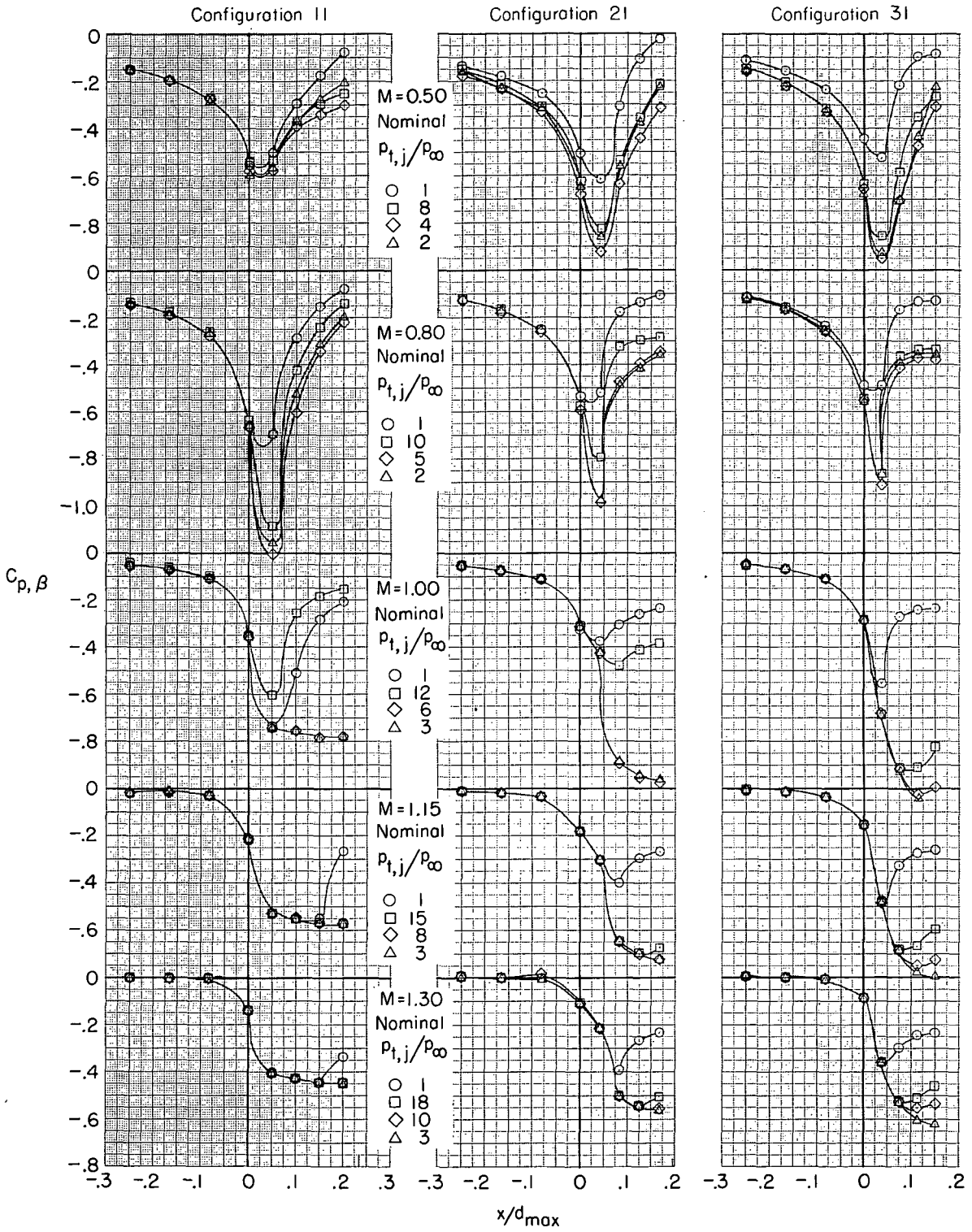

(a) Configurations 11, 21, and 31.

Figure 5.- Effect of jet total-pressure ratio on boattail pressure distribution for various Mach numbers.

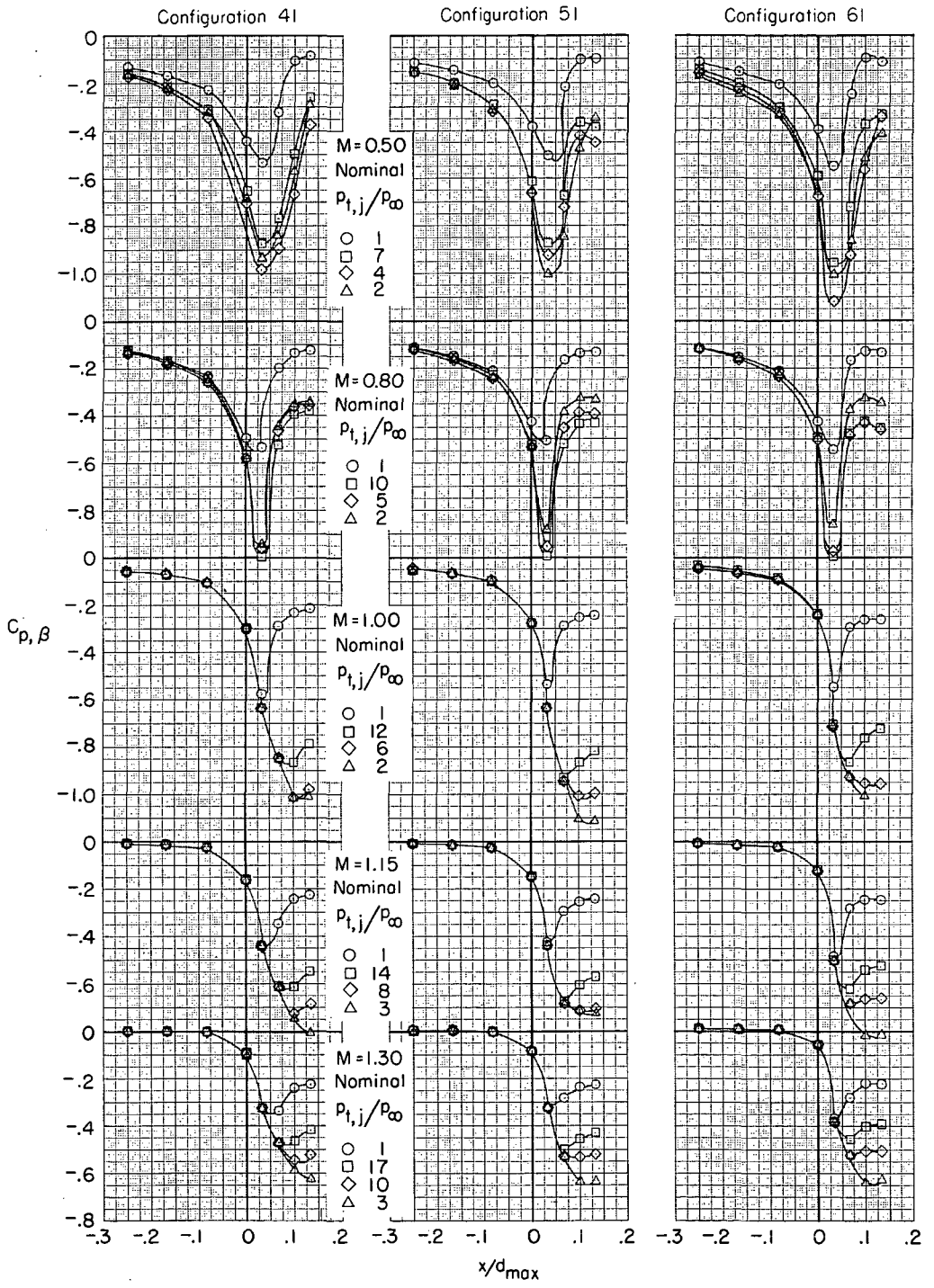

(b) Configurations 41, 51, and 61.

Figure 5.- Continued.

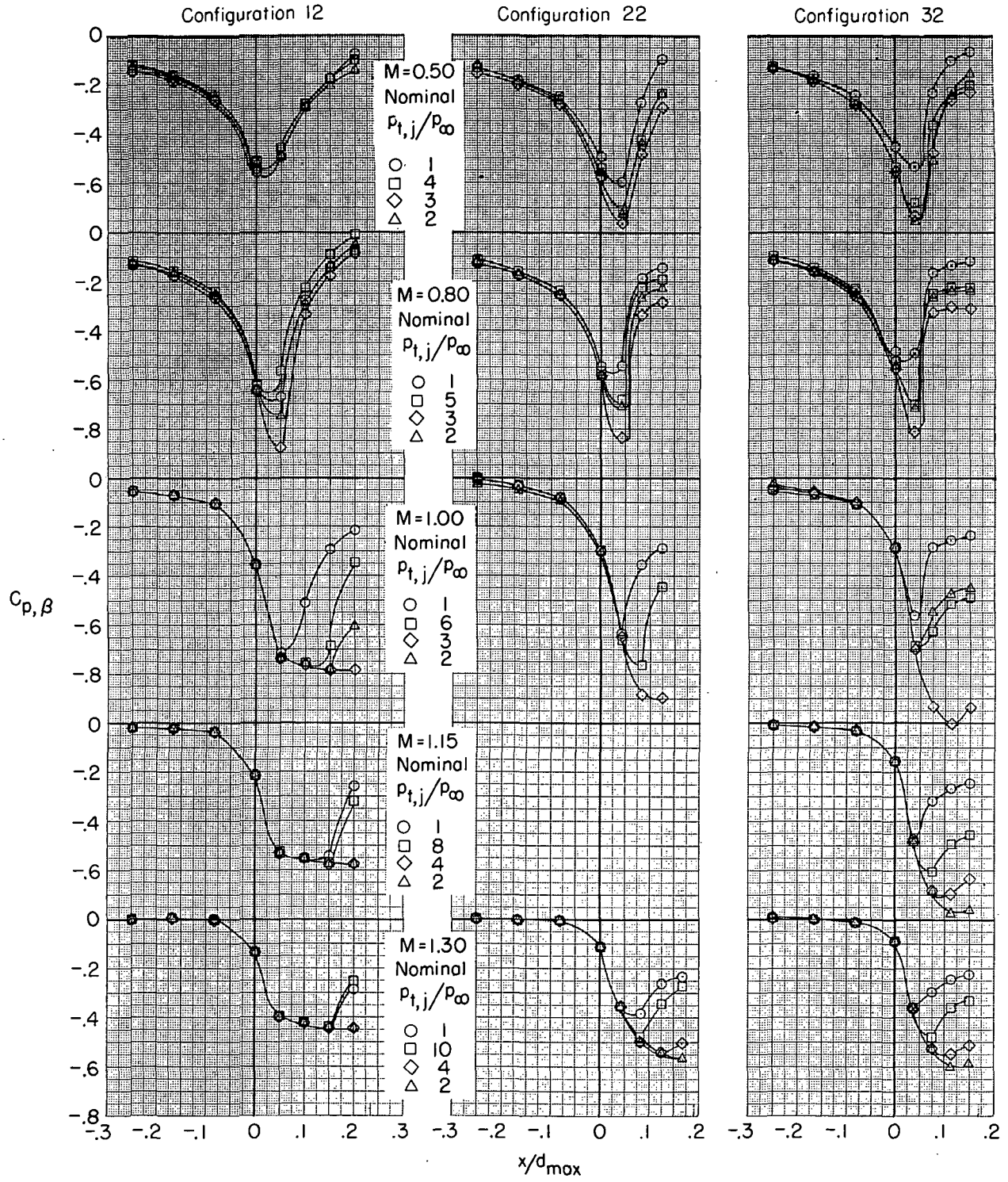

(c) Configurations 12, 22, and 32.

Figure 5.- Continued.

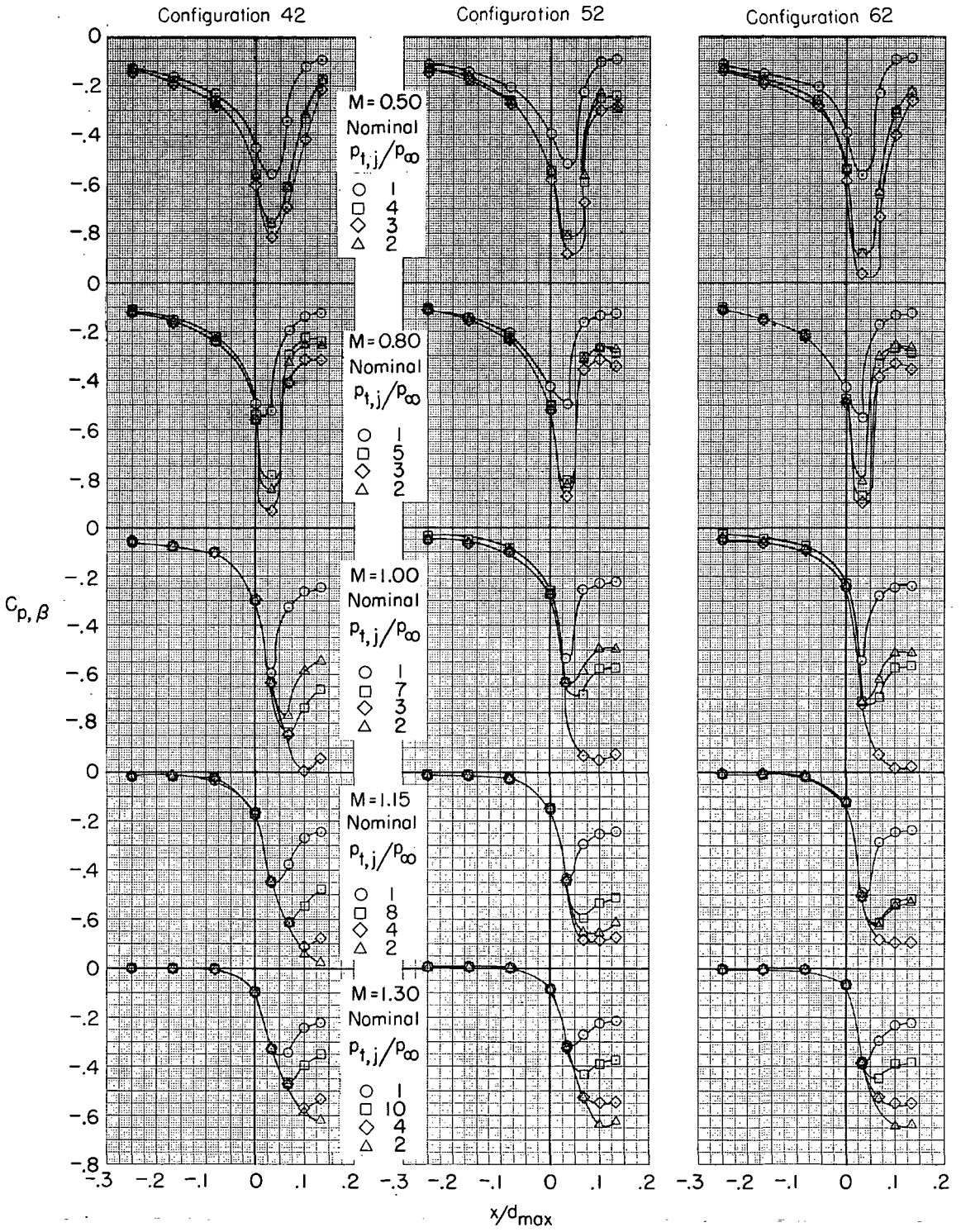

(d) Configurations 42, 52, and 62.

Figure 5.- Concluded.

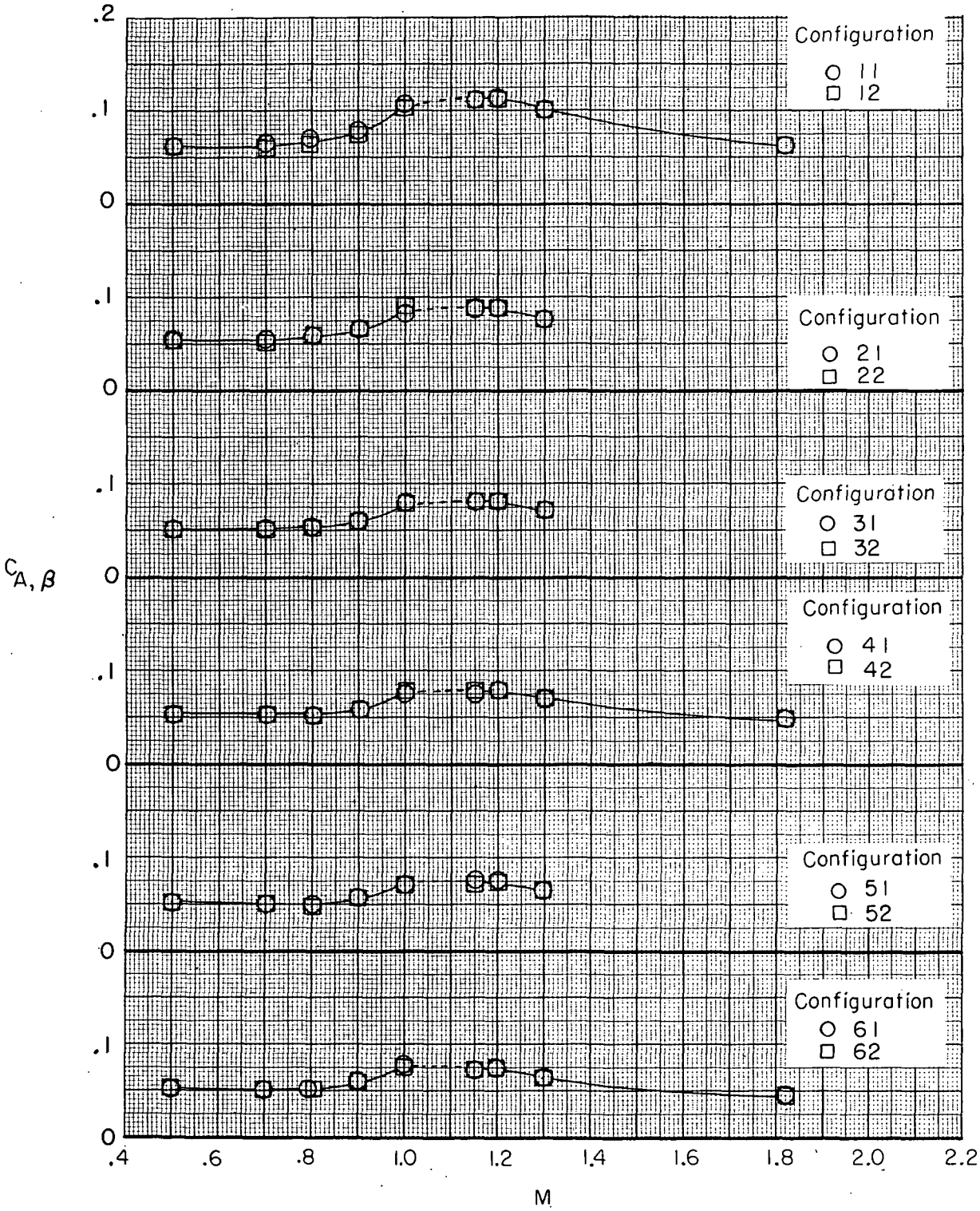

Figure 6.- Variation of boattail drag coefficient with Mach number for various configurations. Jet off.

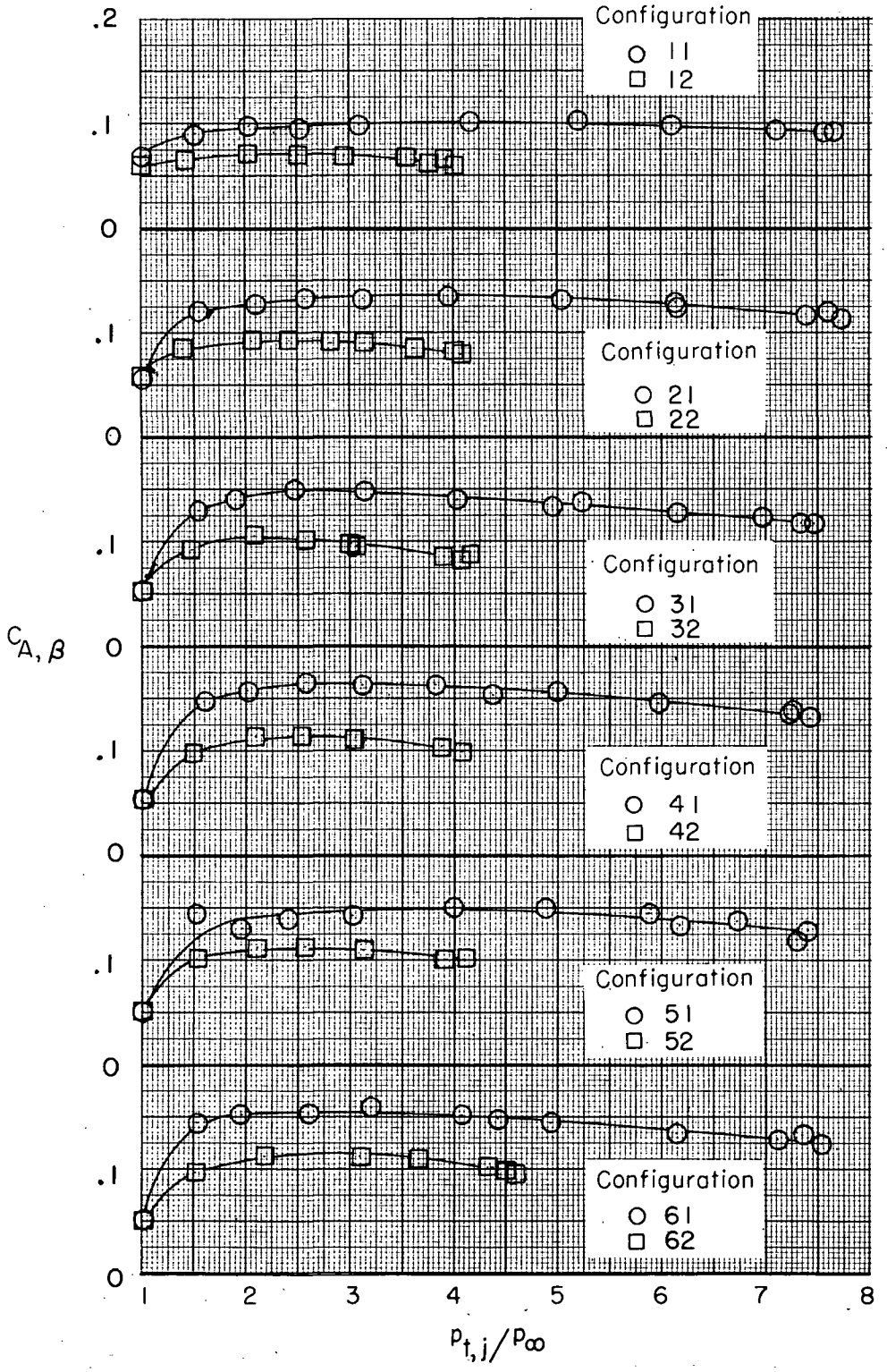

(a) M = 0.50.

Figure 7.- Variation of boattail drag coefficient with jet total-pressure ratio.

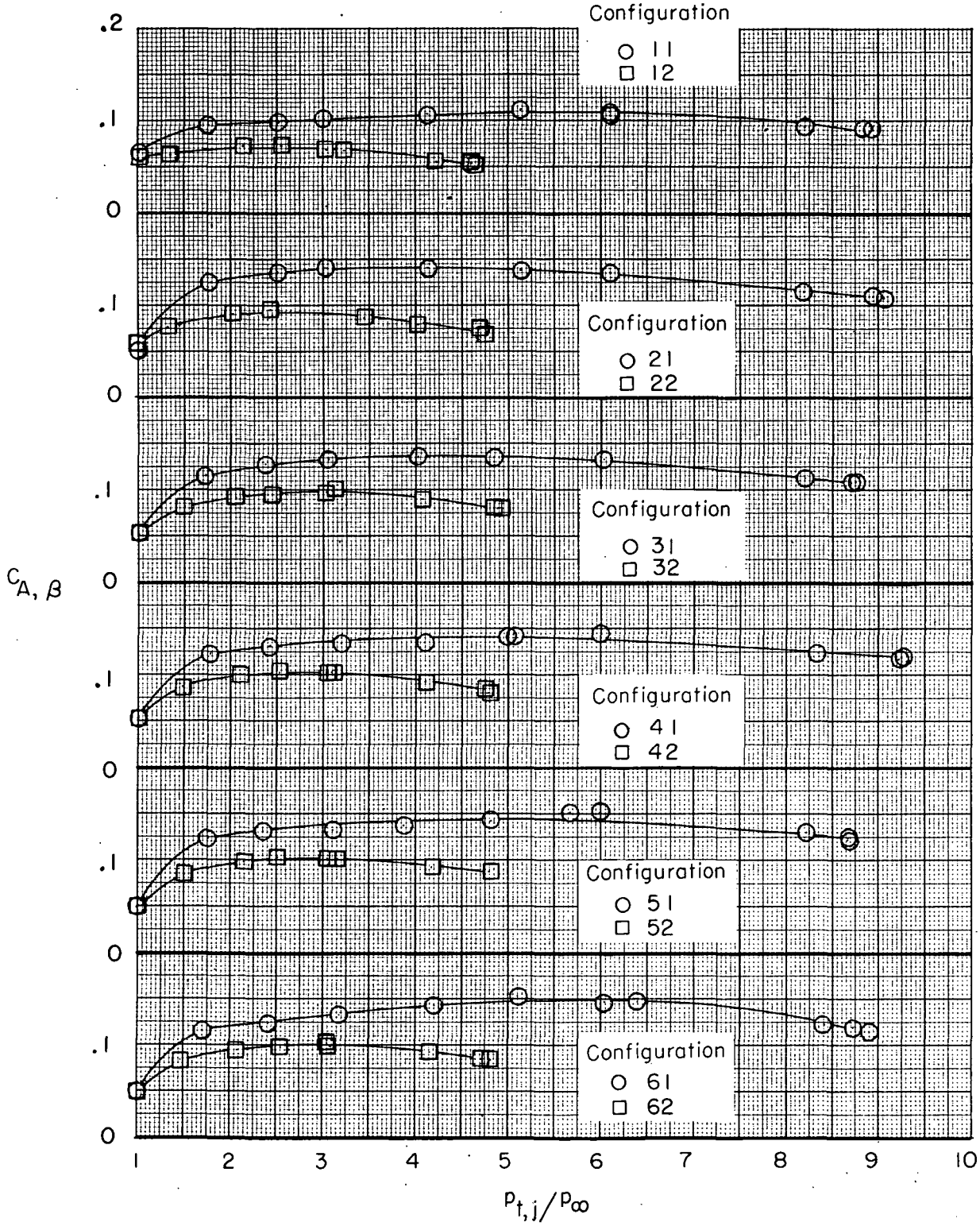

(b) M = 0.70.

Figure 7.- Continued.

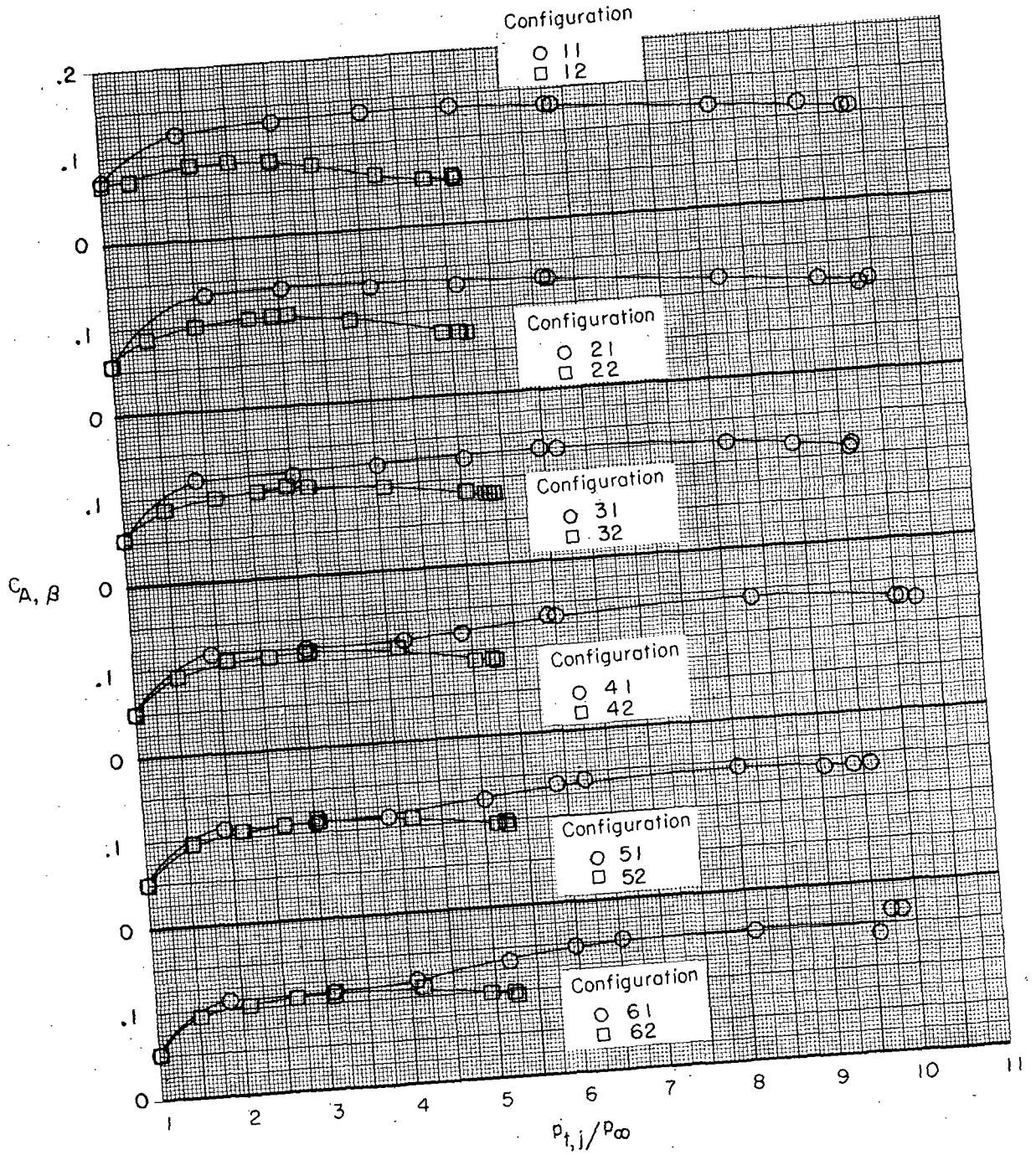

(c) M = 0.80.

Figure 7.- Continued.

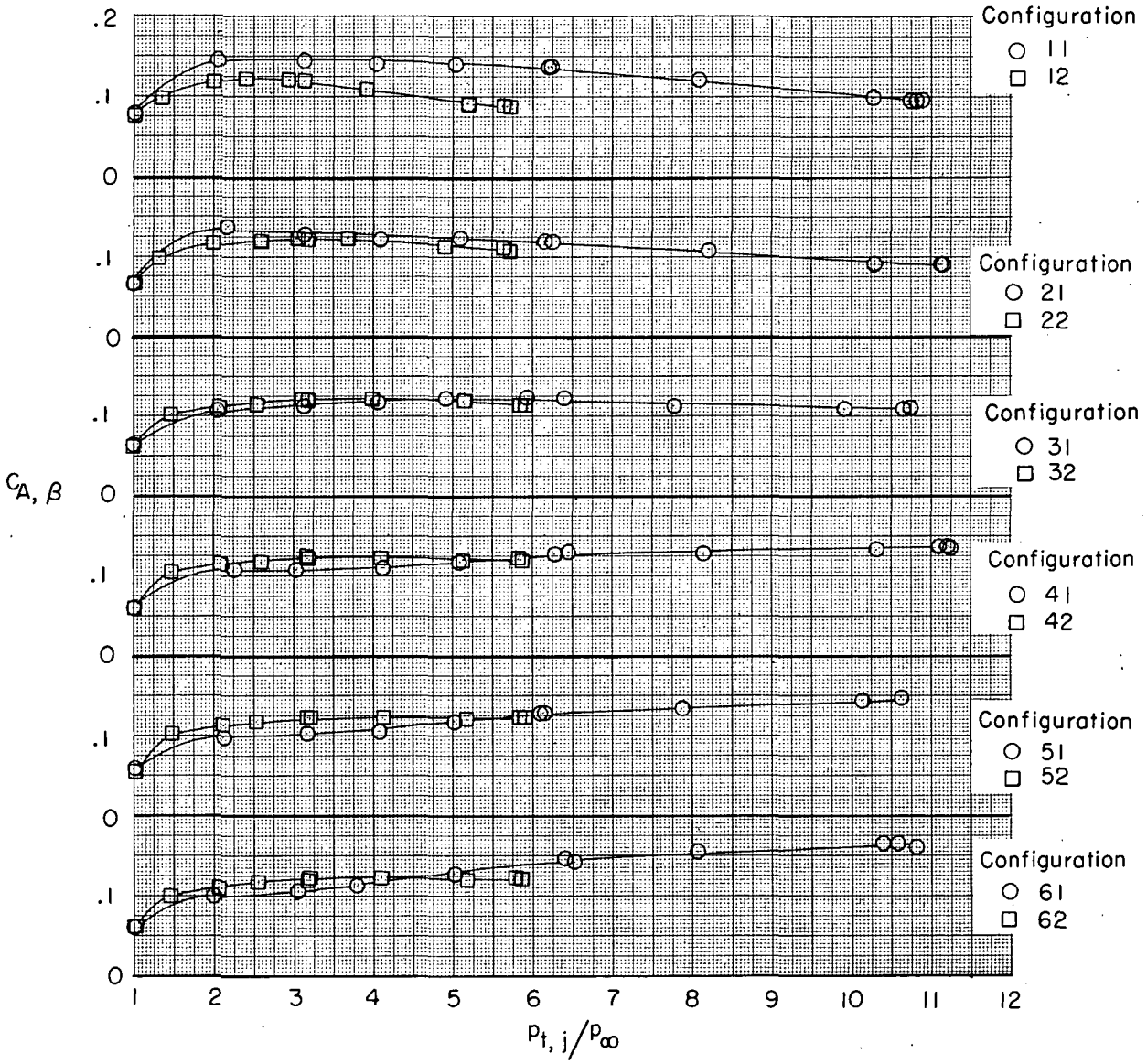

(d) M = 0.90.

Figure 7.- Continued.

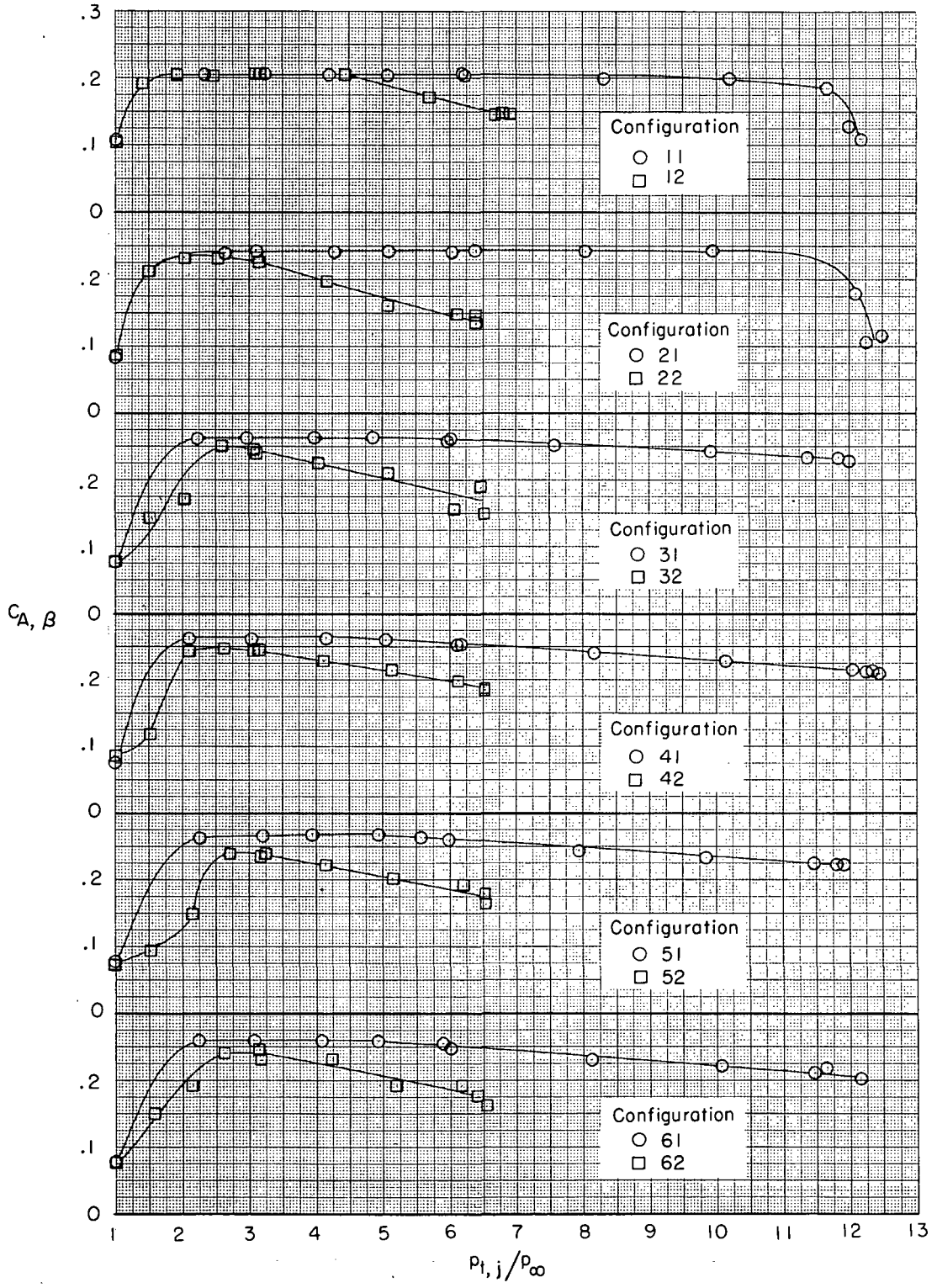

(e) M = 1.00.

Figure 7.- Continued.

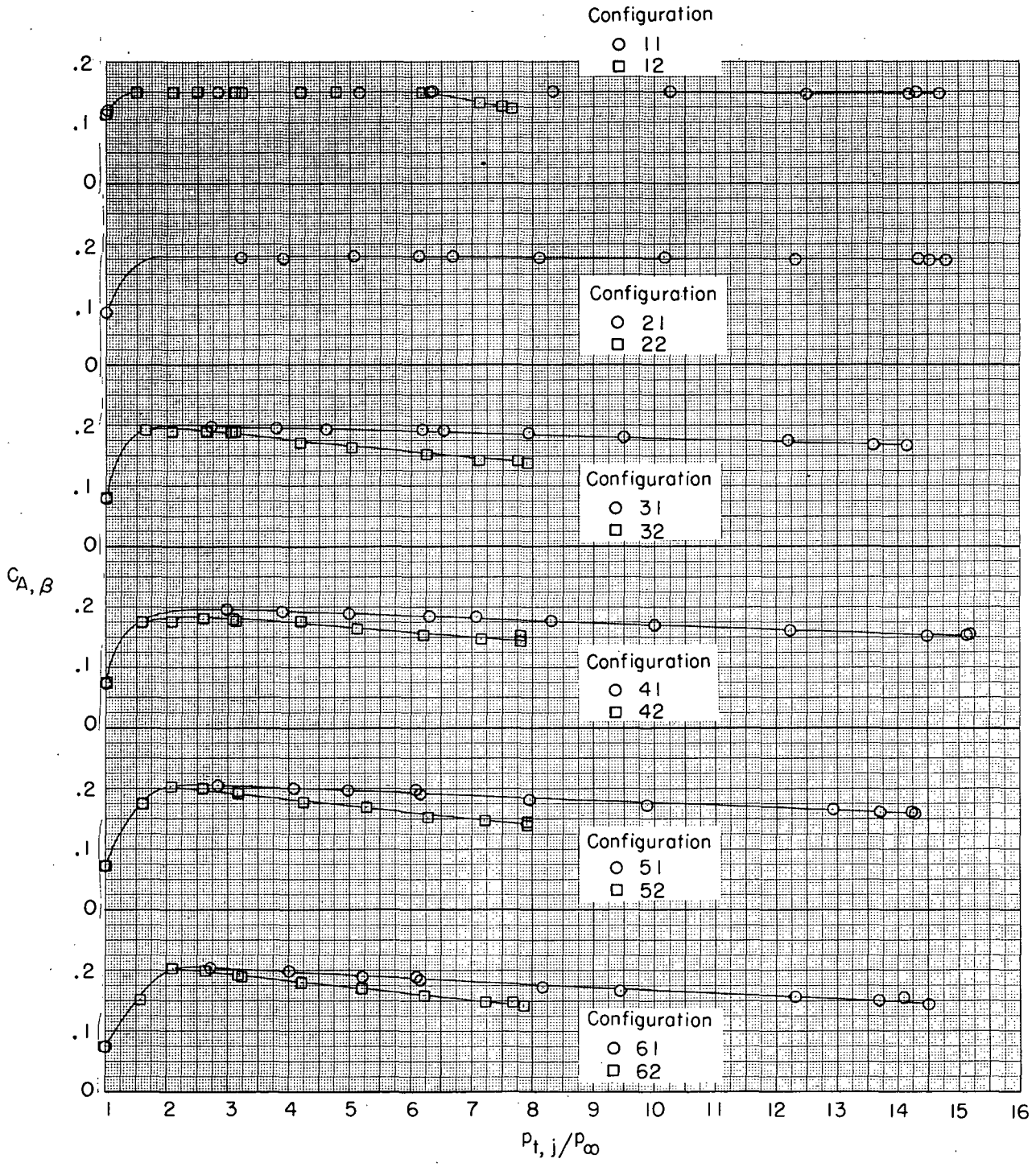

(f) M = 1.15.

Figure 7.- Continued.

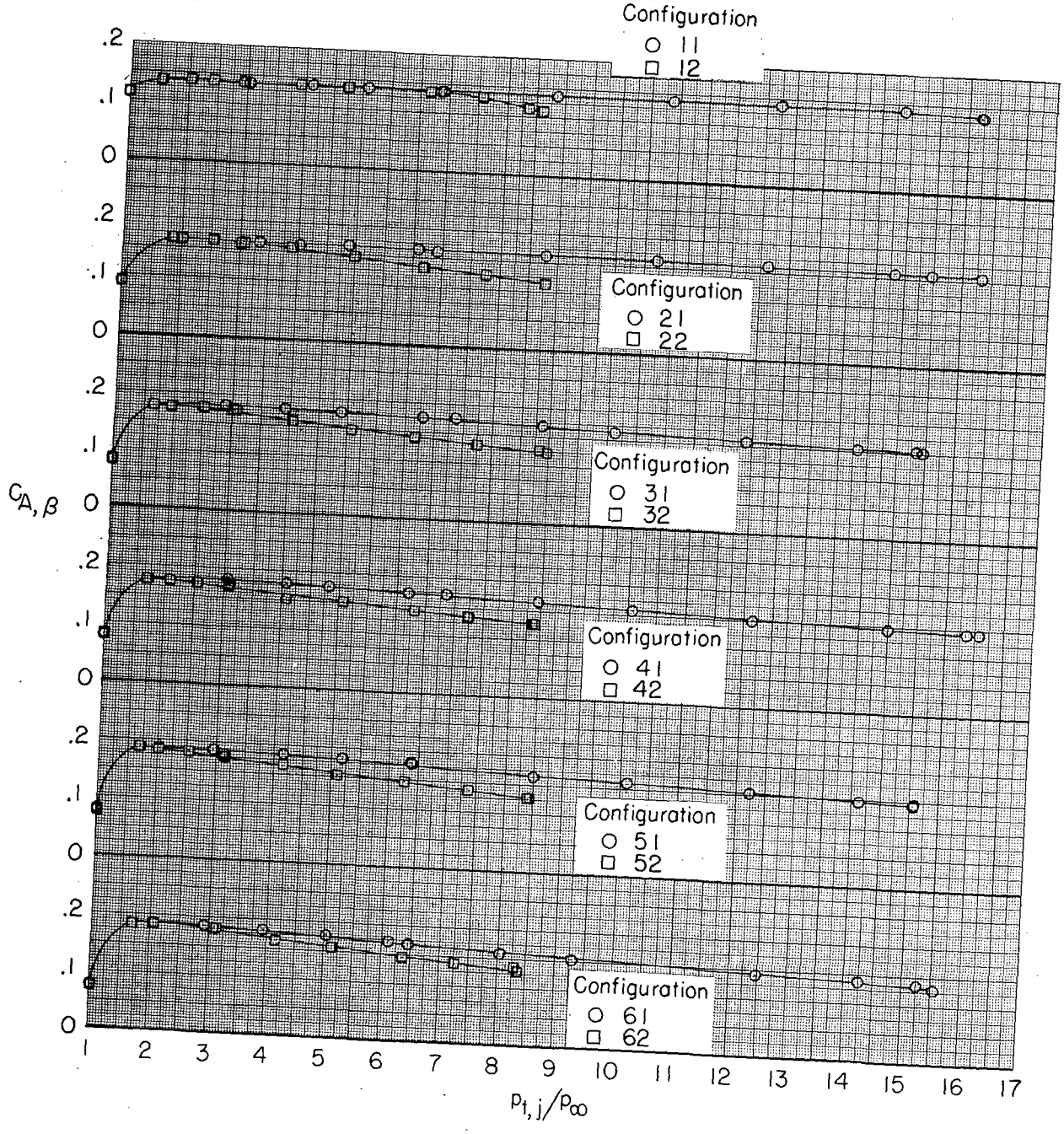

(g) M = 1.20.

Figure 7.- Continued.

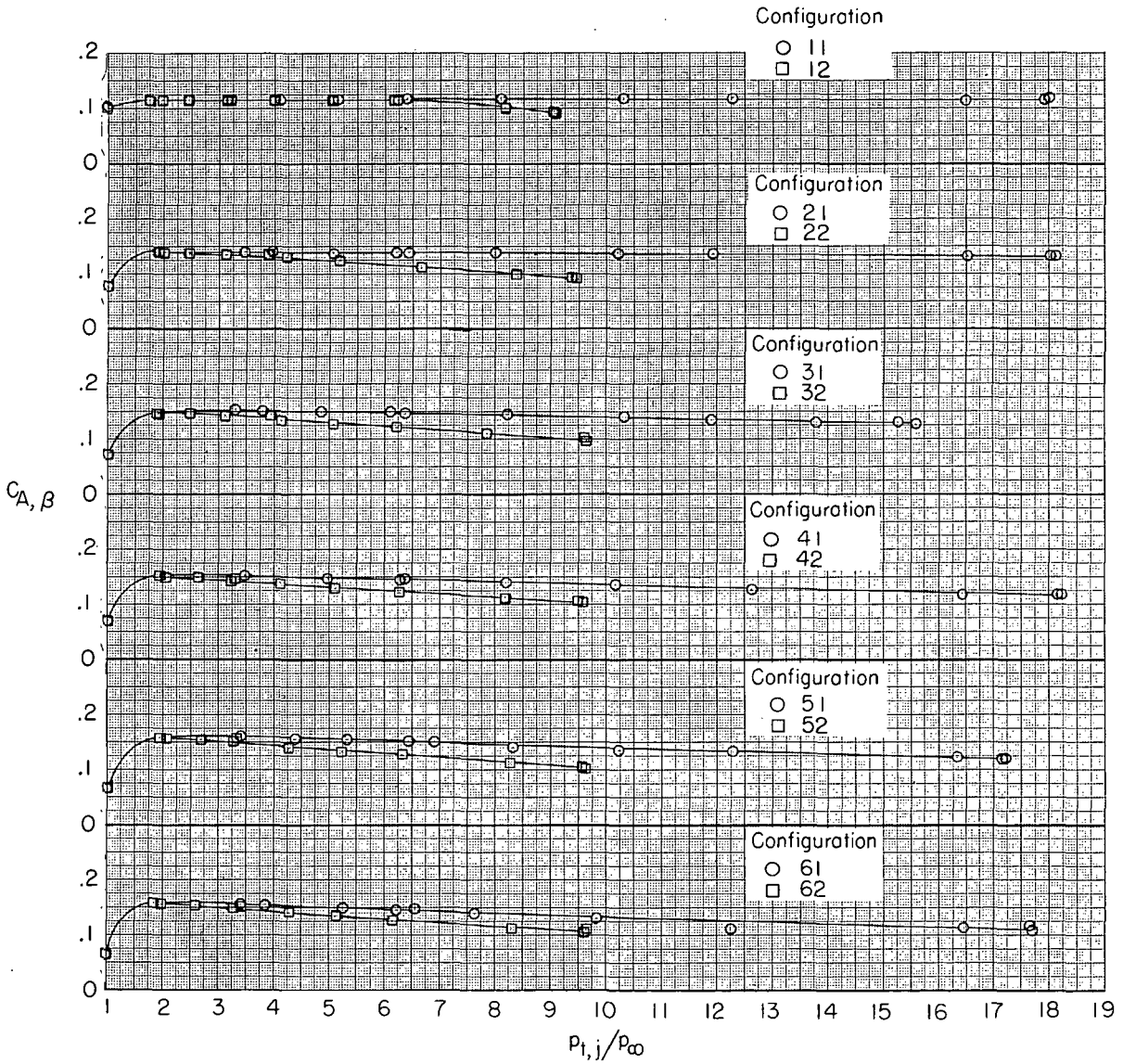

(h) M = 1.30.

Figure 7.- Continued.

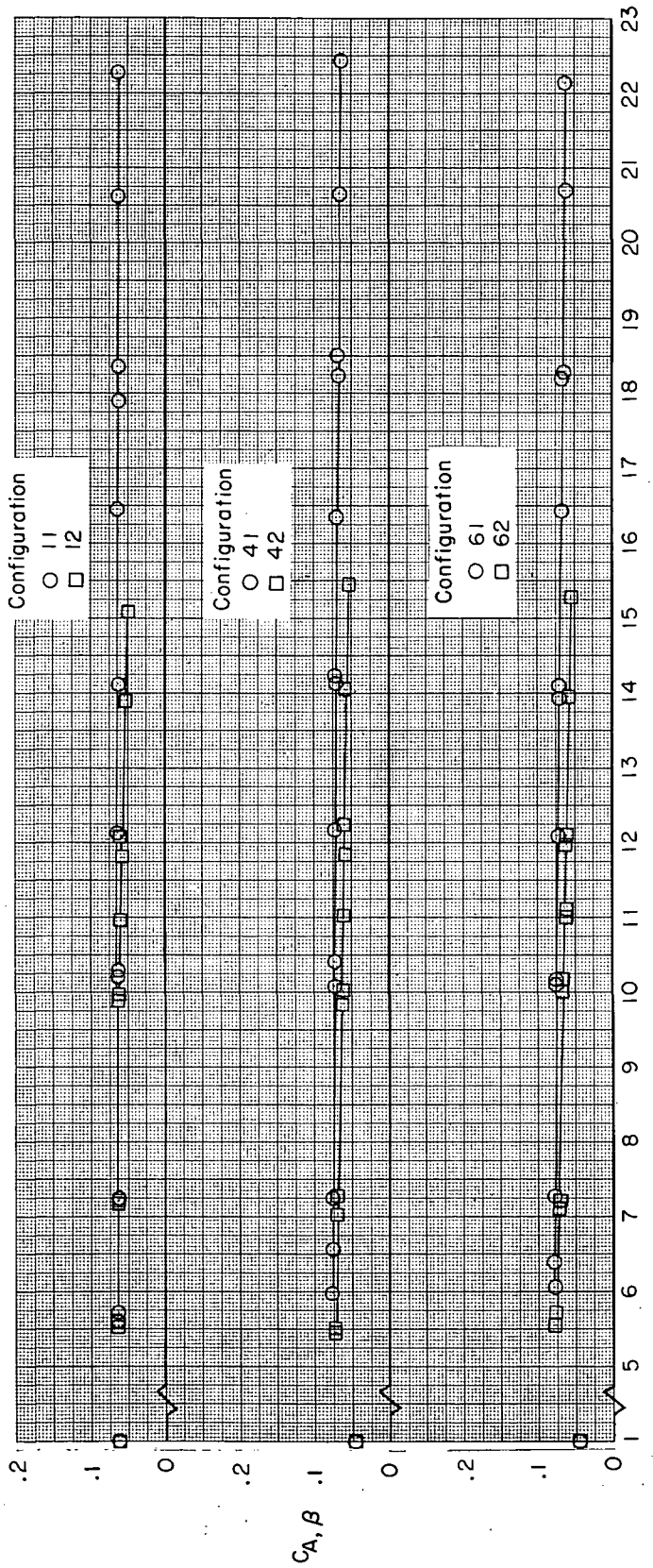

(i) M = 1.82.

Figure 7.- Concluded.

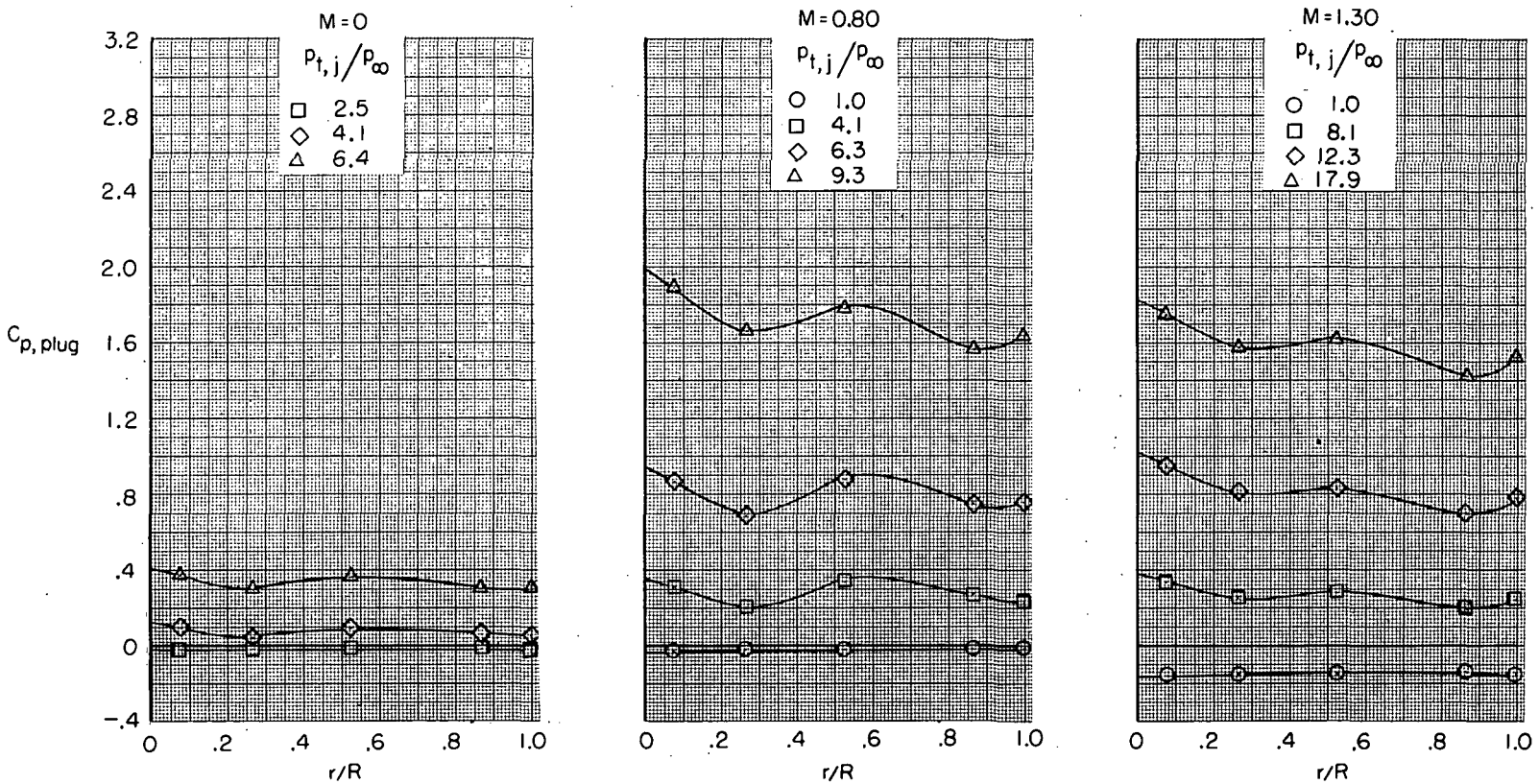

(a) Configuration 11.

Figure 8.- Typical pressure distributions on semitoroidal plug for various jet total-pressure ratios and Mach numbers.

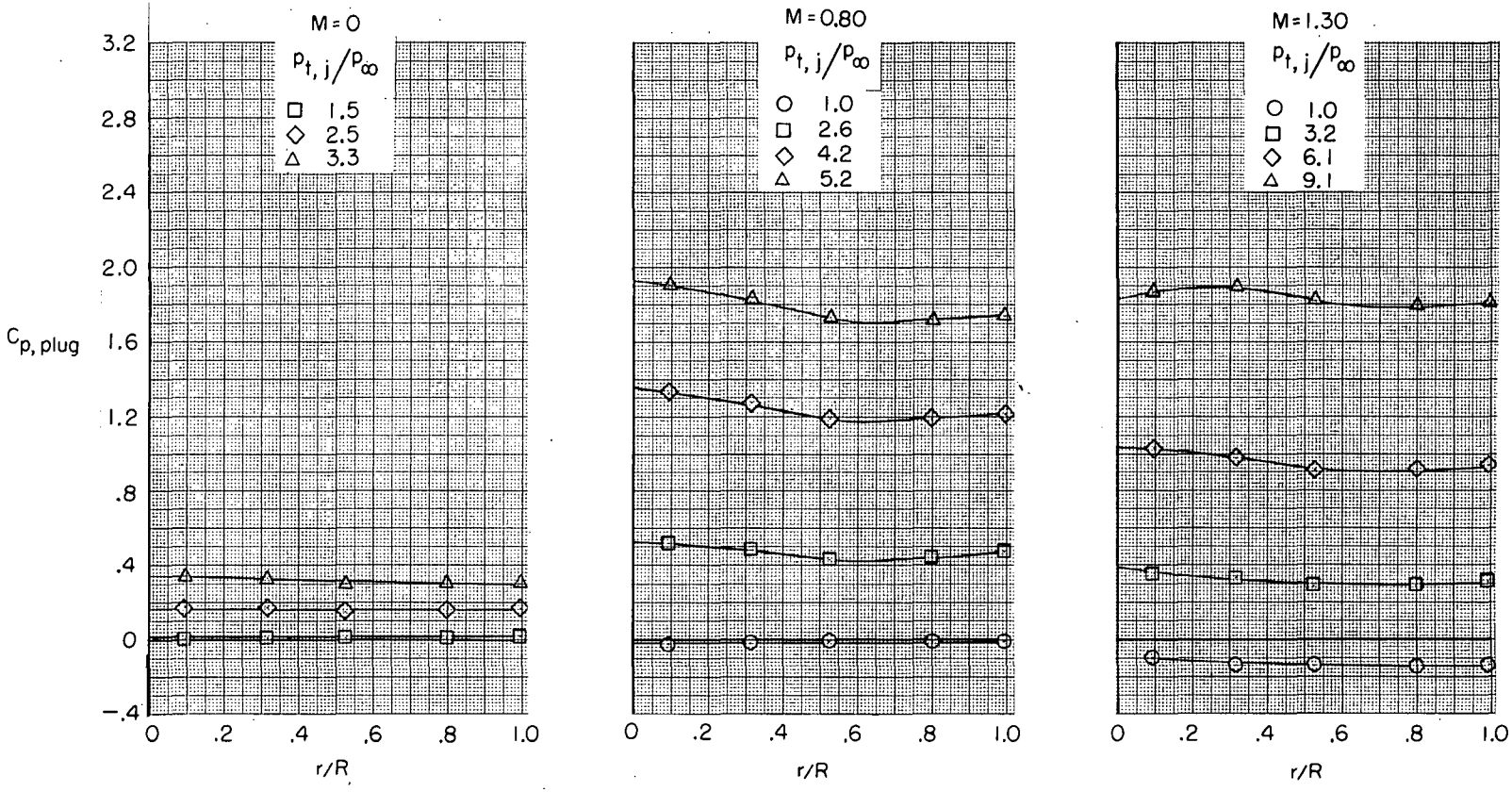

(b) Configuration 12.

Figure 8.- Continued.

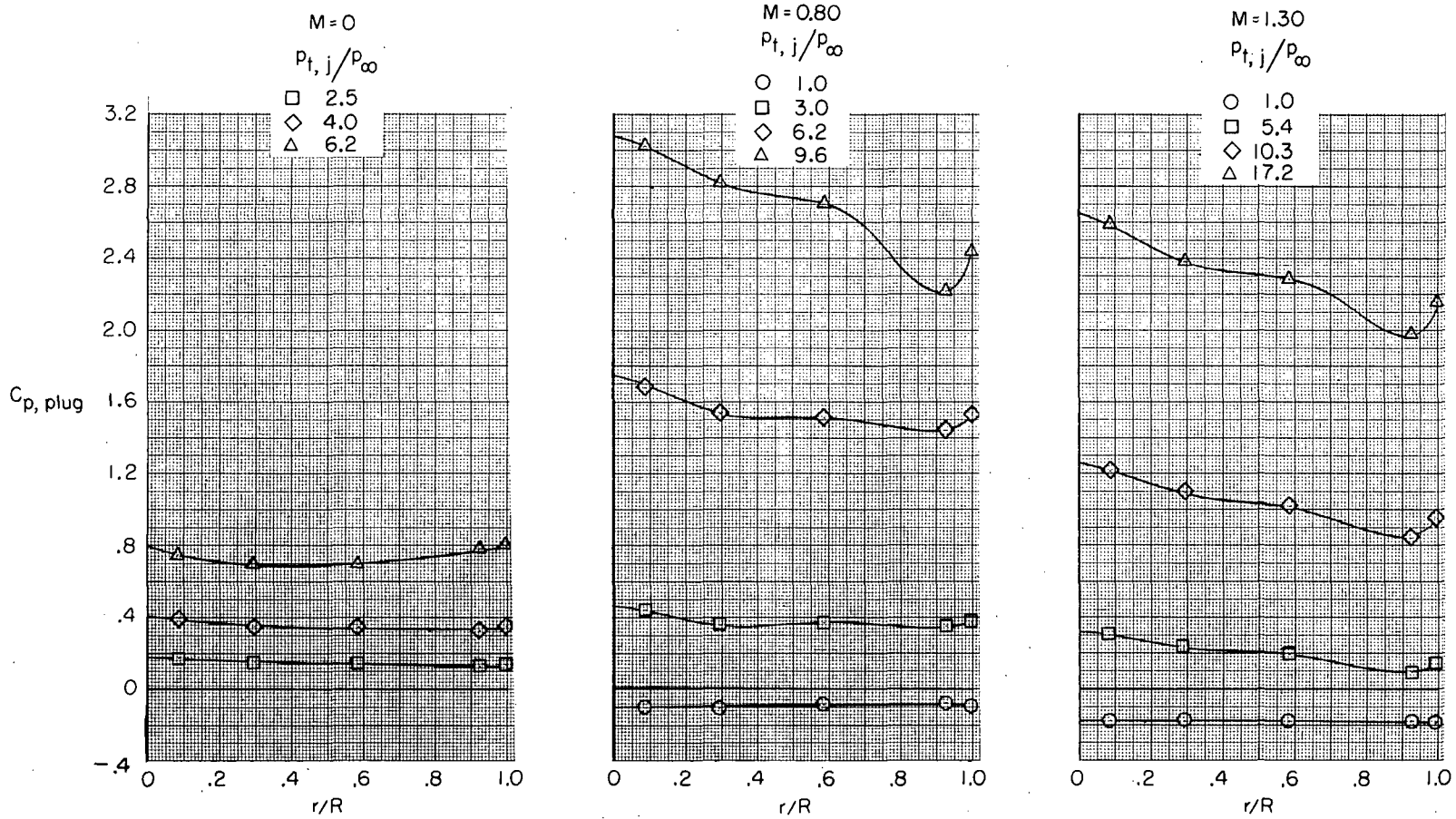

(c) Configuration 51.

Figure 8.- Continued.

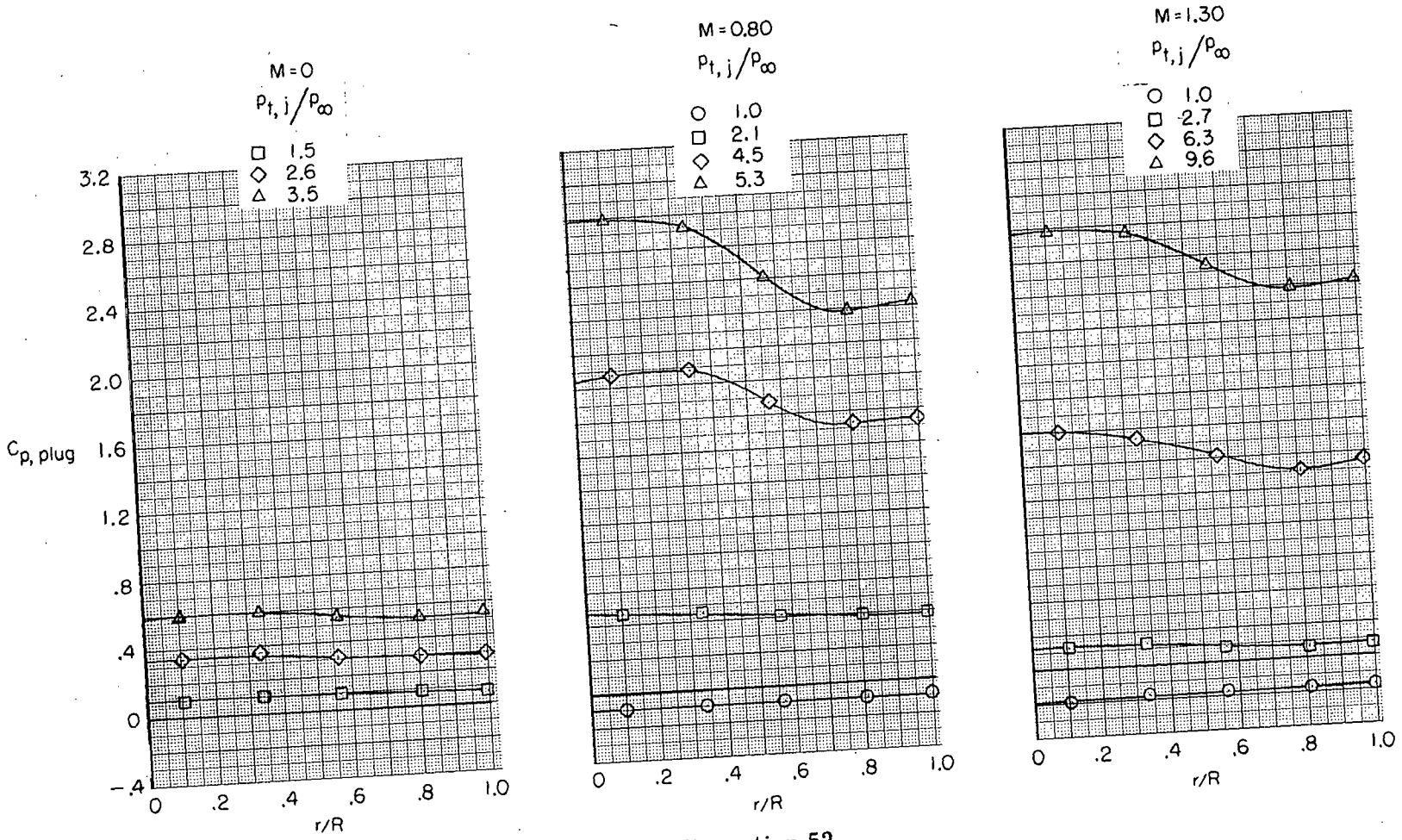

(d) Configuration 52.

Figure 8.- Concluded.

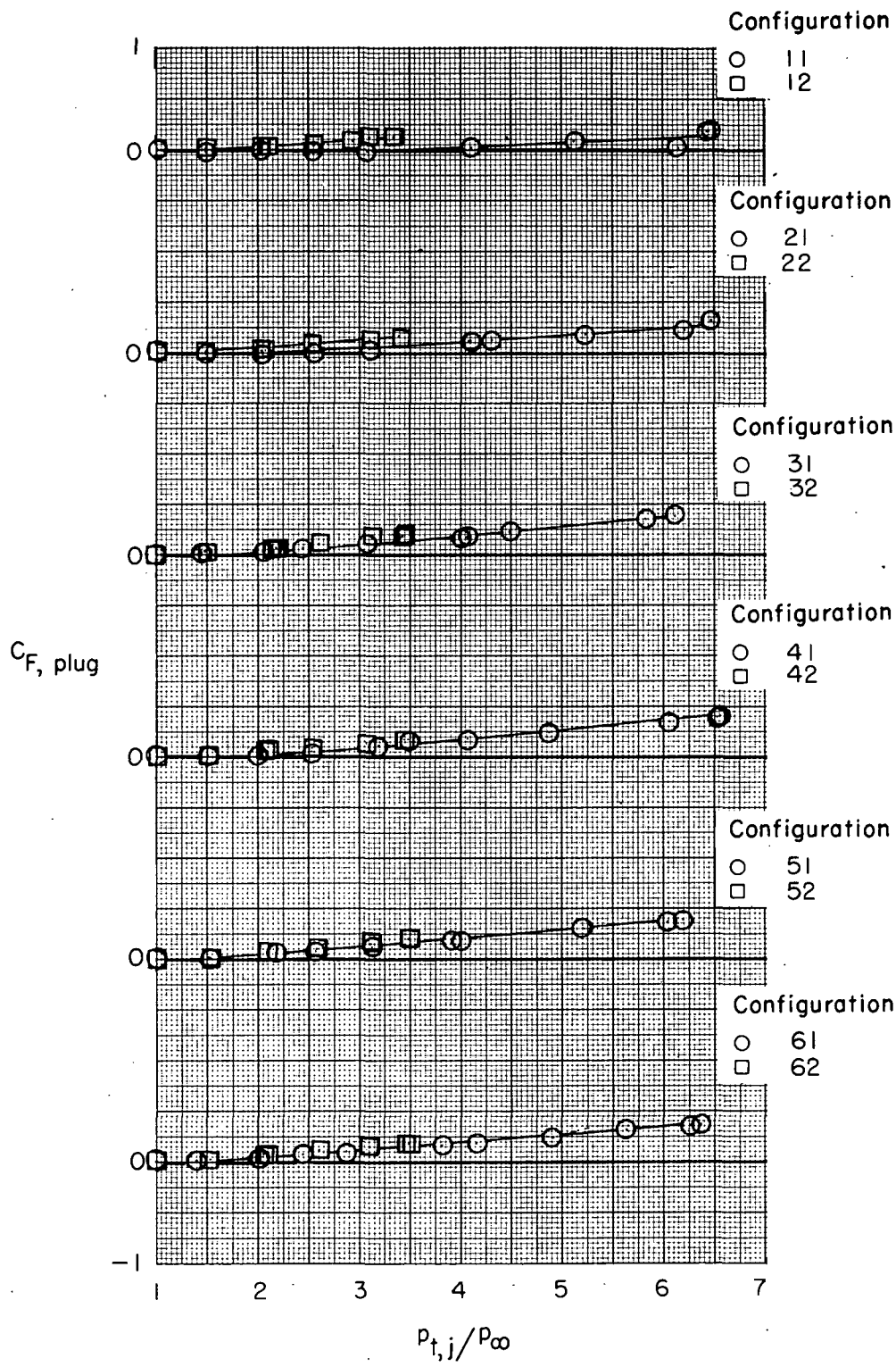

(a) M = 0.

Figure 9.- Variation of plug thrust with jet total-pressure ratio for various configurations.

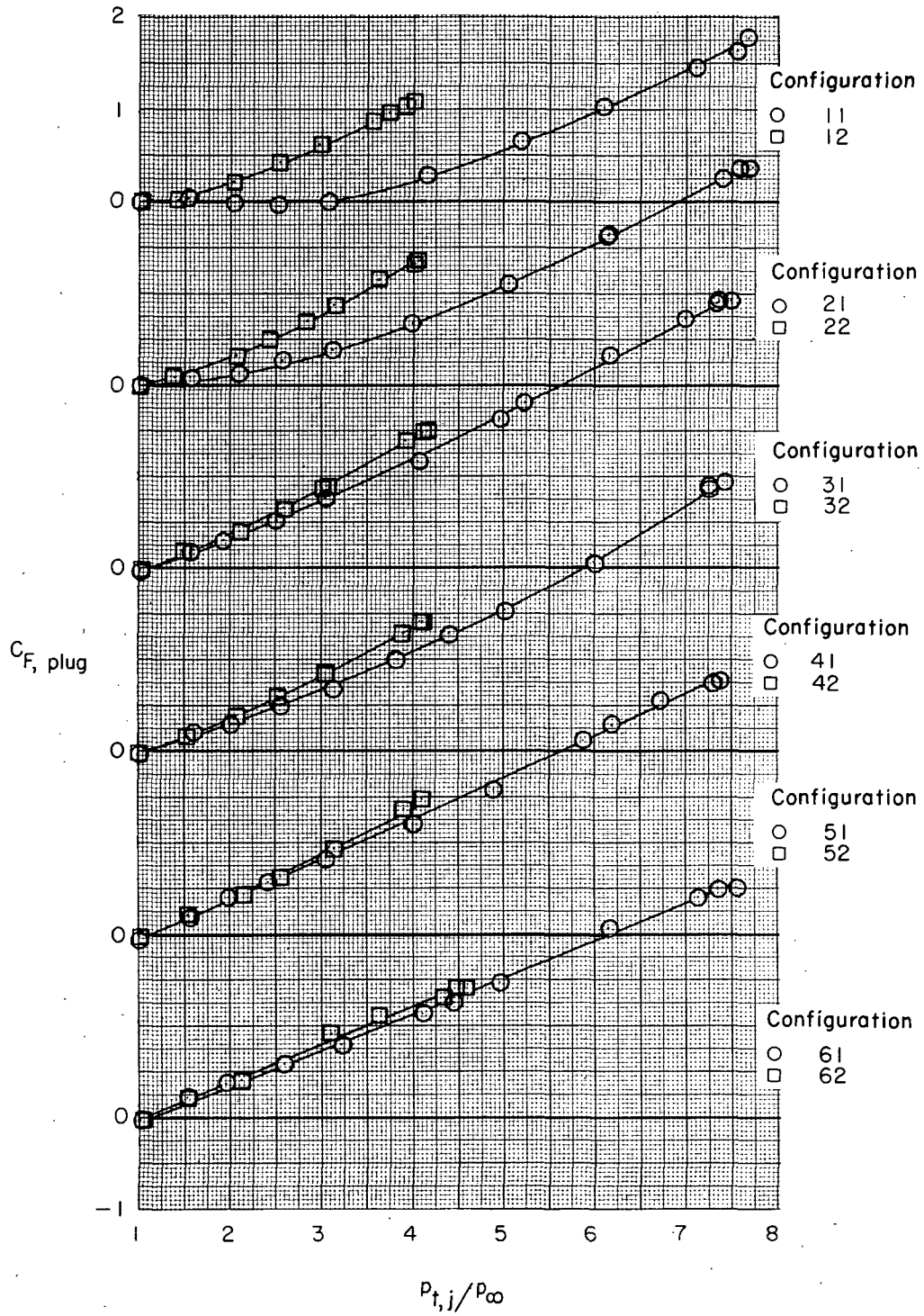

(b) M = 0.50.

Figure 9.- Continued.

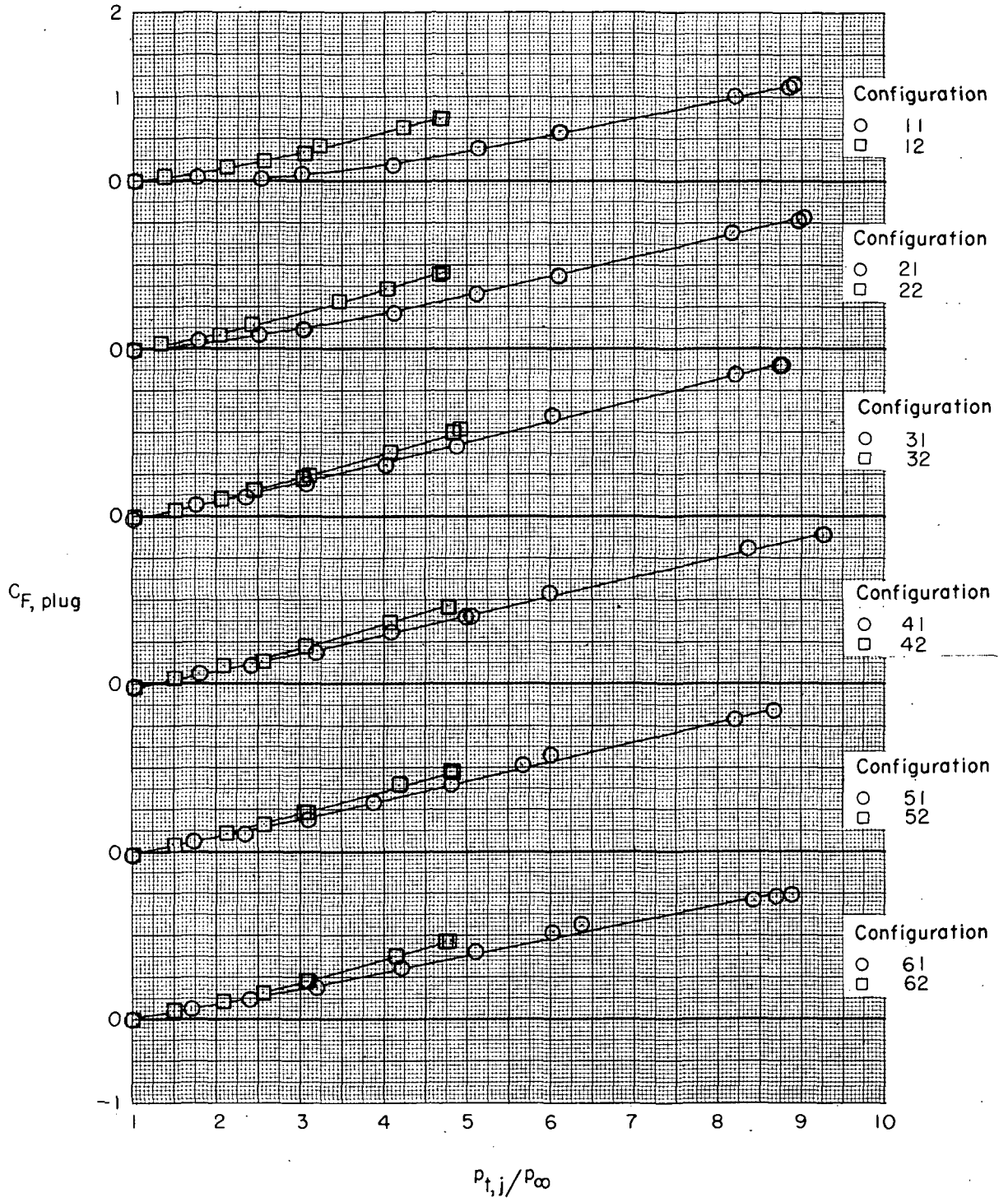

(c) M = 0.70.

Figure 9.- Continued.

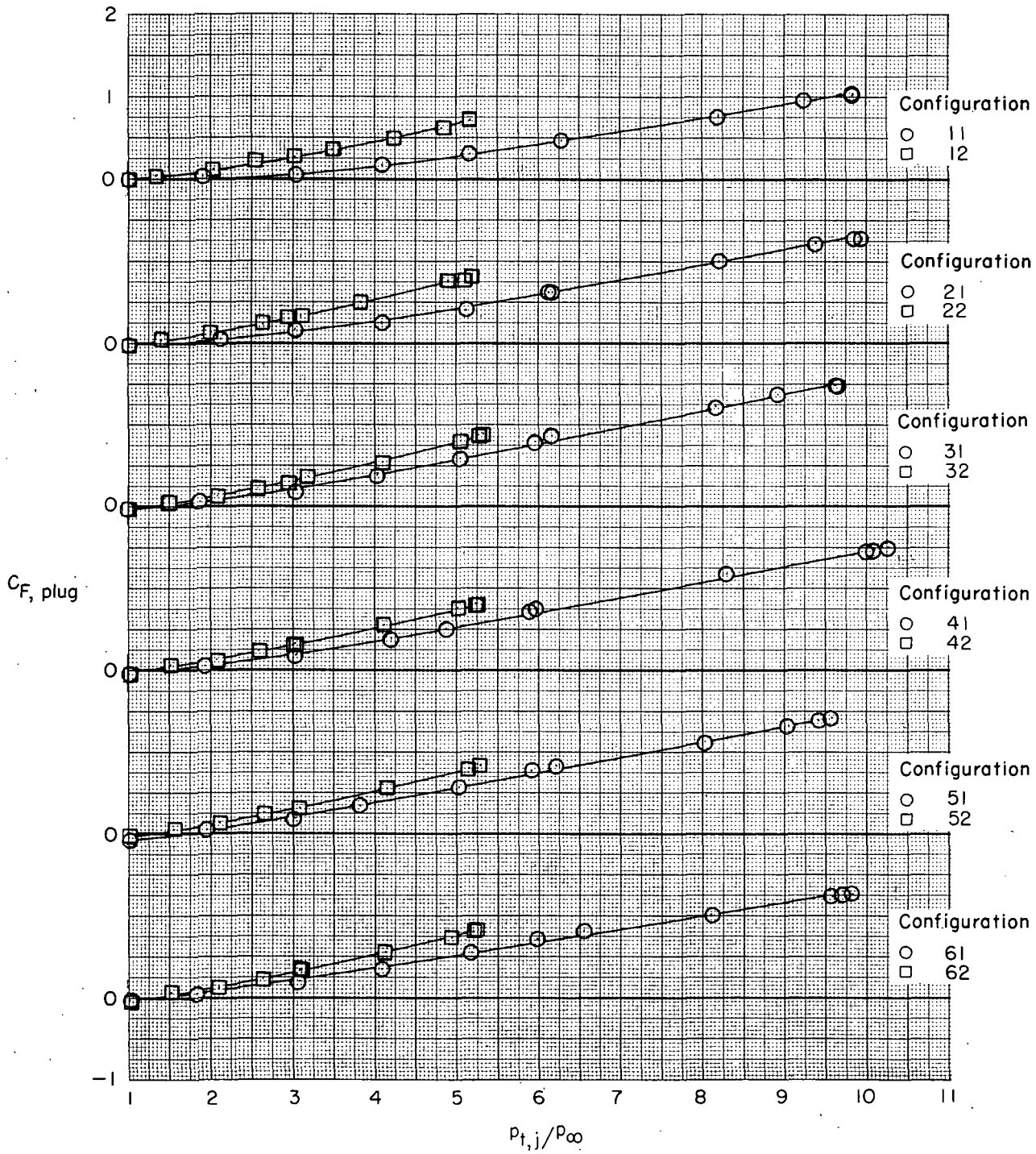

(d) M = 0.80.

Figure 9.- Continued.

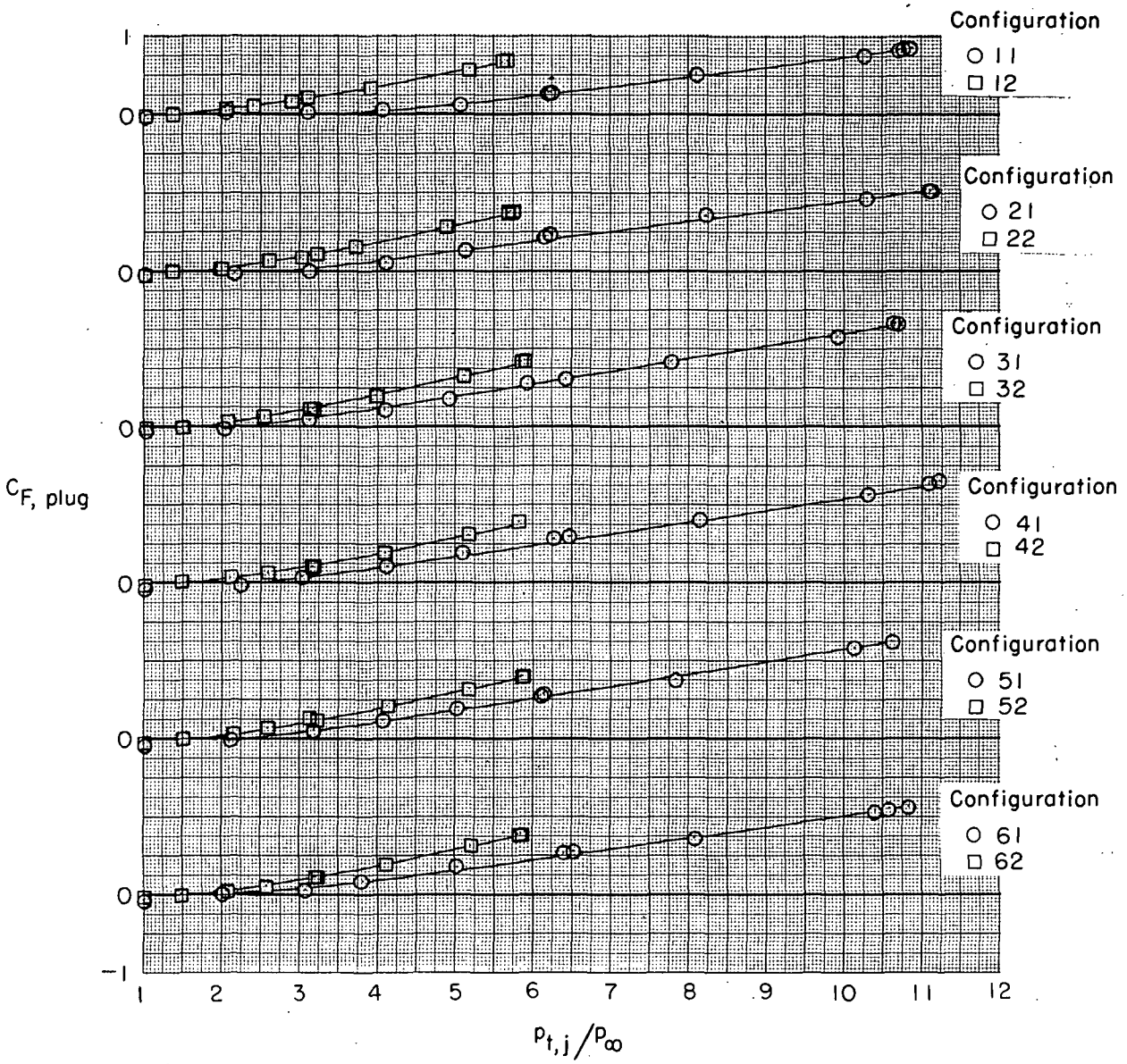

(e) M = 0.90.

Figure 9.- Continued.

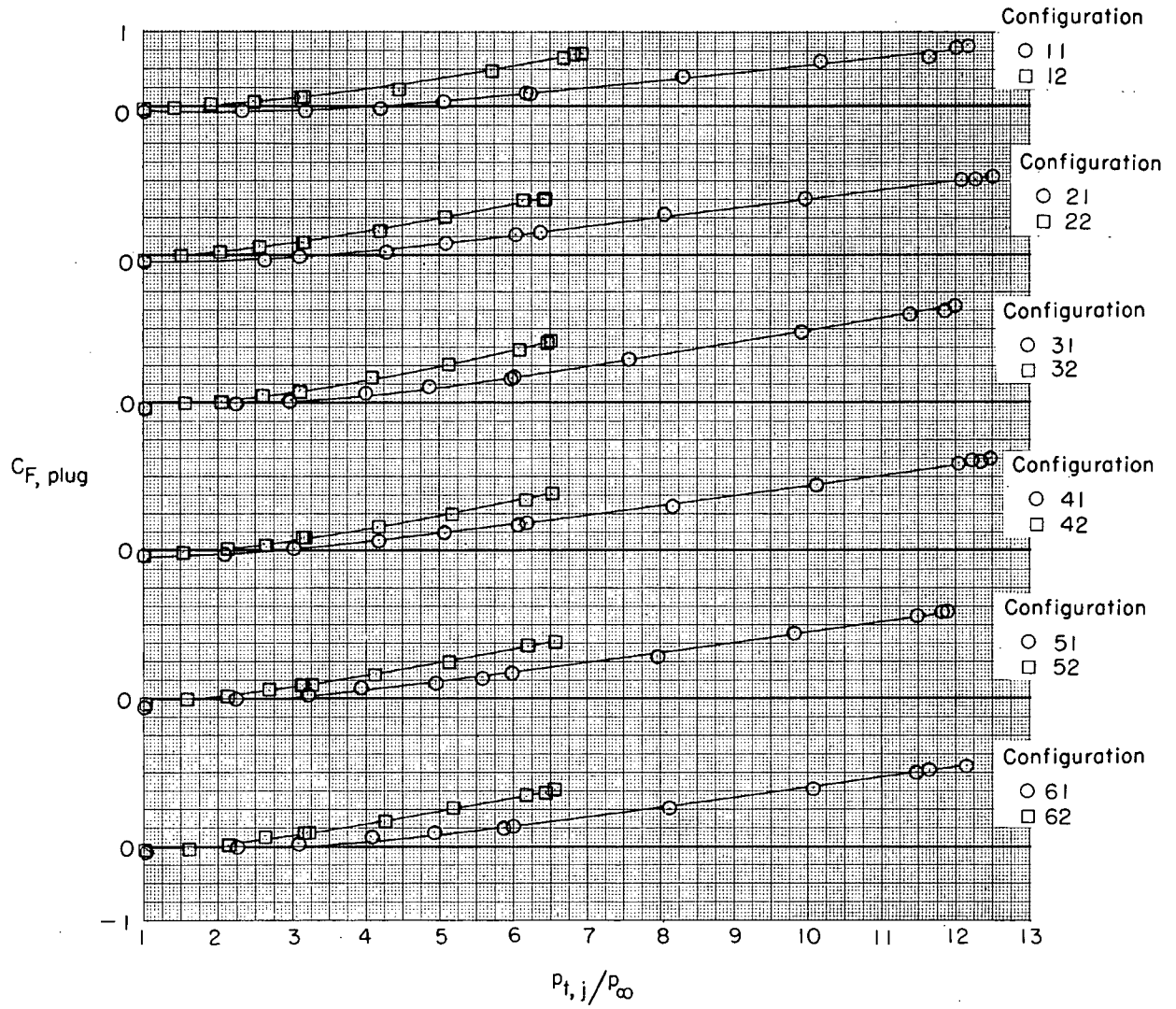

(f) M = 1.00.

Figure 9.- Continued.

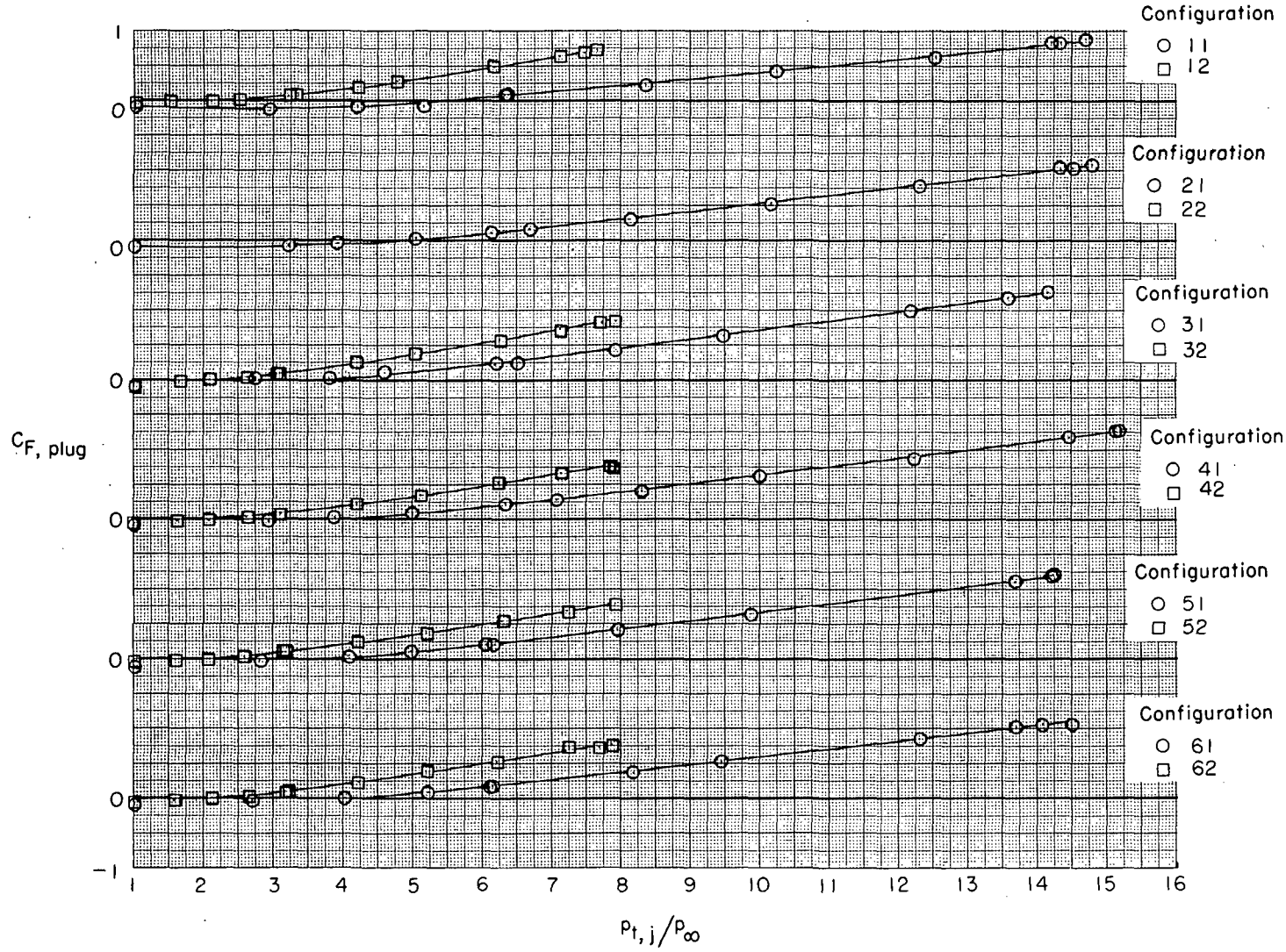

(g) M = 1.15.

Figure 9.- Continued.

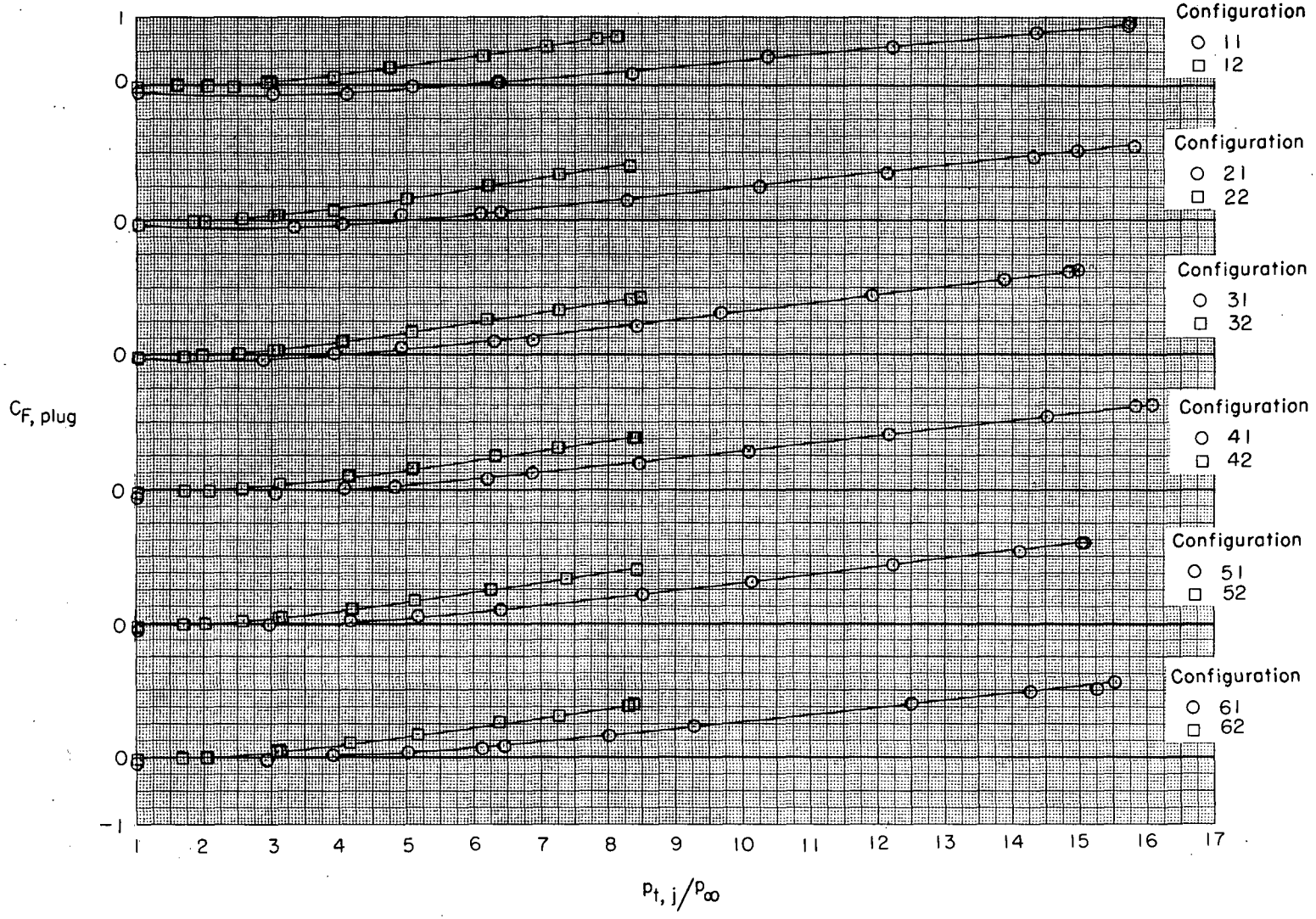

(h) M = 1.20.

Figure 9.- Continued.

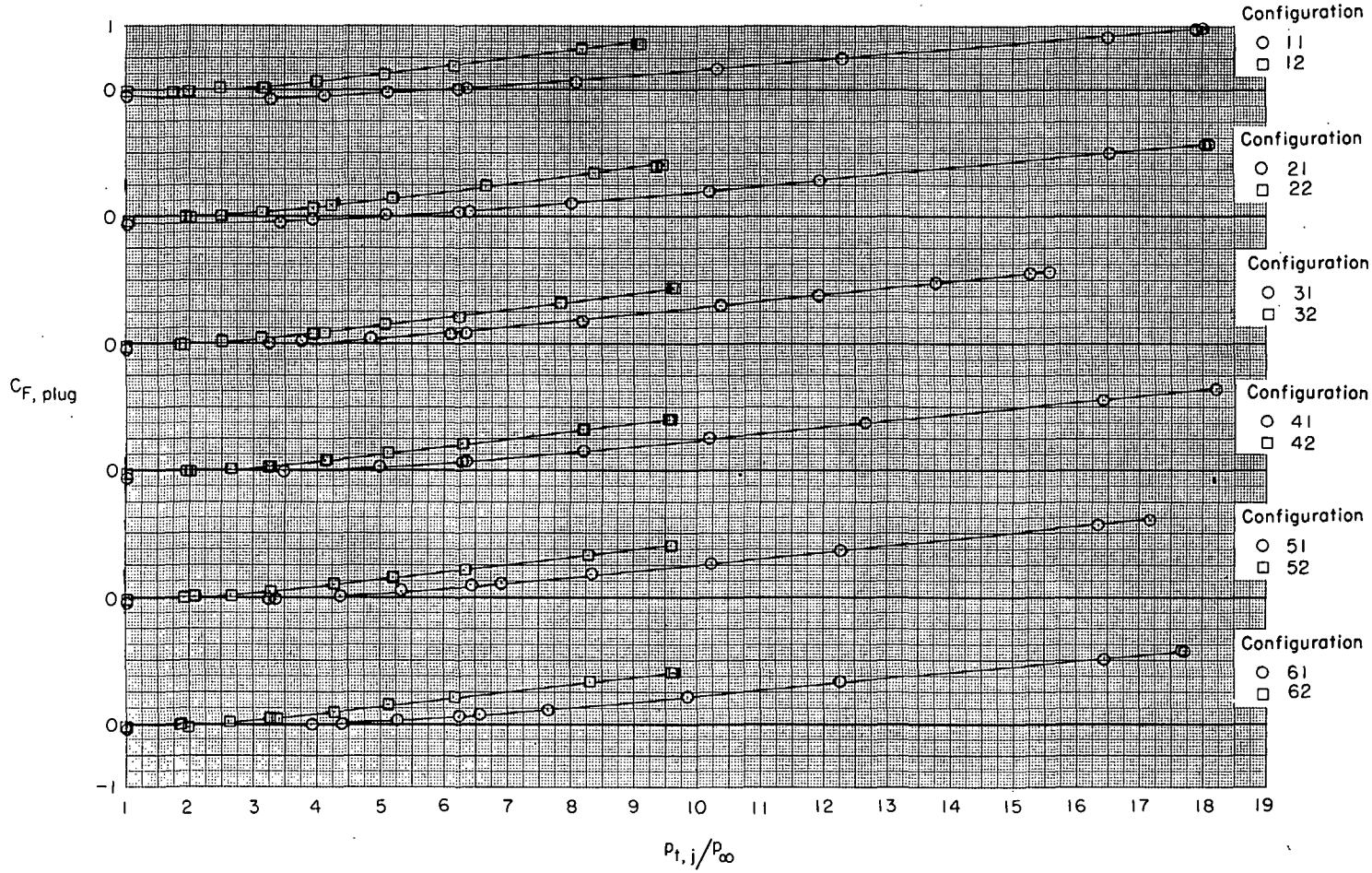

(i) M = 1.30.

Figure 9.- Continued.

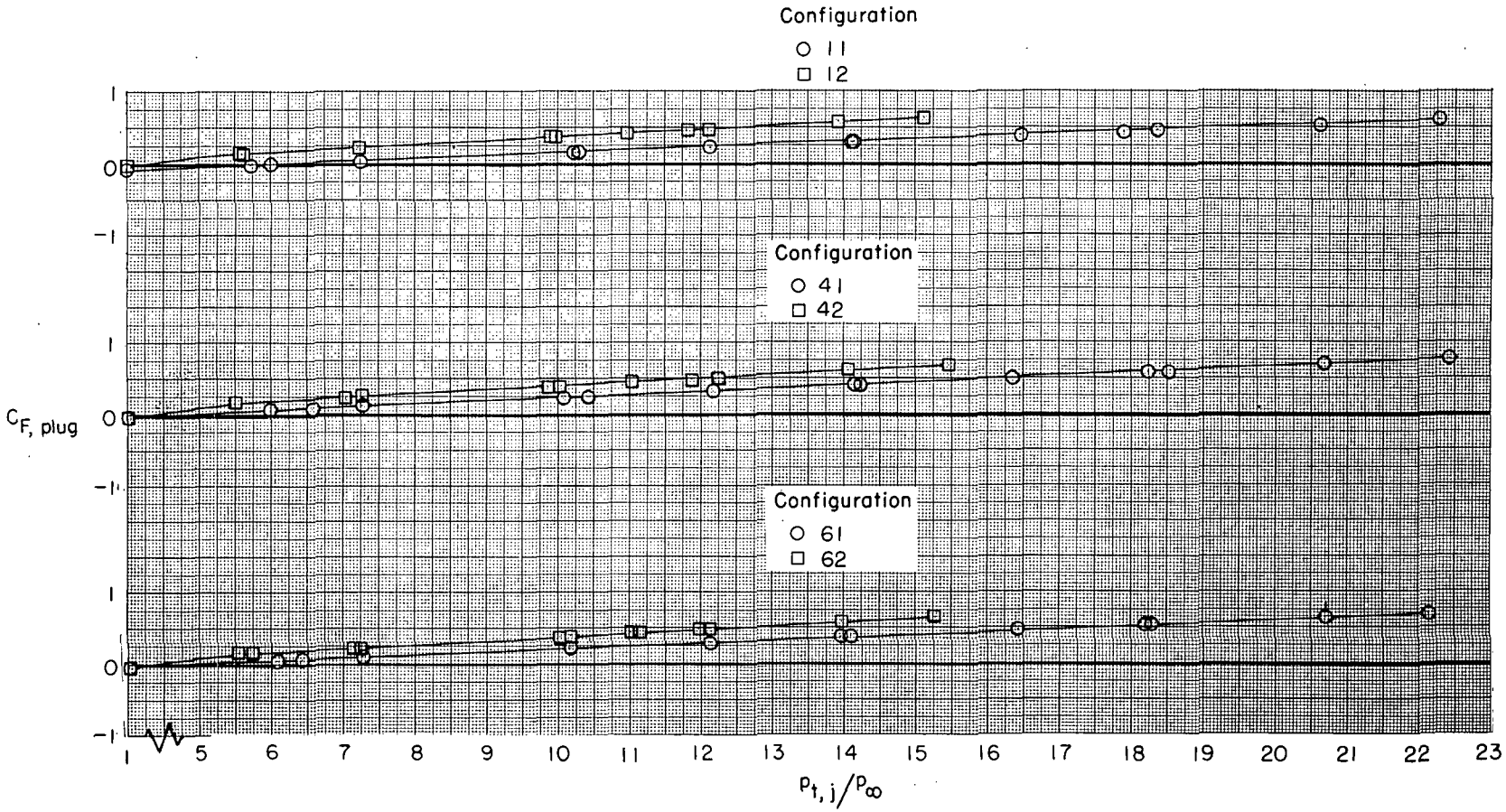

(j) M = 1.82.

Figure 9.- Concluded.

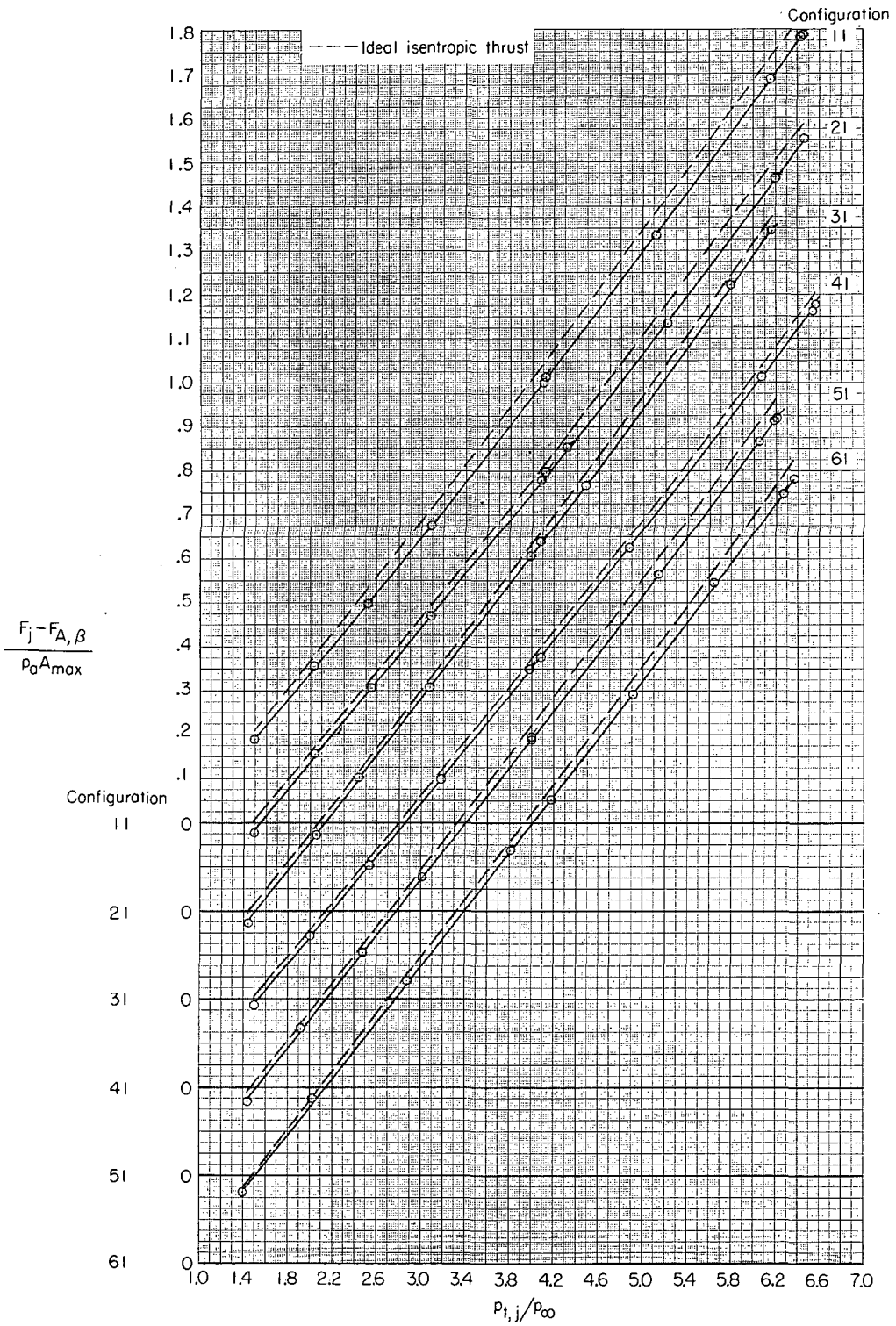

(a) Configurations 11, 21, 31, 41, 51, and 61.

Figure 10.- Variation of static thrust coefficient with jet total-pressure ratio. Flagged symbols denote increasing pressure ratio.

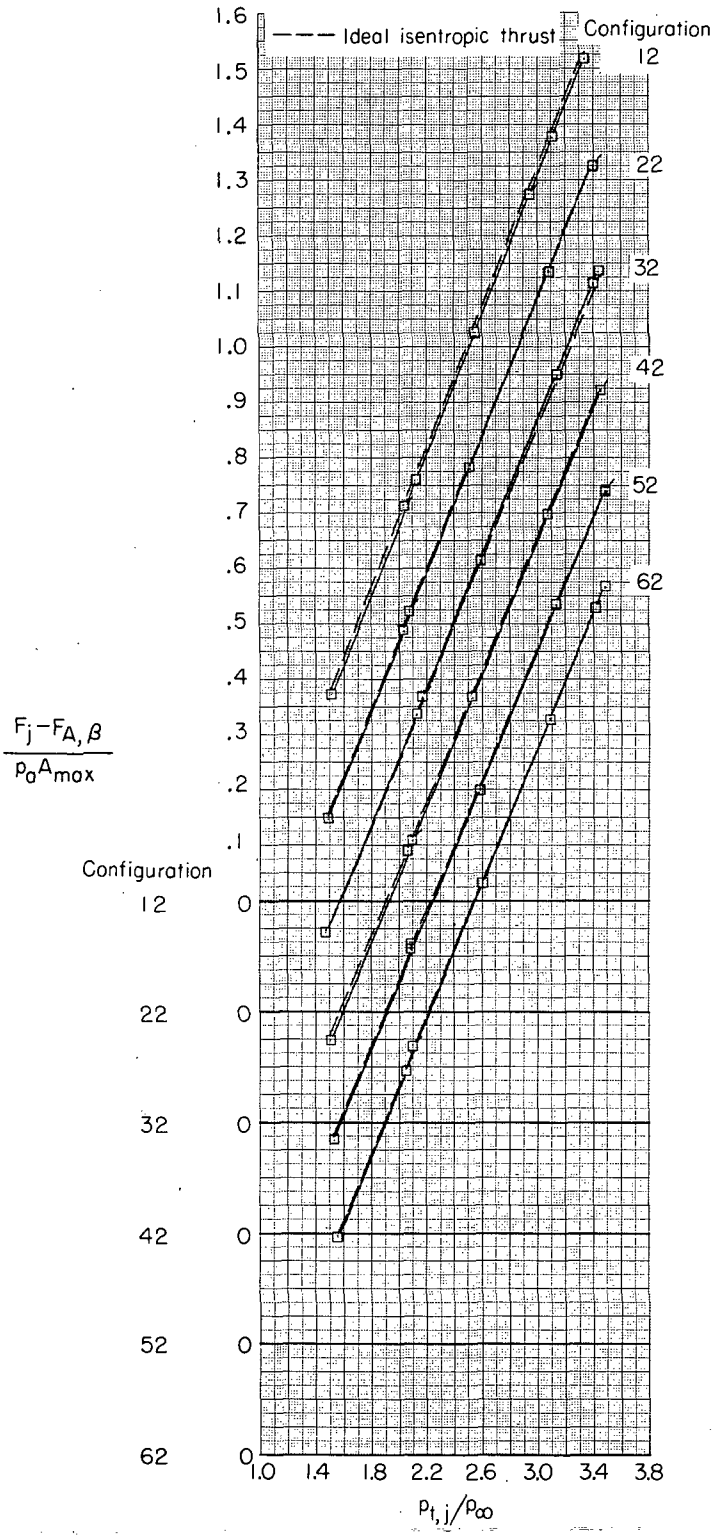

(b) Configurations 12, 22, 32, 42, 52, and 62.

Figure 10.- Concluded.

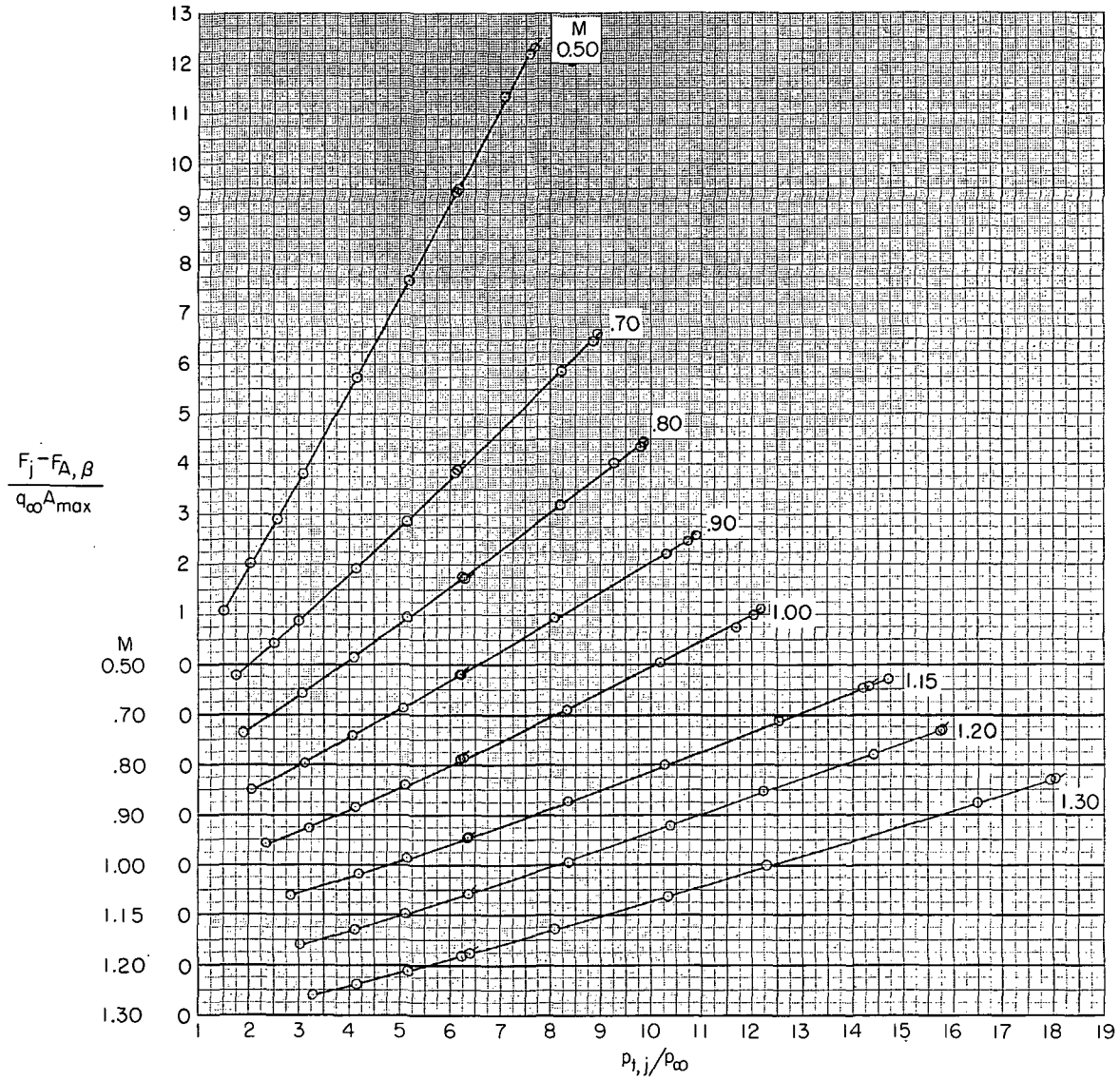

(a) Configuration 11.

Figure 11.- Variation of thrust-minus-boattail-drag coefficient with jet total-pressure ratio for various Mach numbers. Flagged symbols denote increasing pressure ratio.

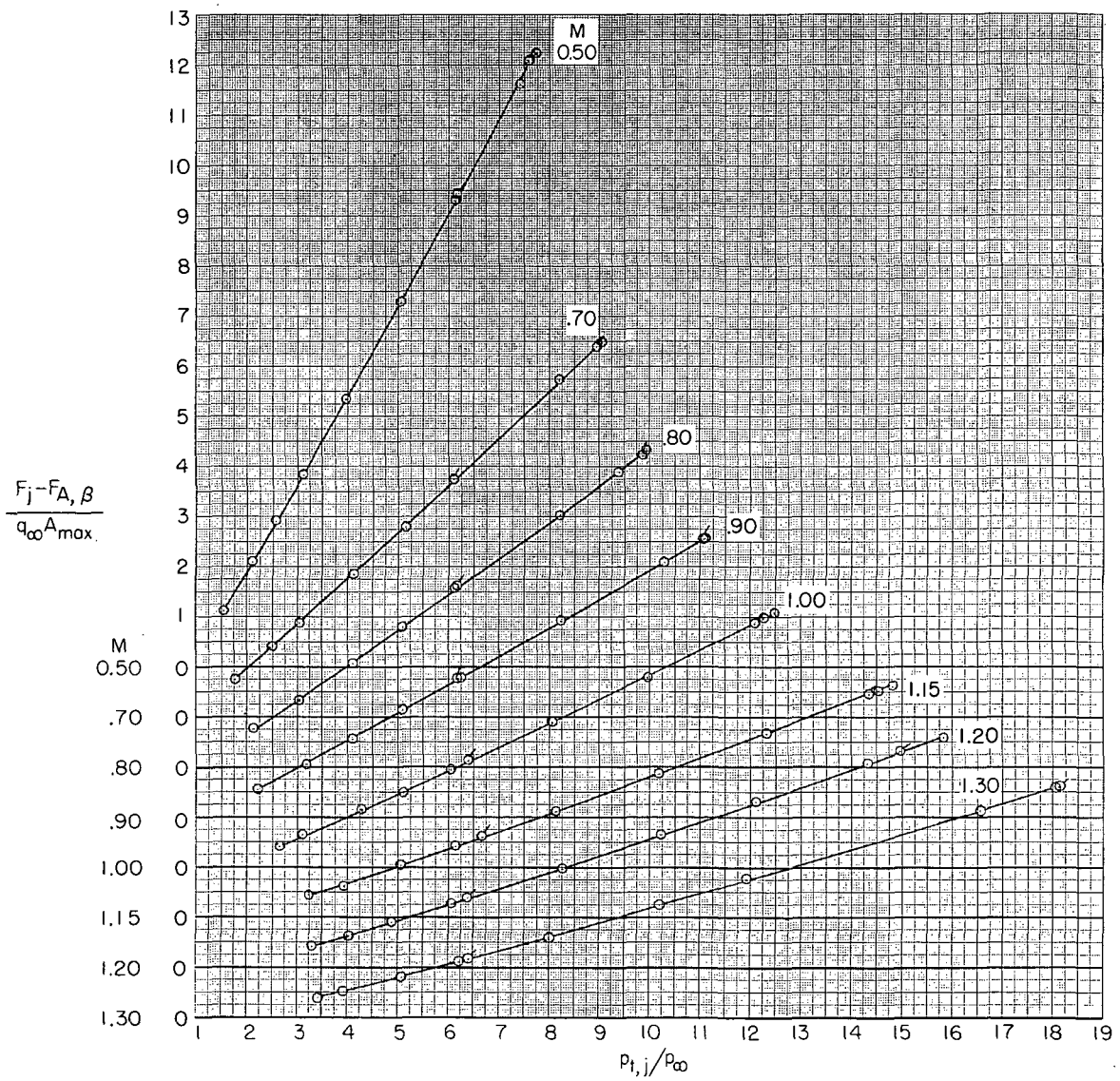

(b) Configuration 21.

Figure 11.- Continued.

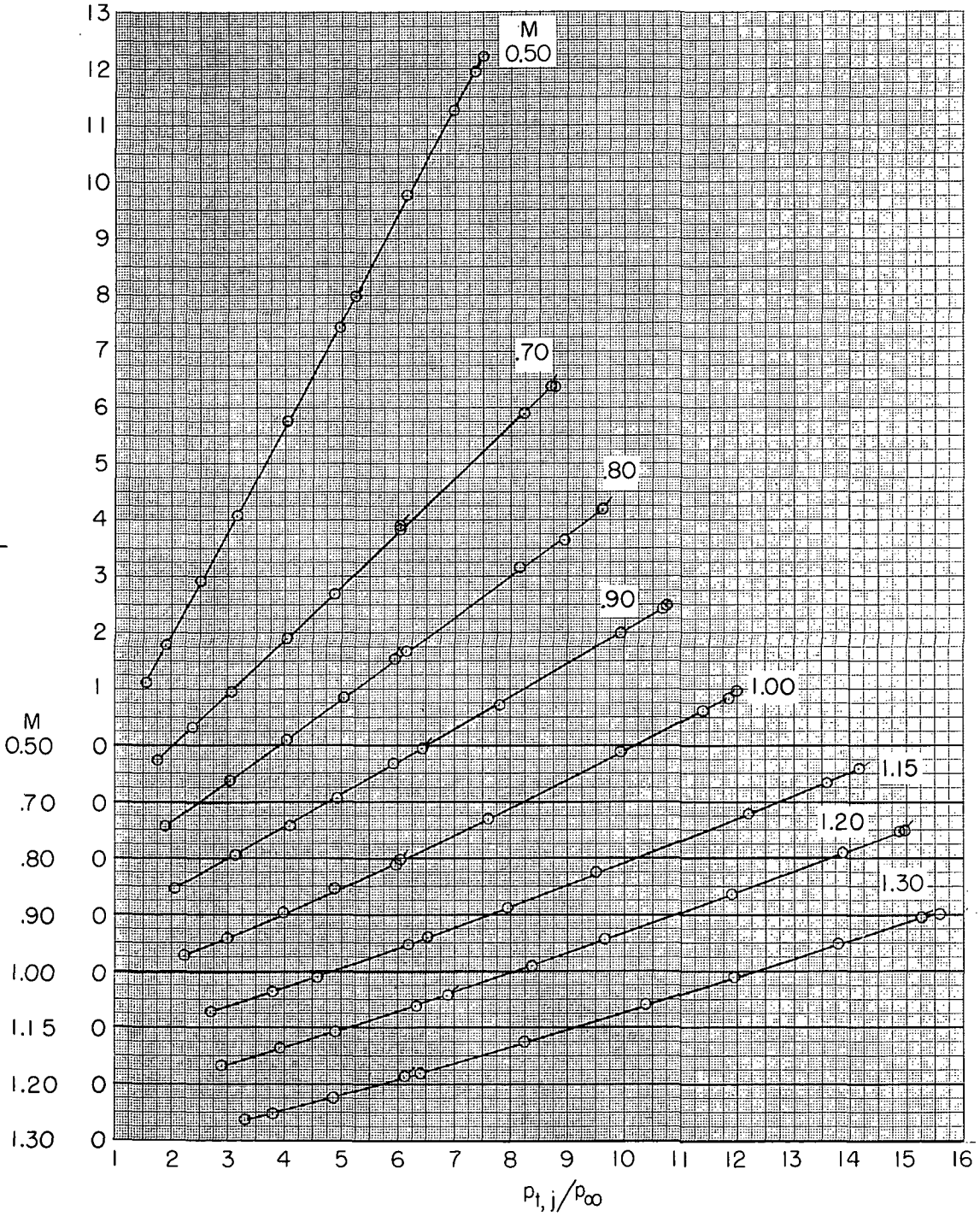

(c) Configuration 31.

Figure 11.- Continued.

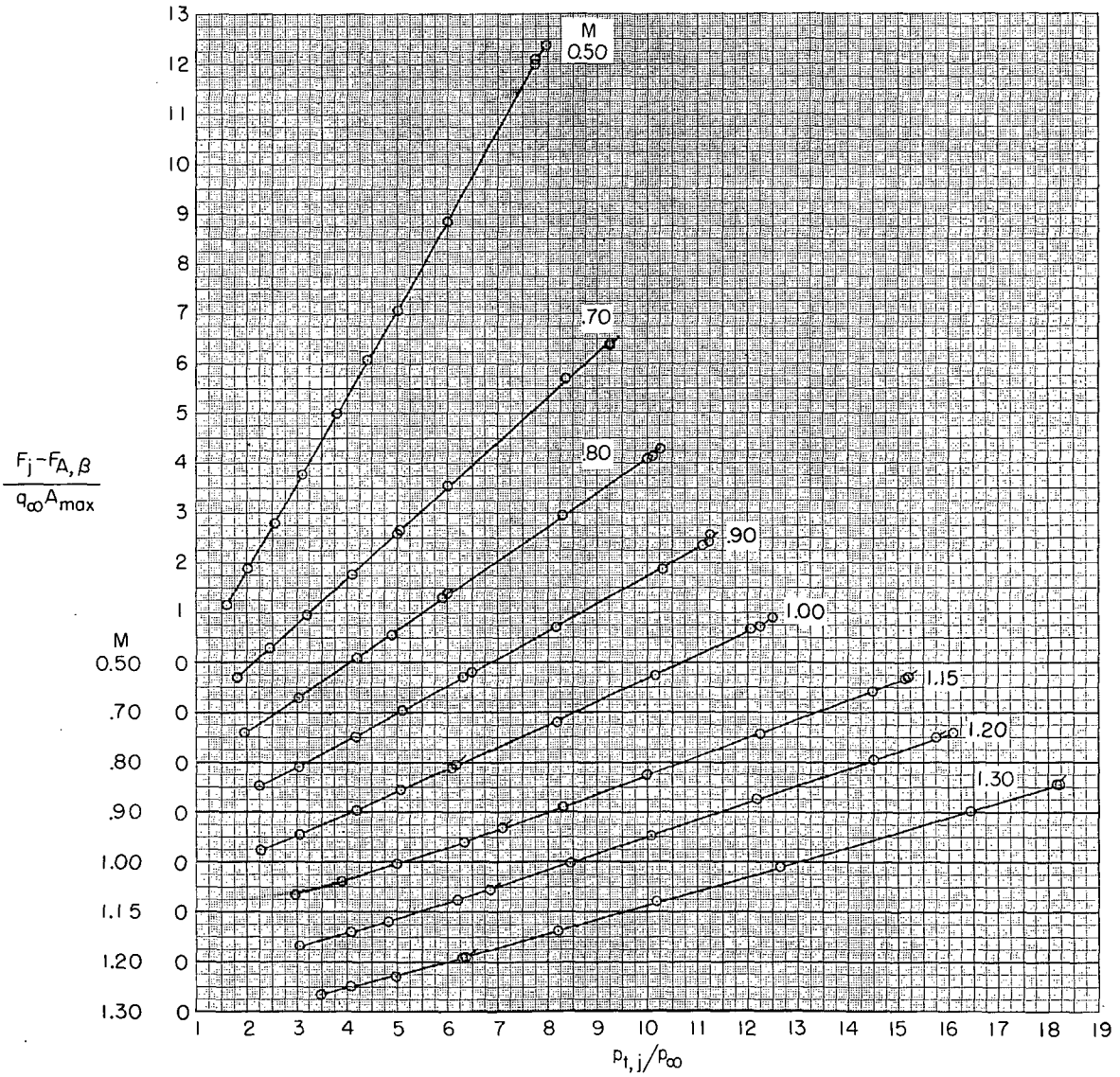

(d) Configuration 41.

Figure 11.- Continued.

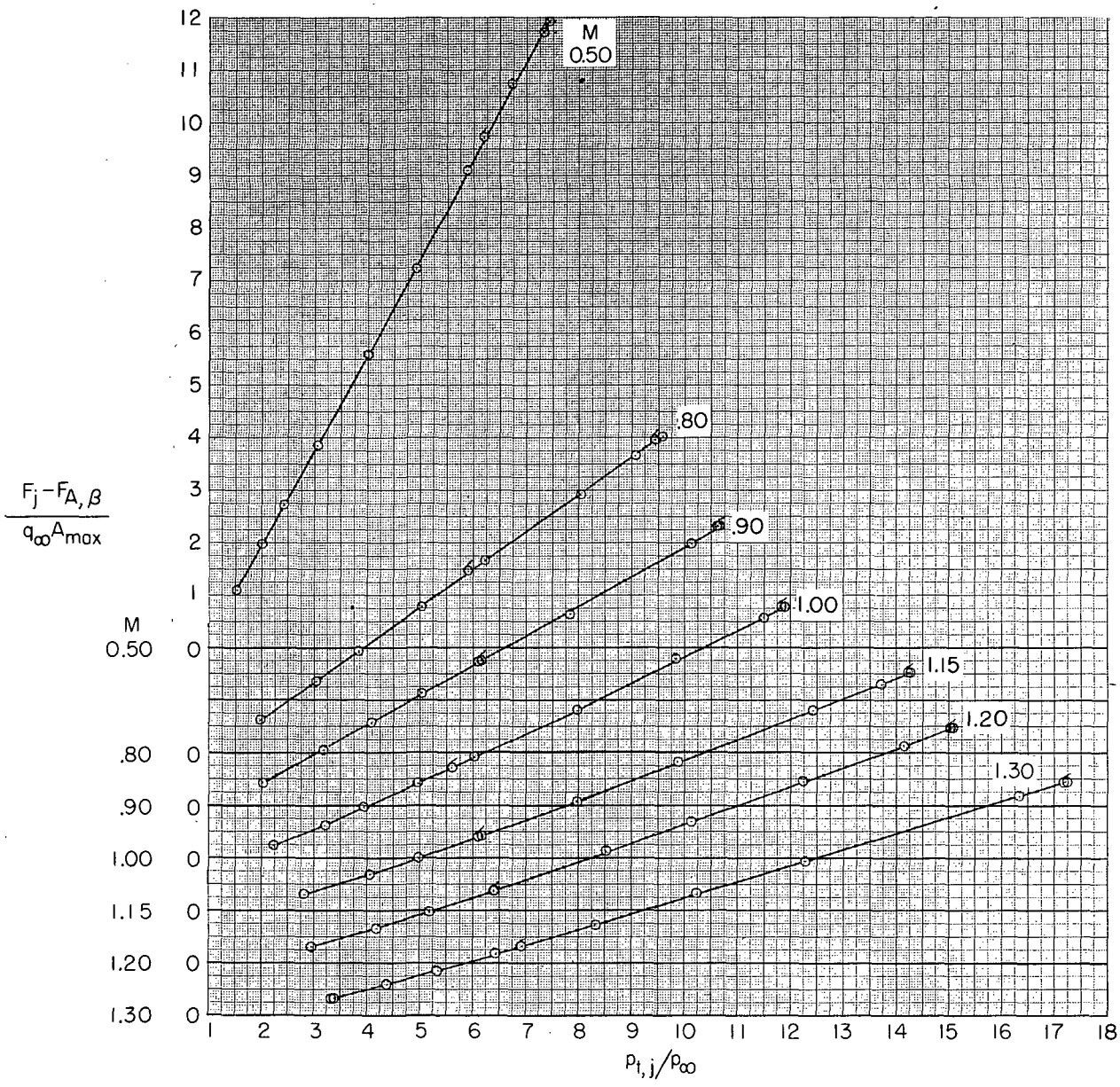

(e) Configuration 51.

Figure 11.- Continued.

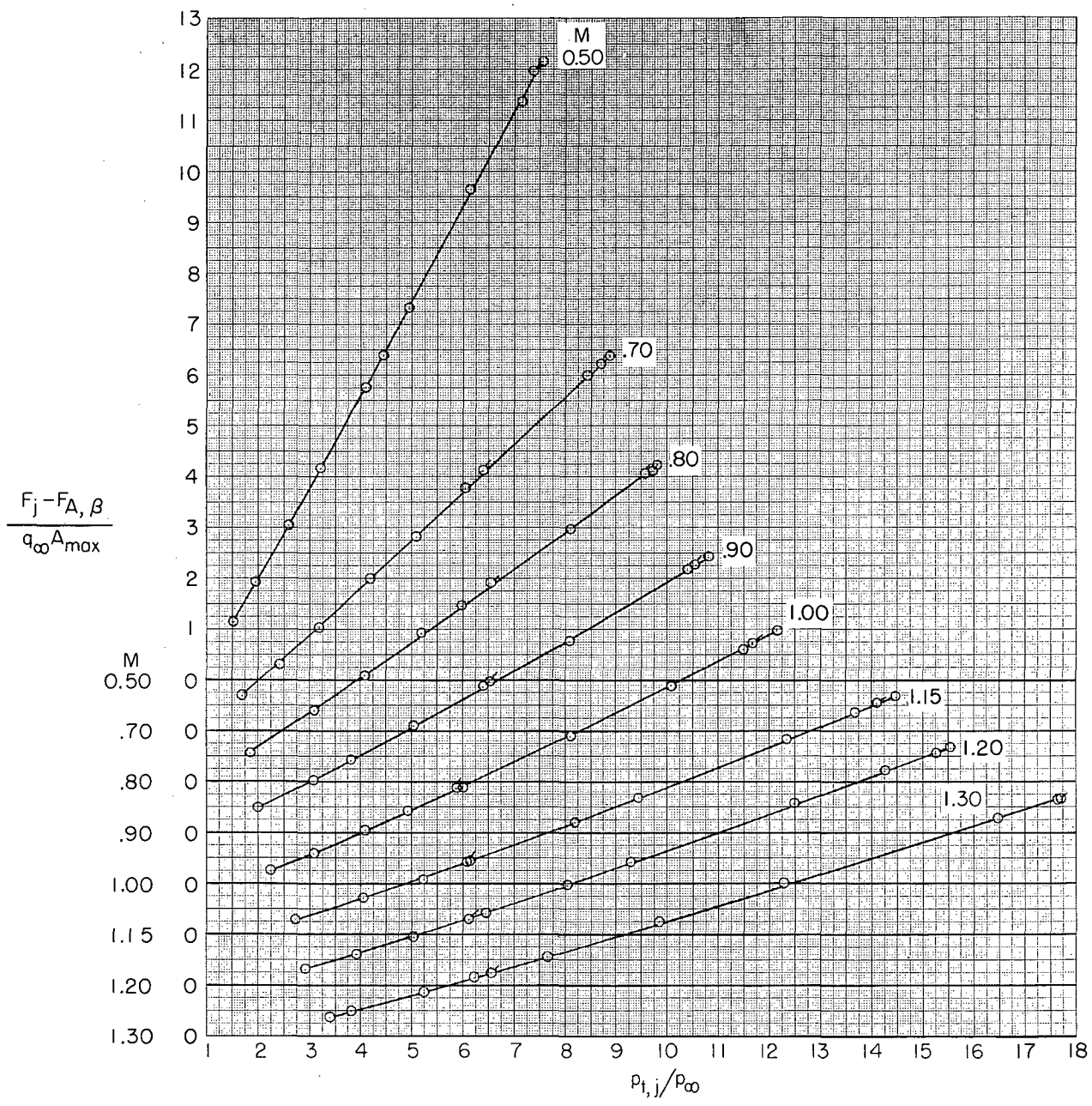

(f) Configuration 61.

Figure 11.- Continued.

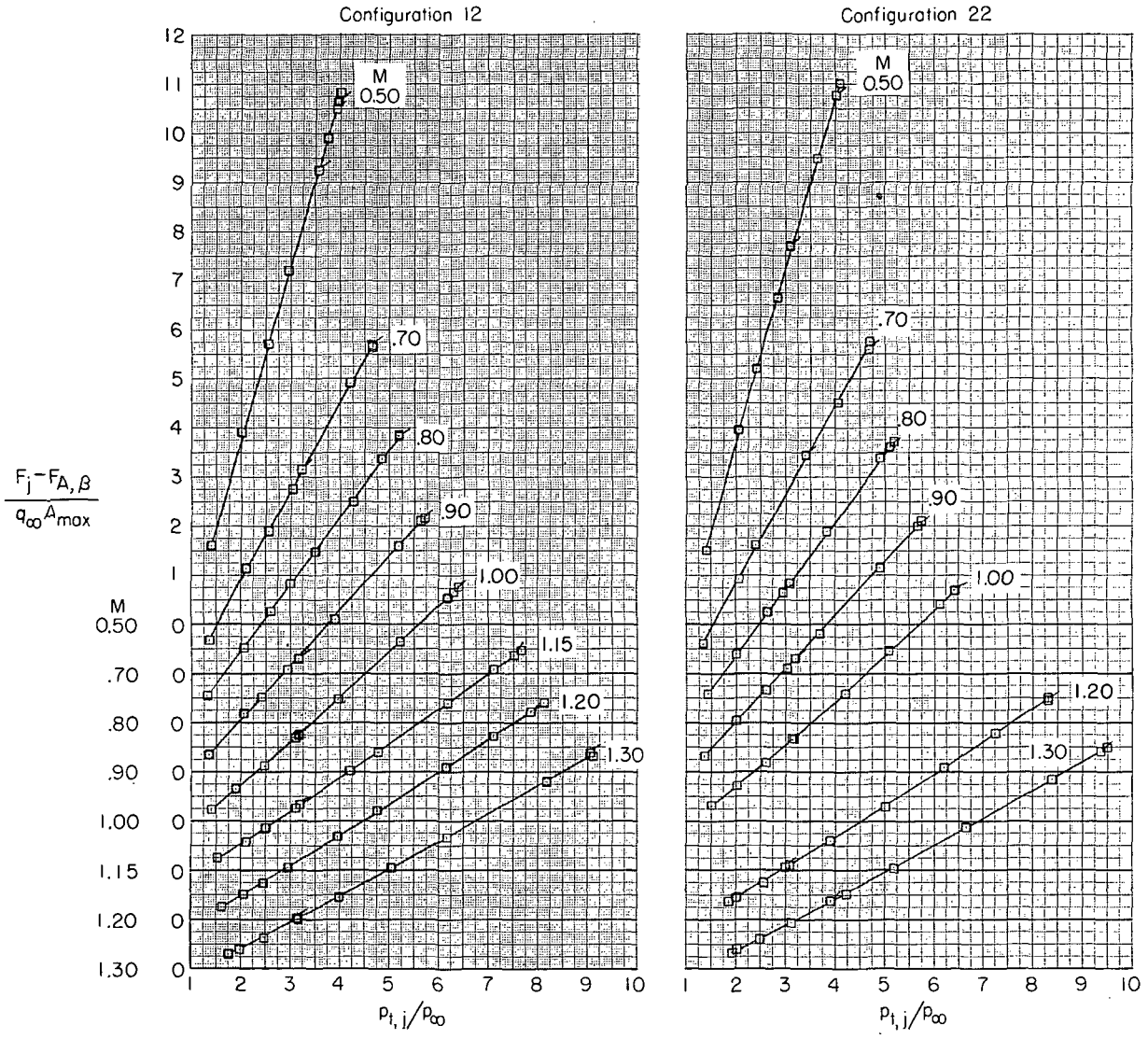

(g) Configurations 12 and 22.

Figure 11.- Continued.

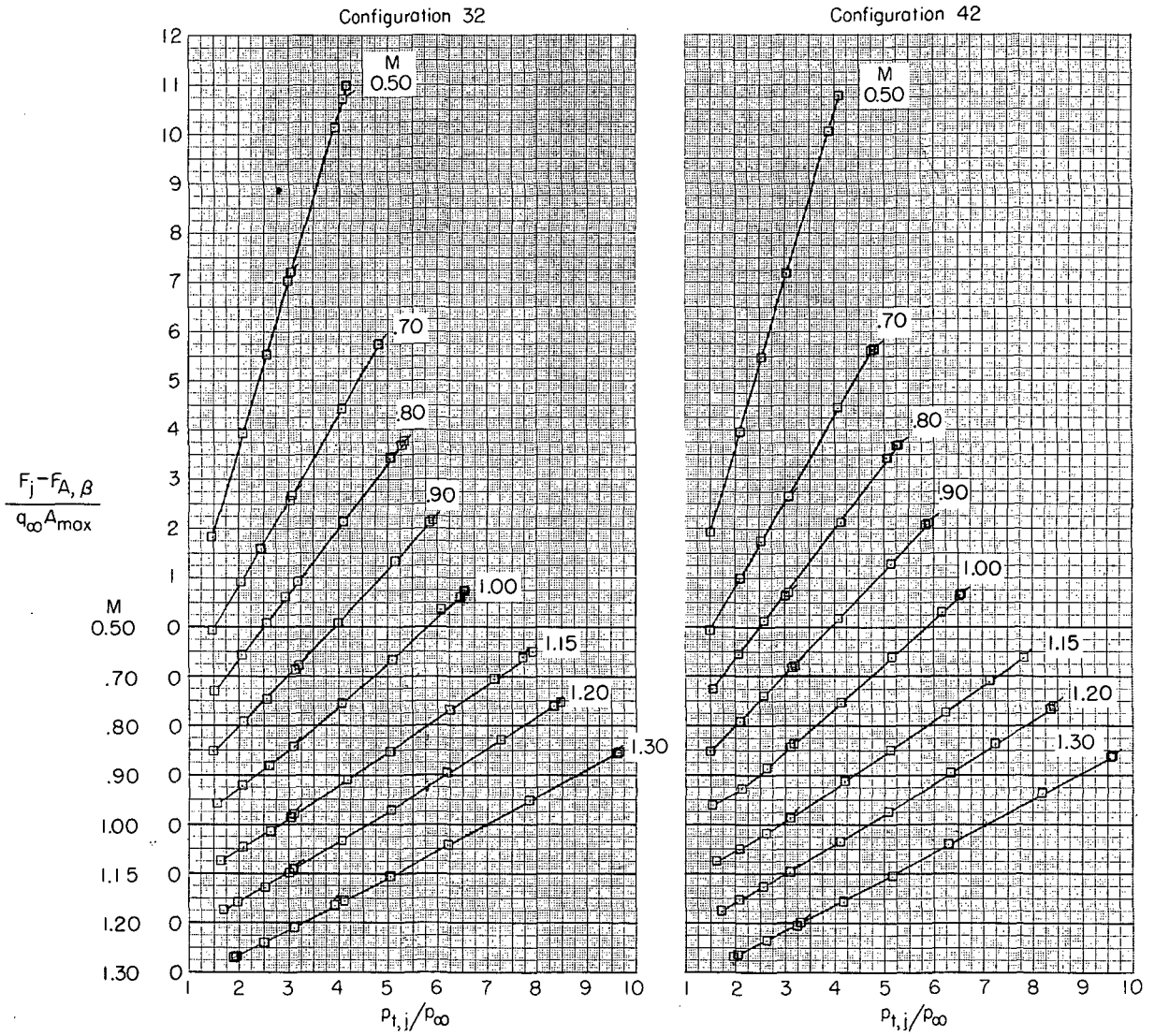

(h) Configurations 32 and 42.

Figure 11.- Continued.

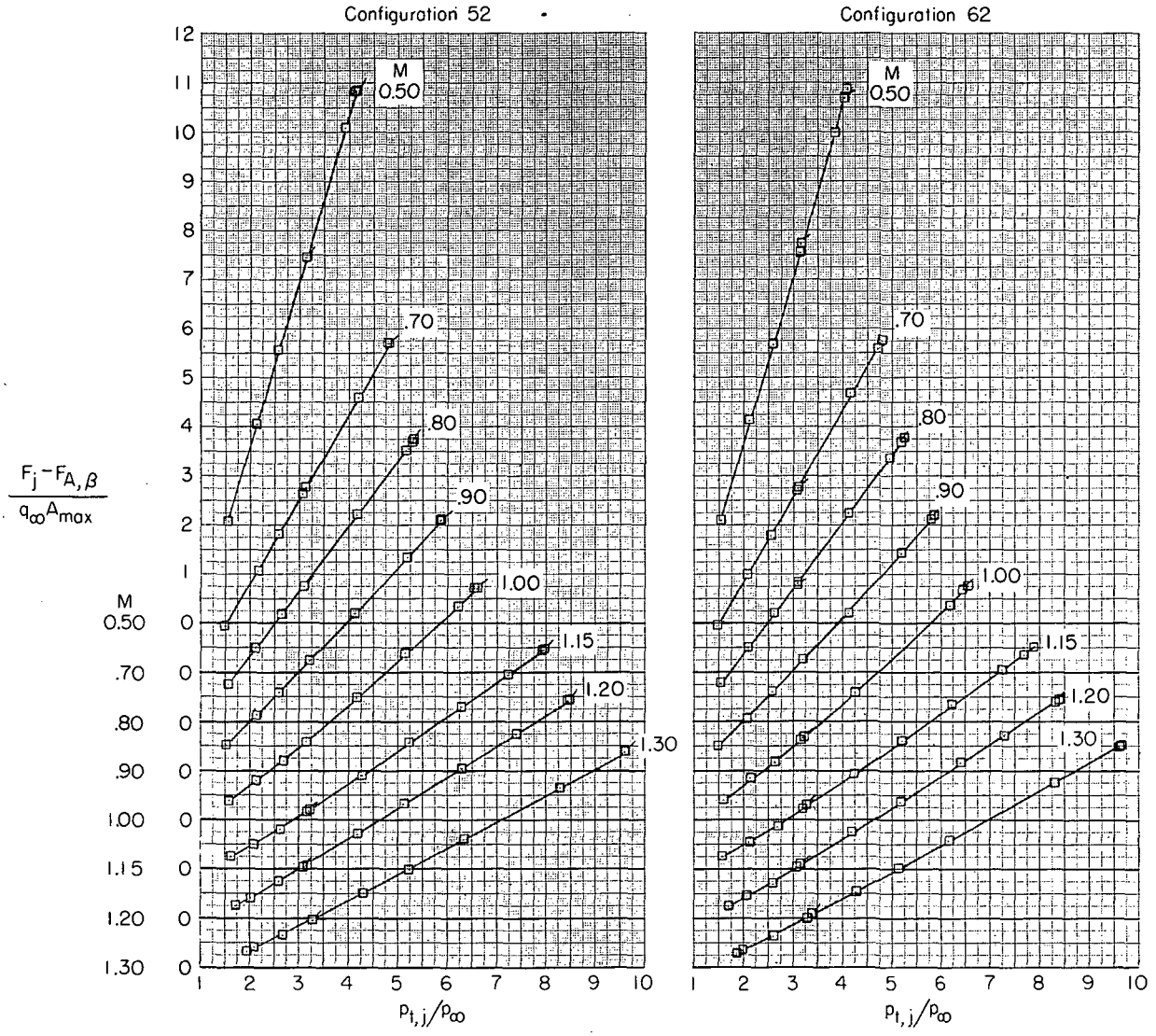

(i) Configurations 52 and 62.

Figure 11.- Continued.

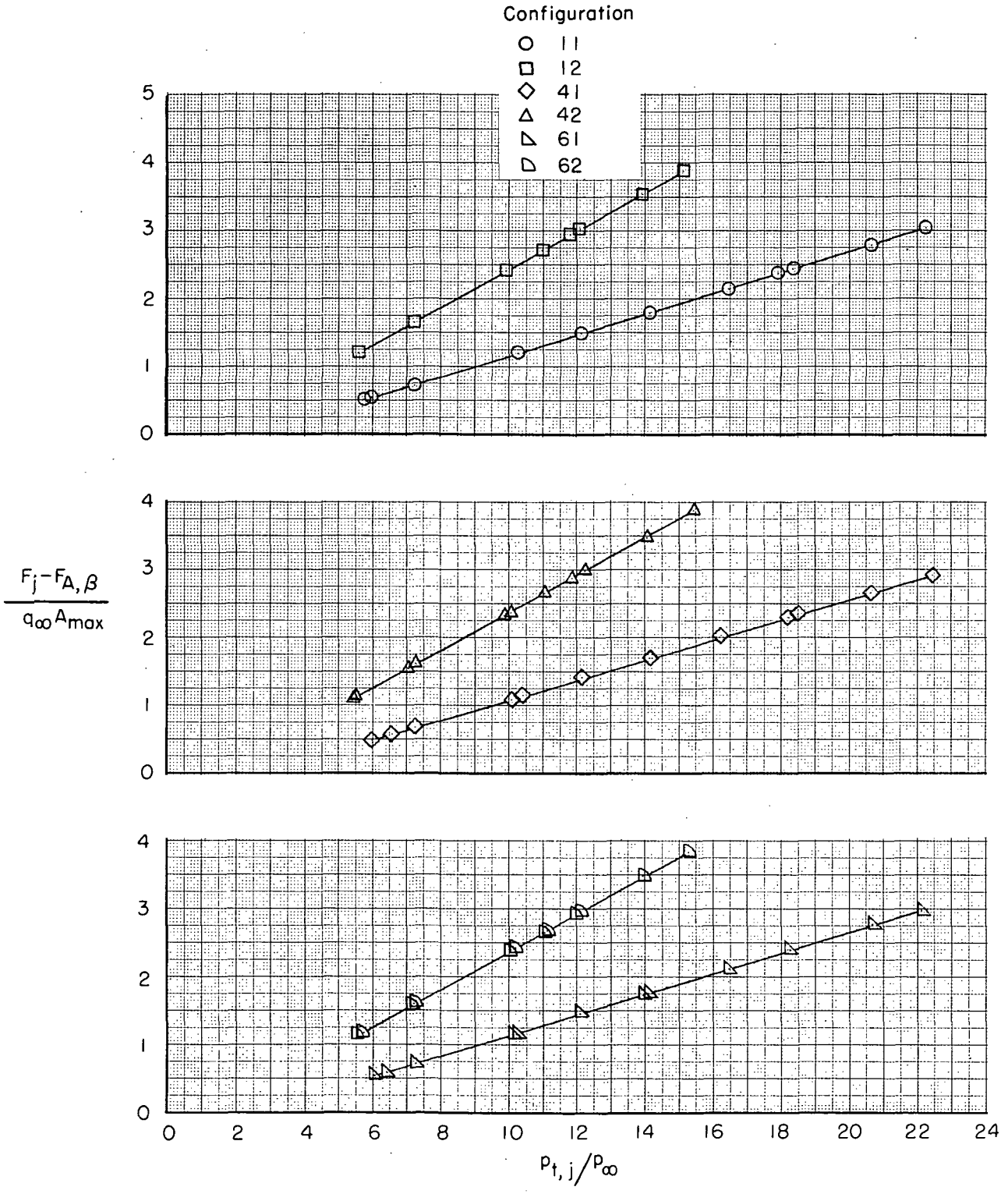

(j) M = 1.82.

Figure 11.- Concluded.

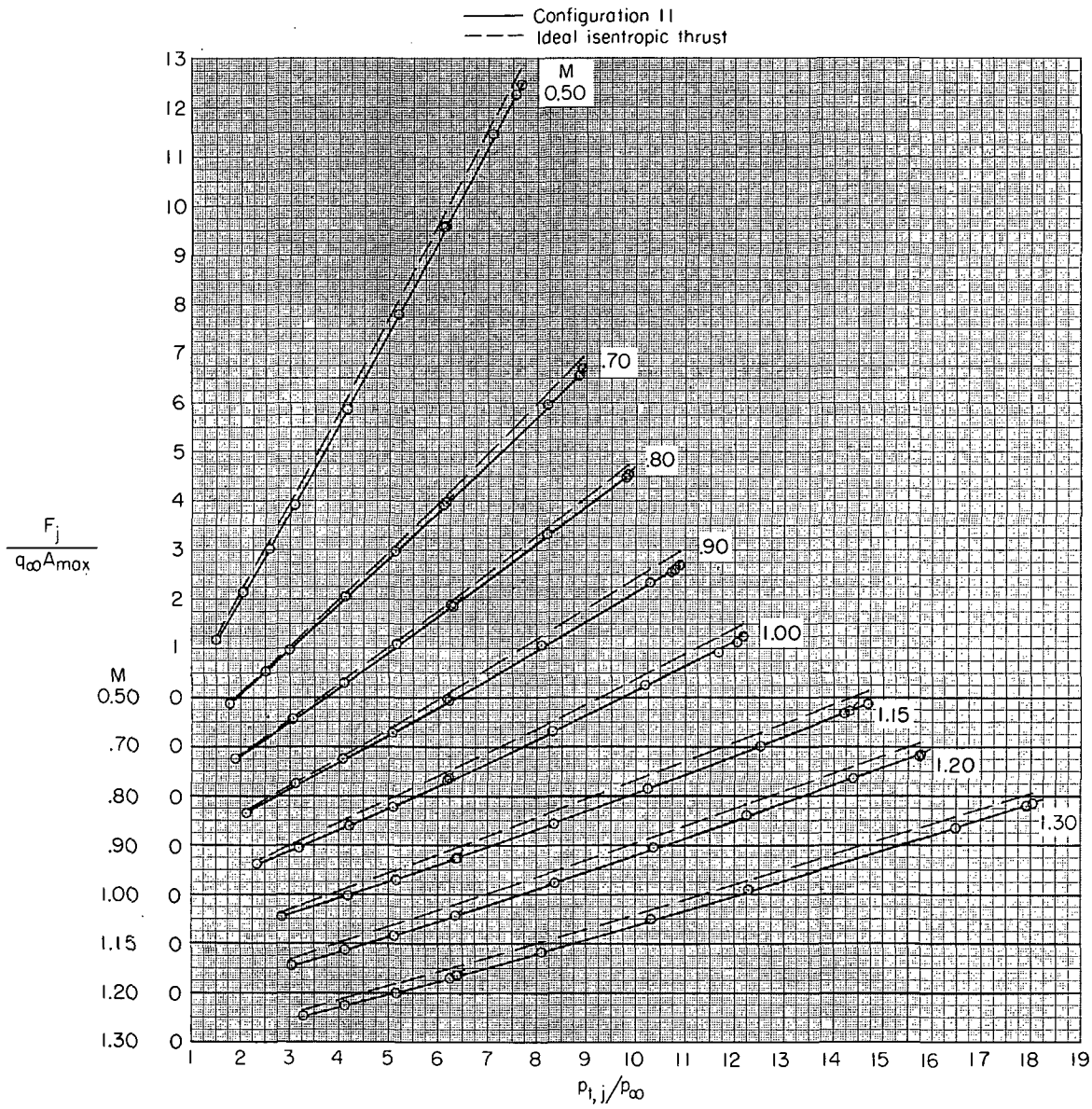

(a) Configuration 11.

Figure 12.- Variation of thrust coefficient with jet total-pressure ratio for various Mach numbers. Flagged symbols denote increasing pressure ratio.

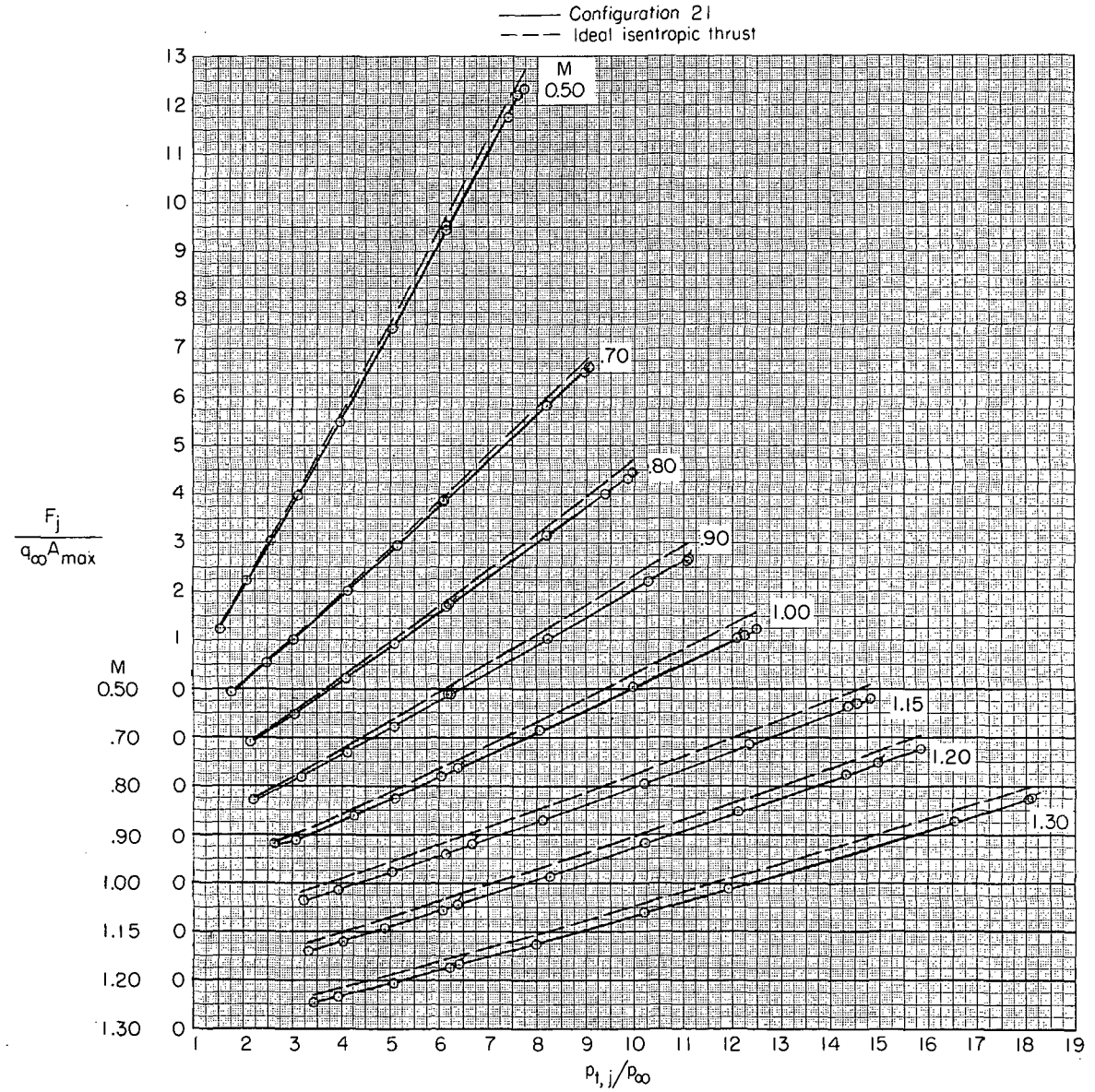

(b) Configuration 21.

Figure 12.- Continued.

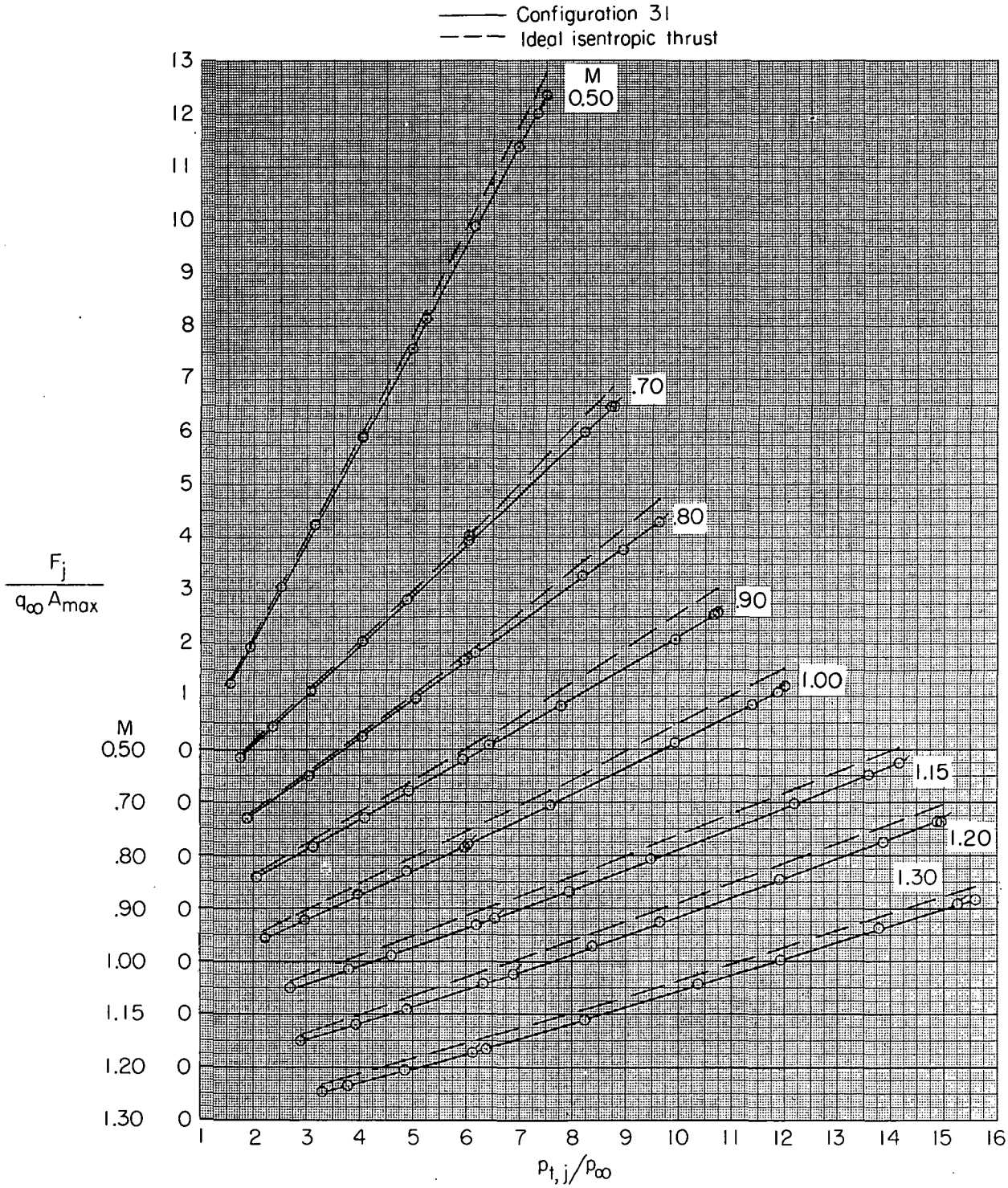

(c) Configuration 31.

Figure 12.- Continued.

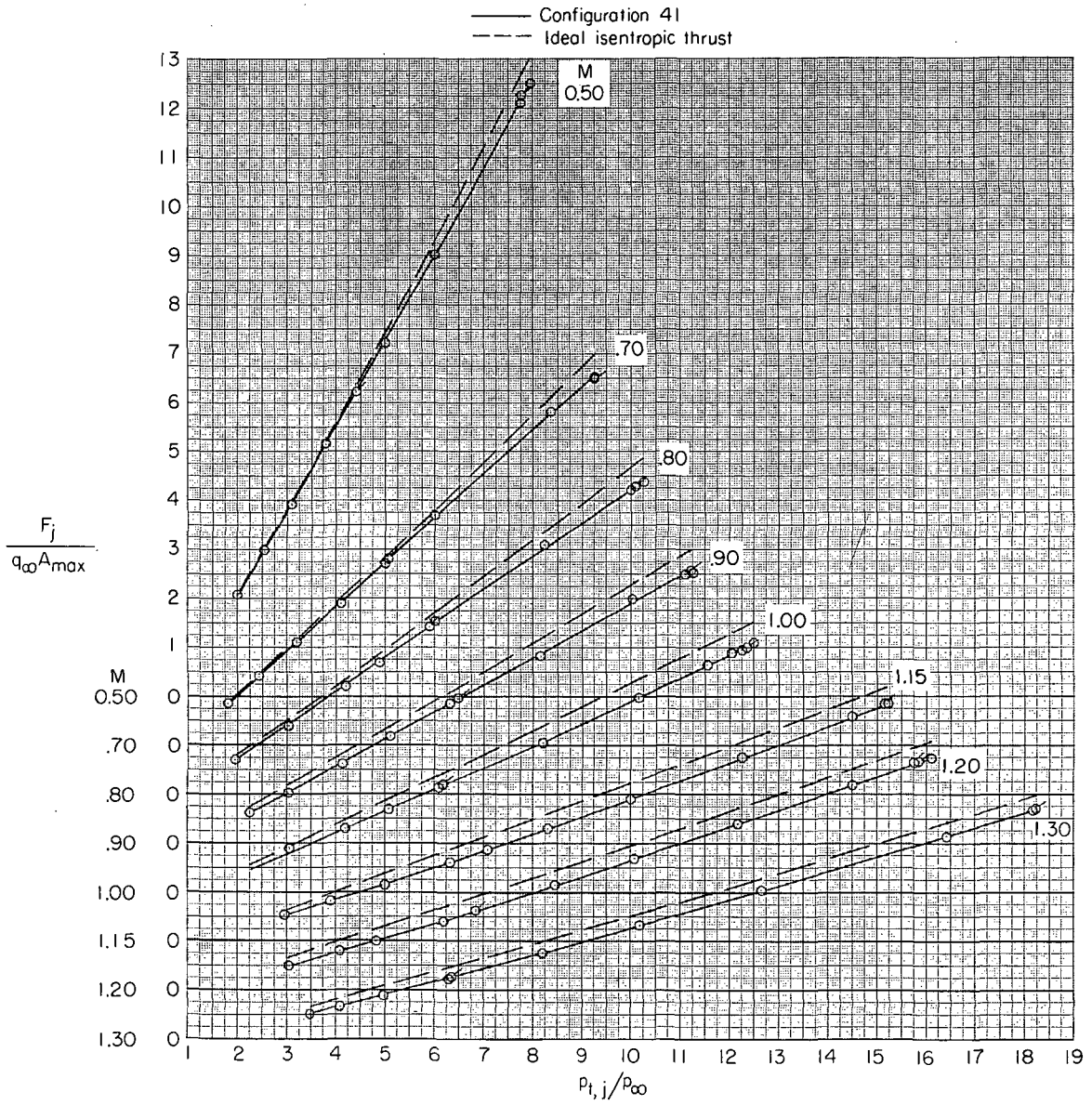

(d) Configuration 41.

Figure 12.- Continued.

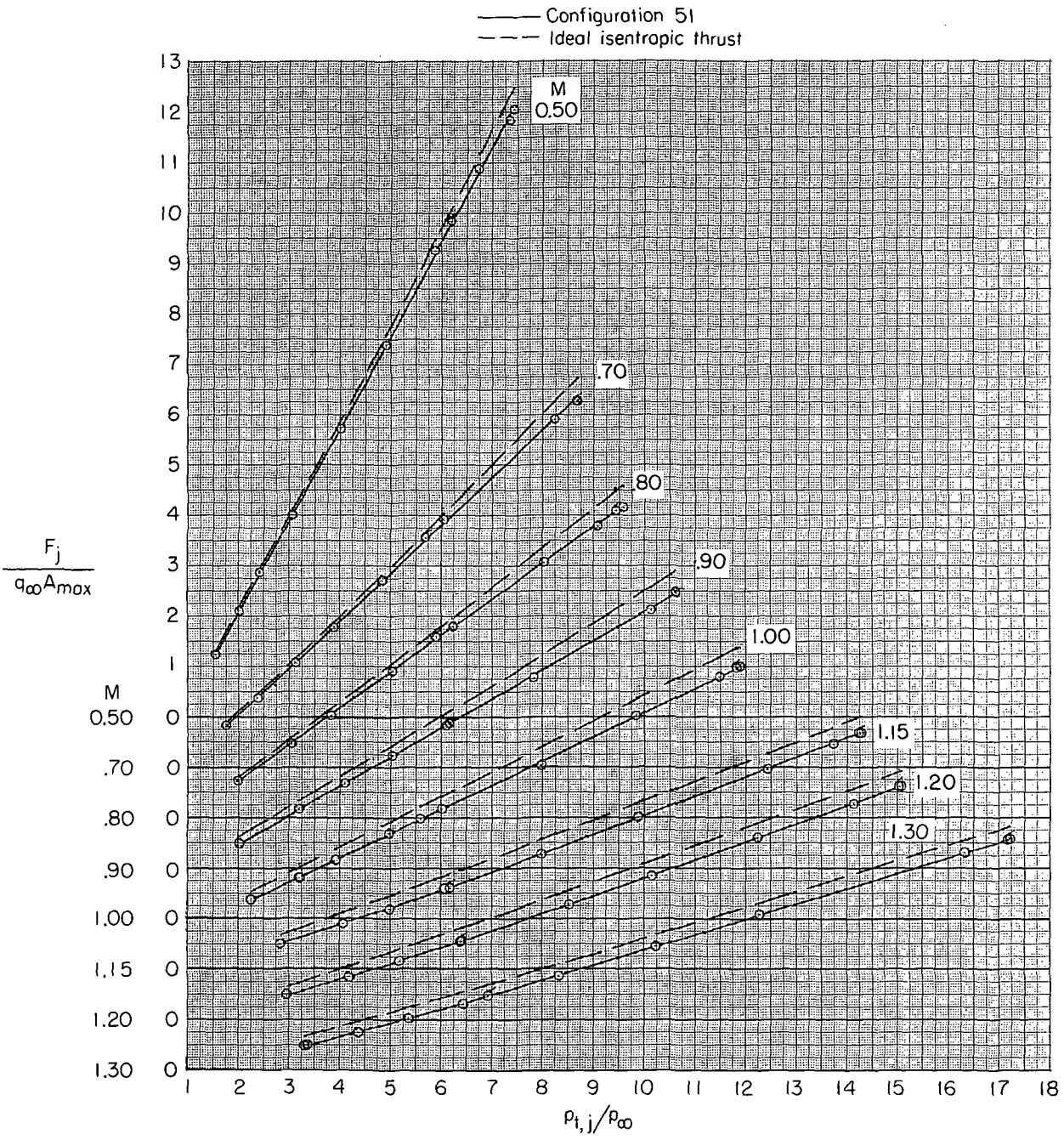

(e) Configuration 51.

Figure 12.- Continued.

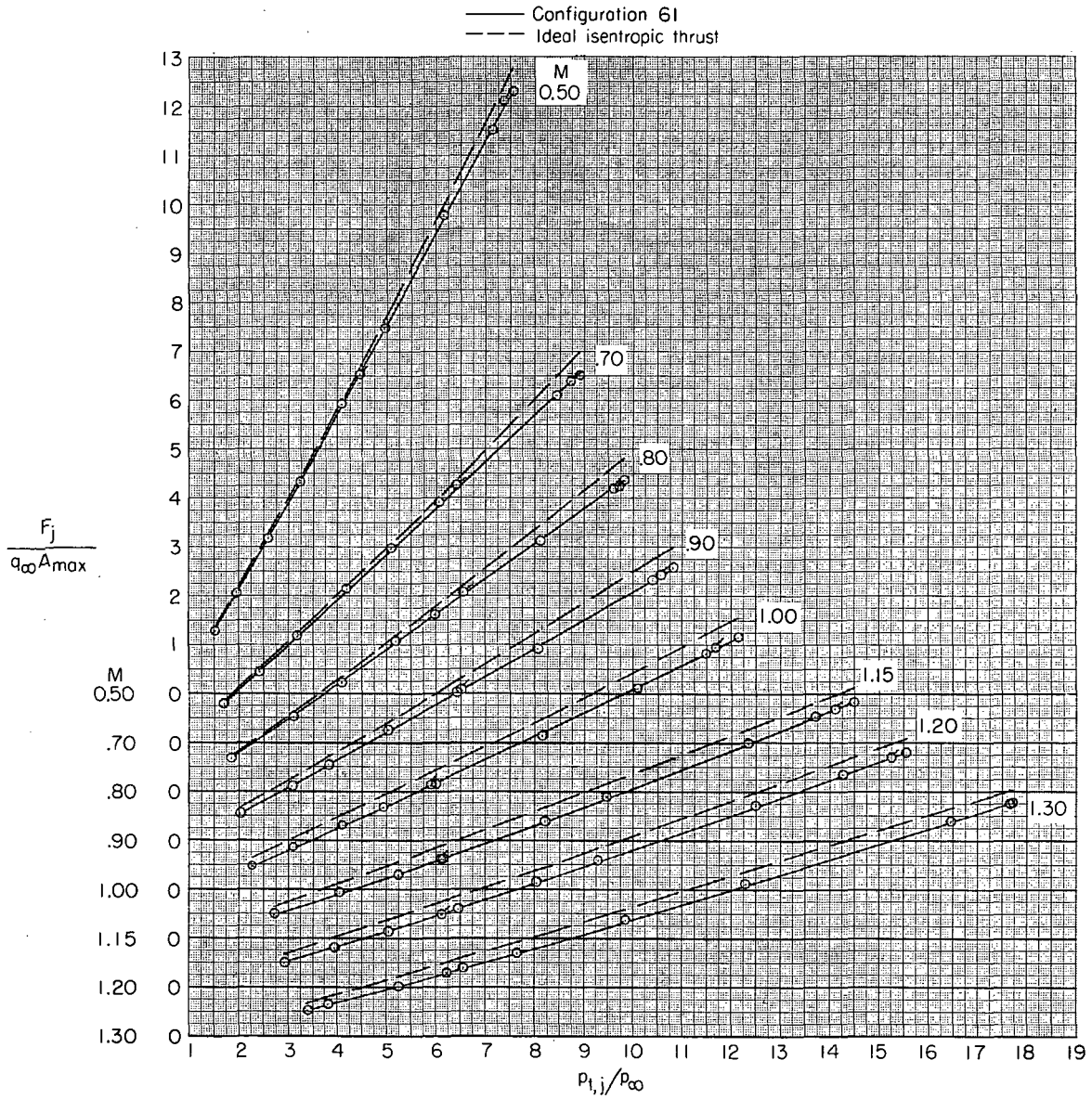

(f) Configuration 61.

Figure 12.- Continued.

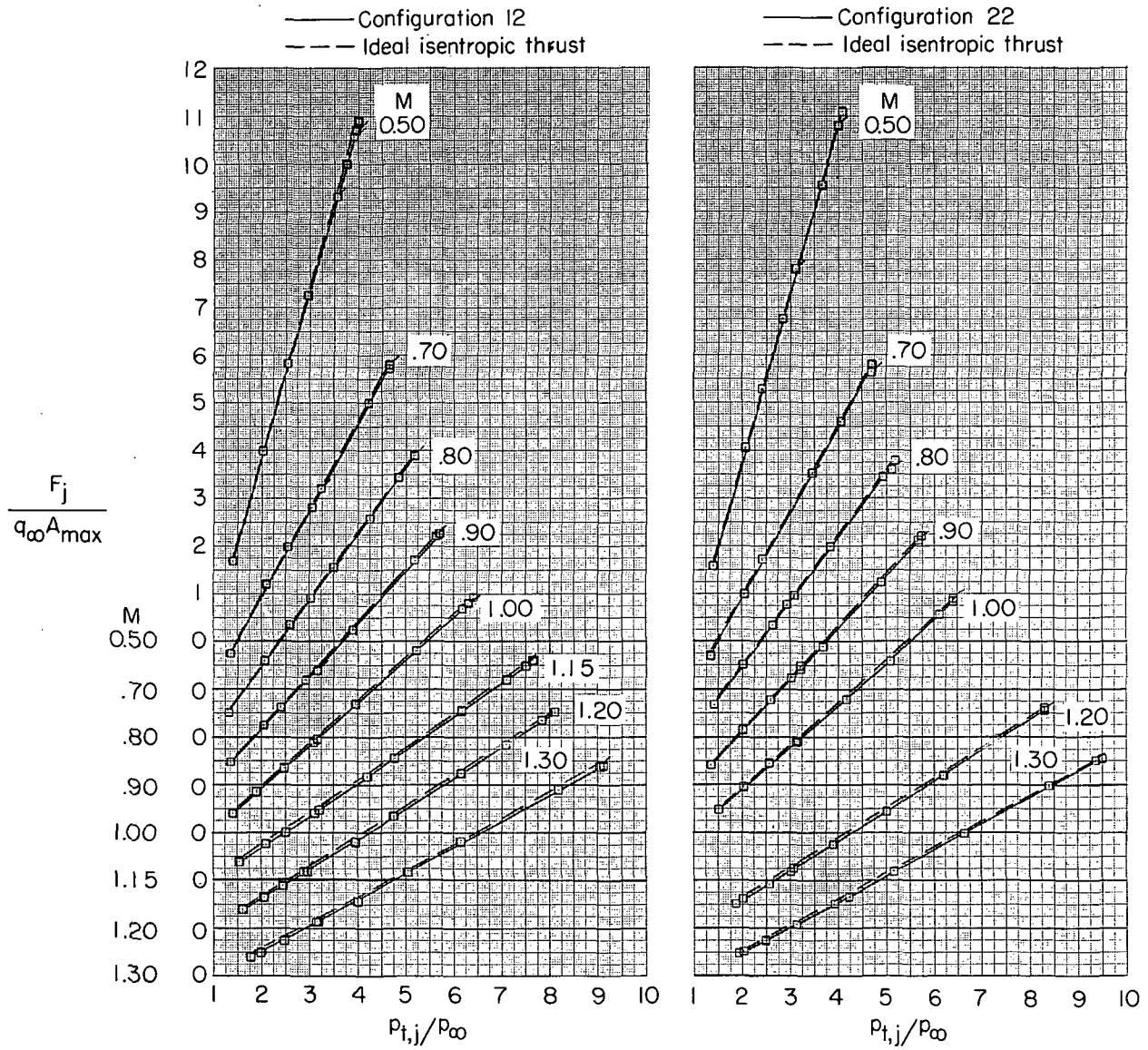

(g) Configurations 12 and 22.

Figure 12.- Continued.

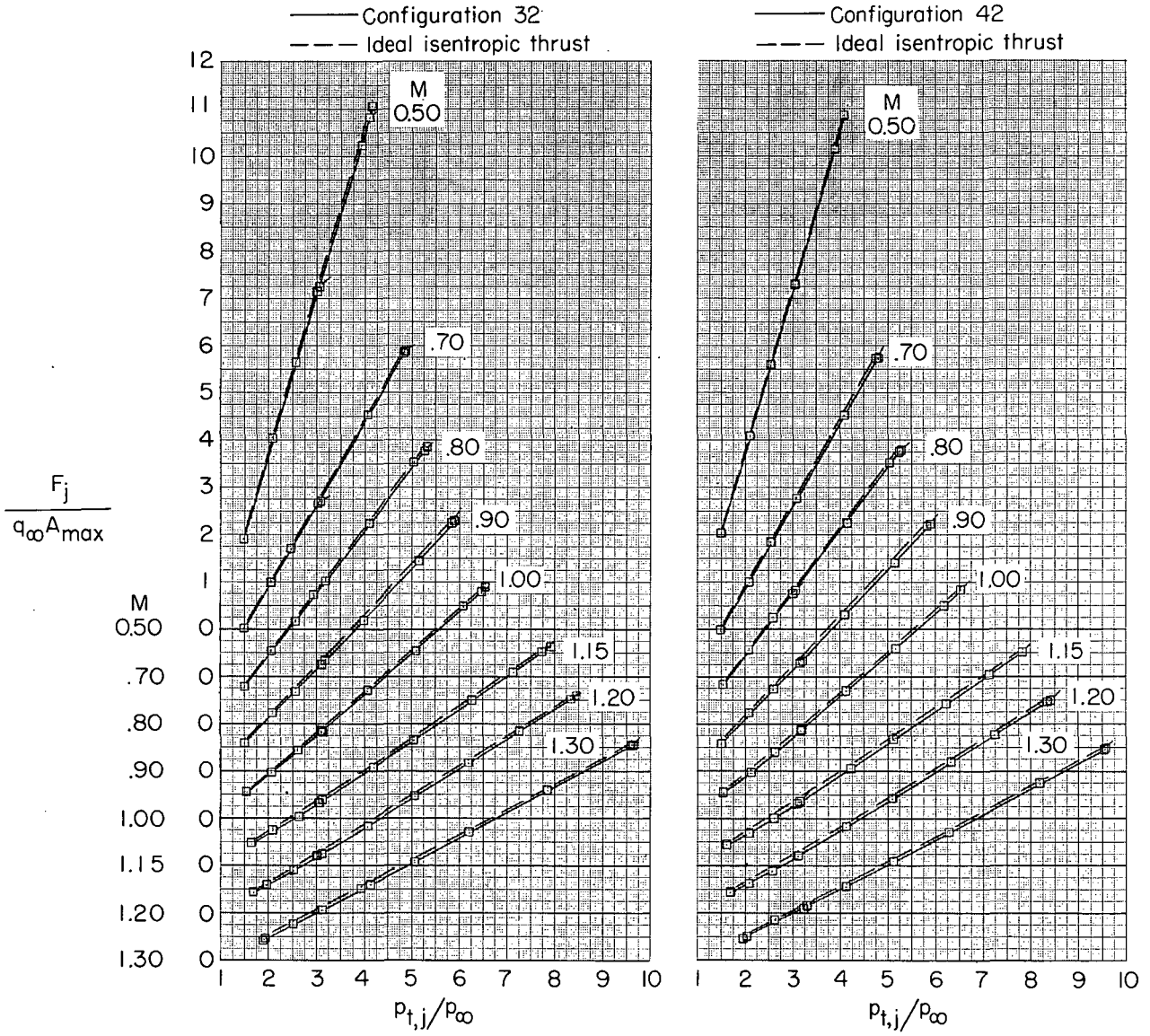

(h) Configurations 32 and 42.

Figure 12.- Continued.

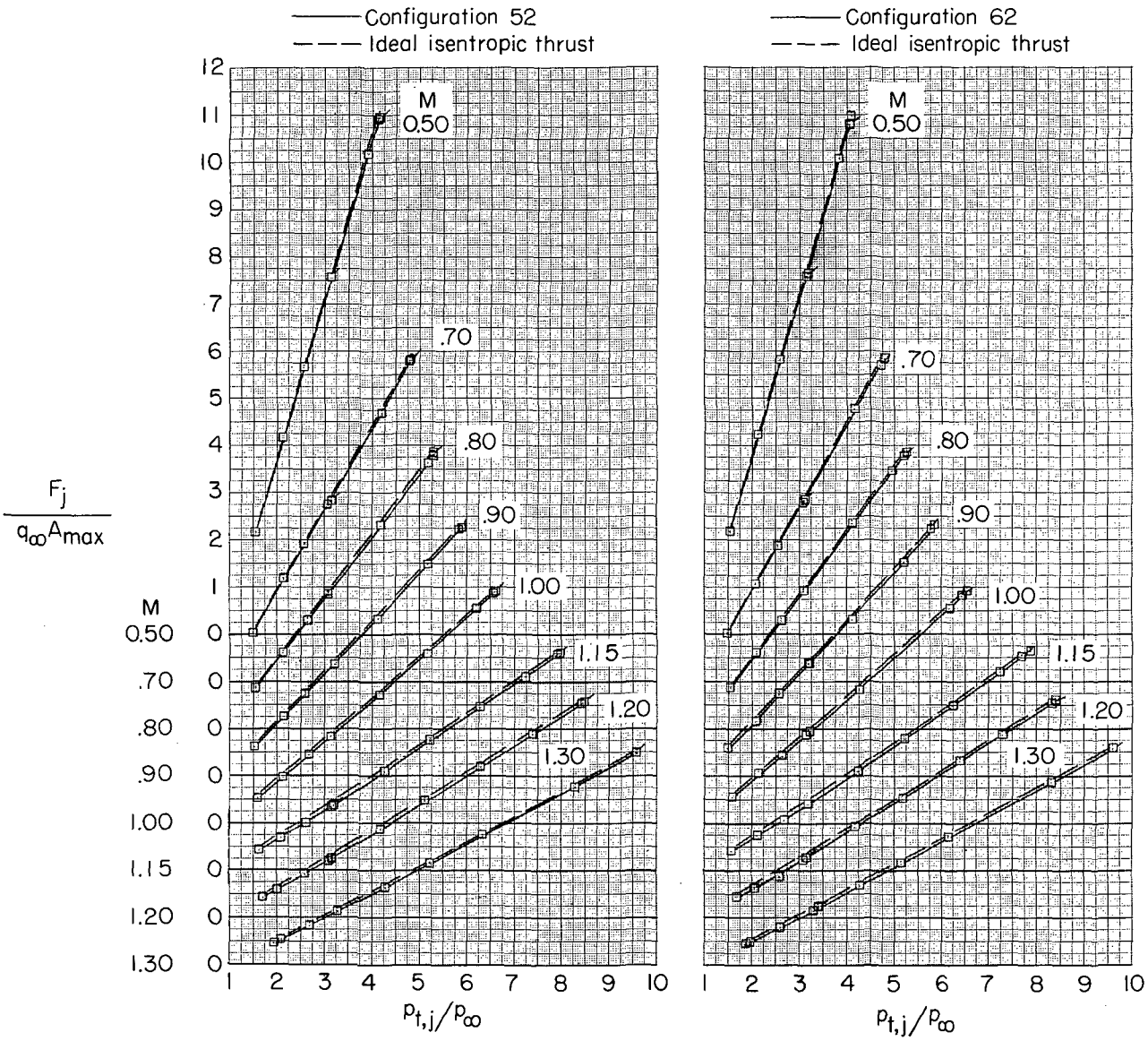

(i) Configurations 52 and 62.

Figure 12.- Continued.

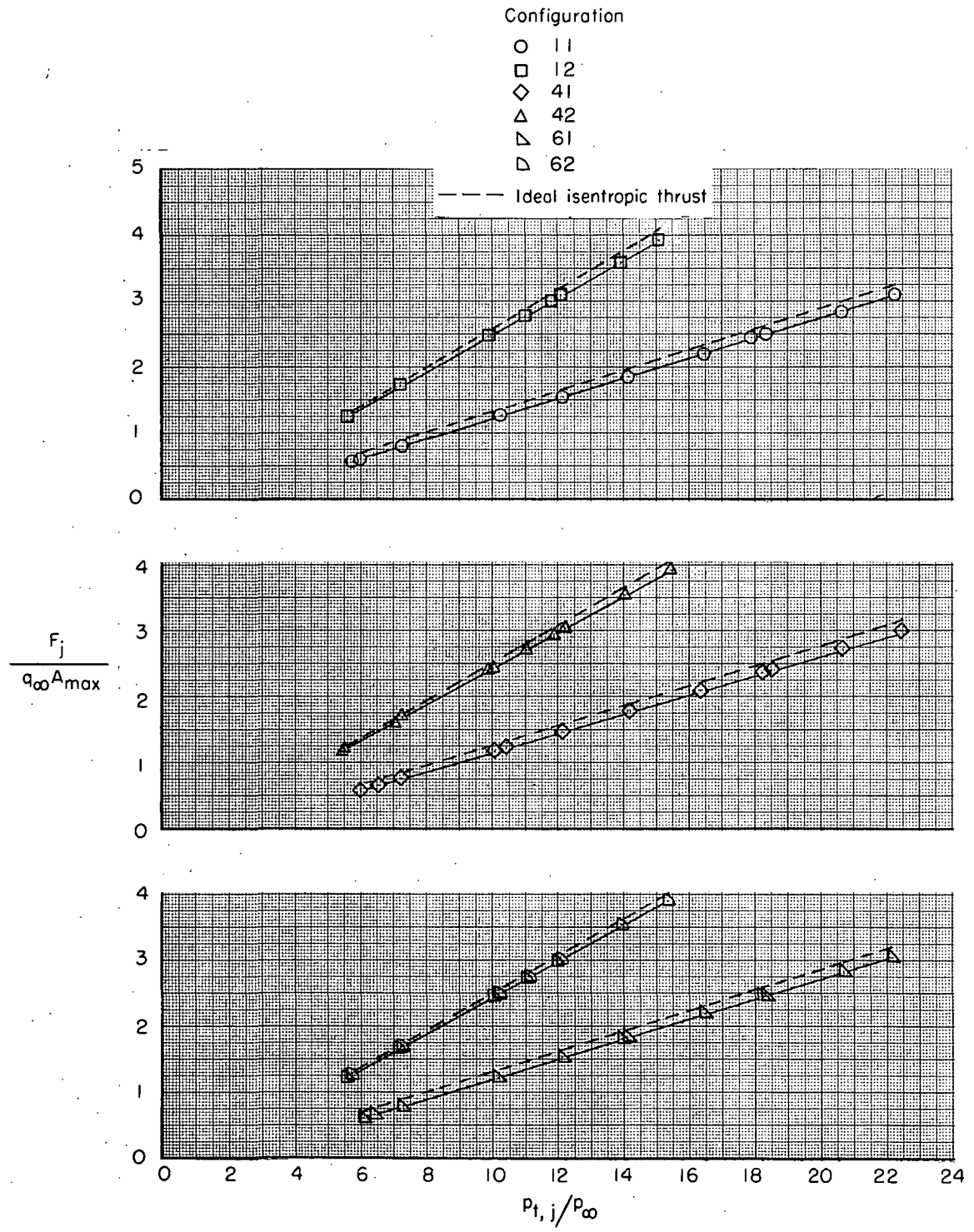

(j) M = 1.82.

Figure 12.- Concluded.

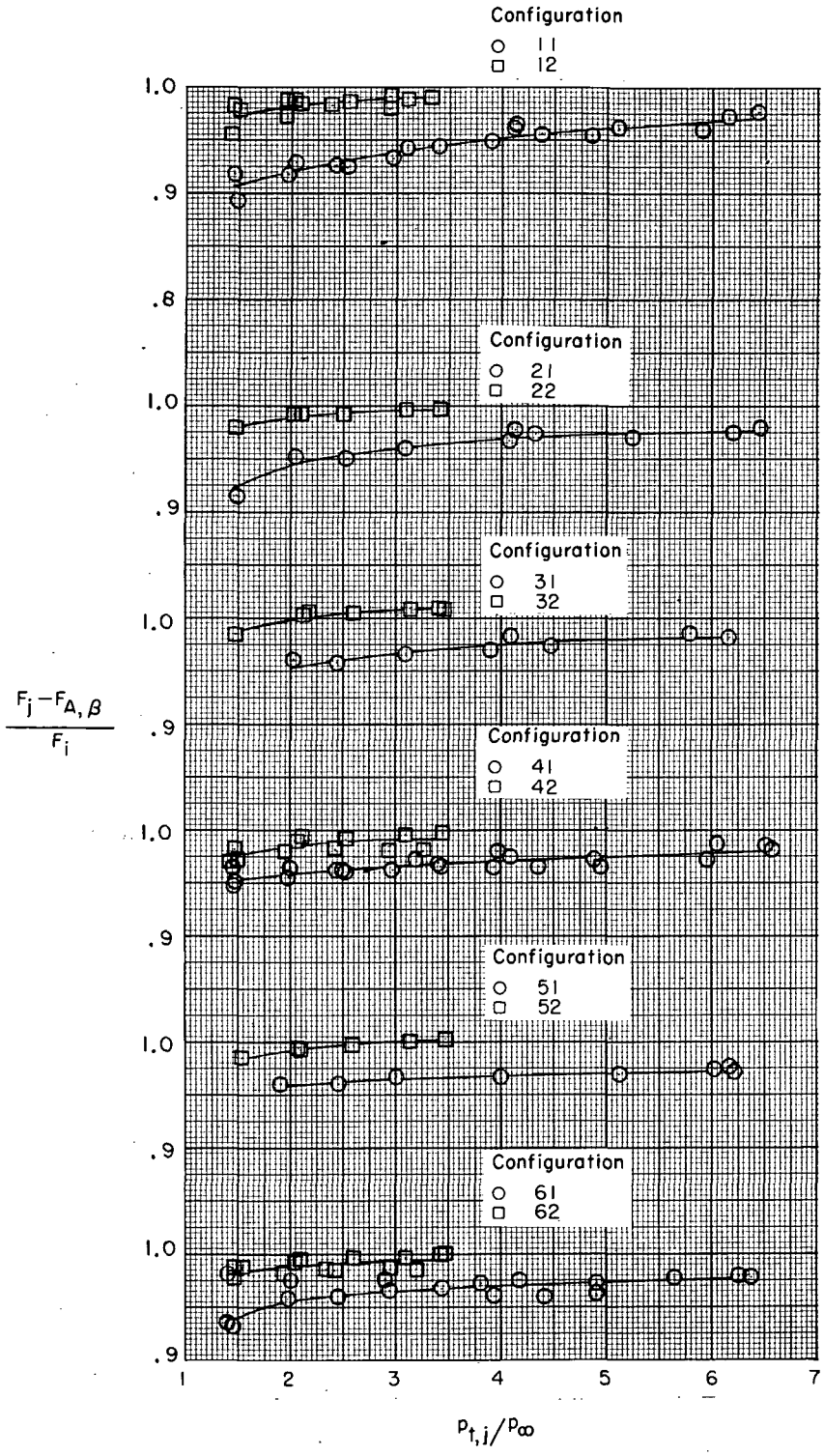

(a) M = 0.

Figure 13.- Variation of thrust-minus-drag ratio with jet total-pressure ratio for various Mach numbers.

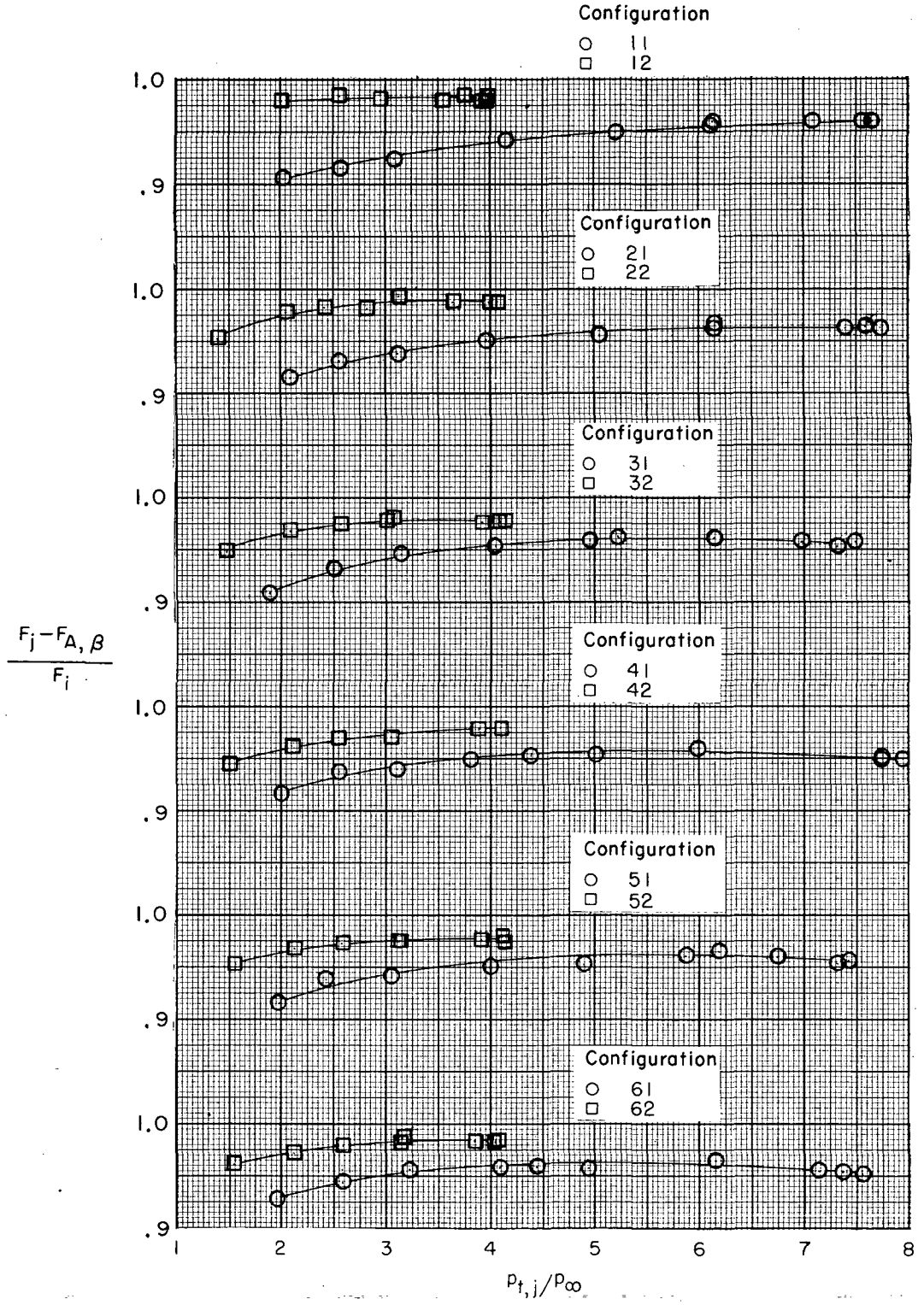

(b) M = 0.50.

Figure 13.- Continued.

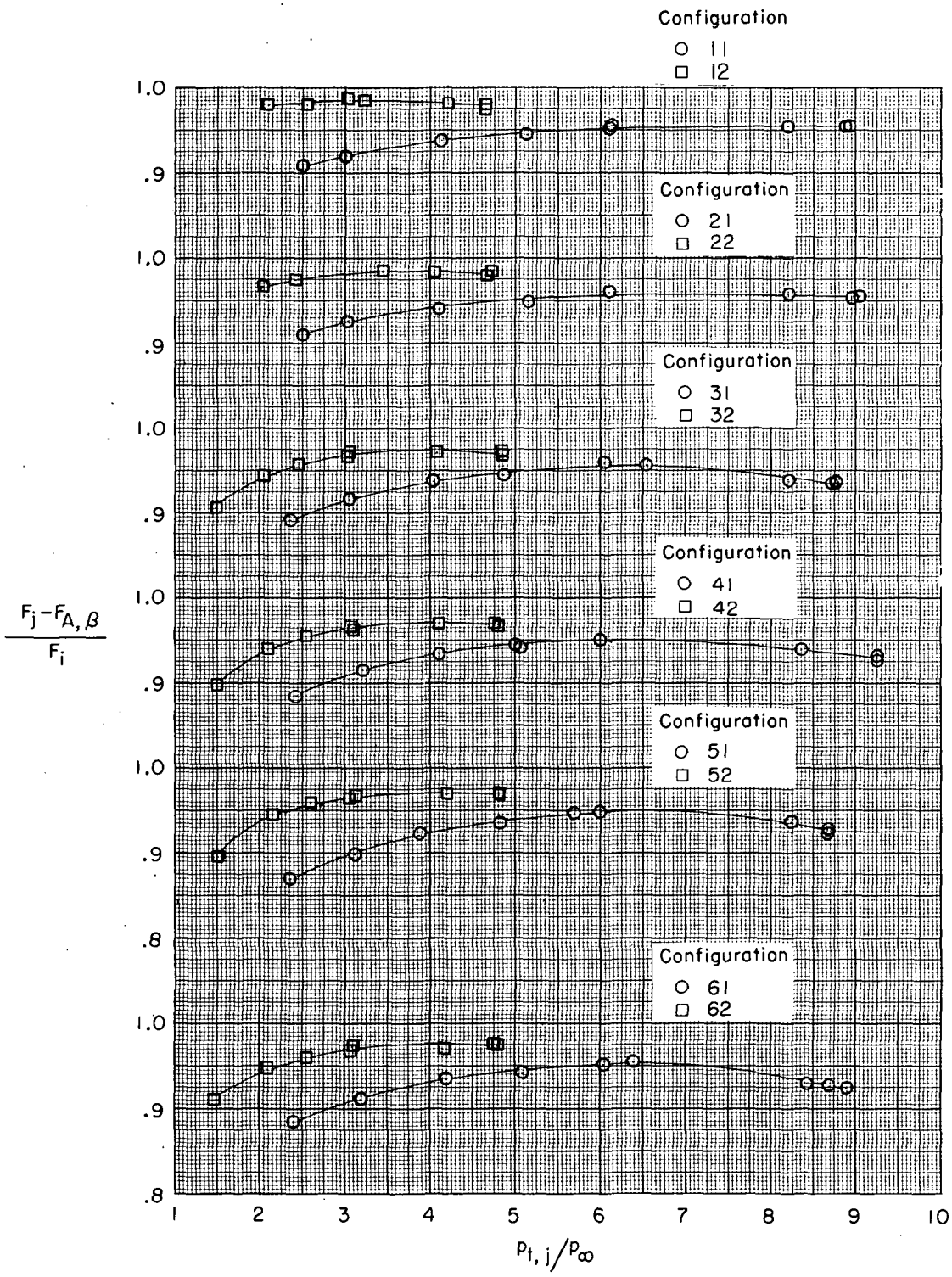

(c) M = 0.70.

Figure 13.- Continued.

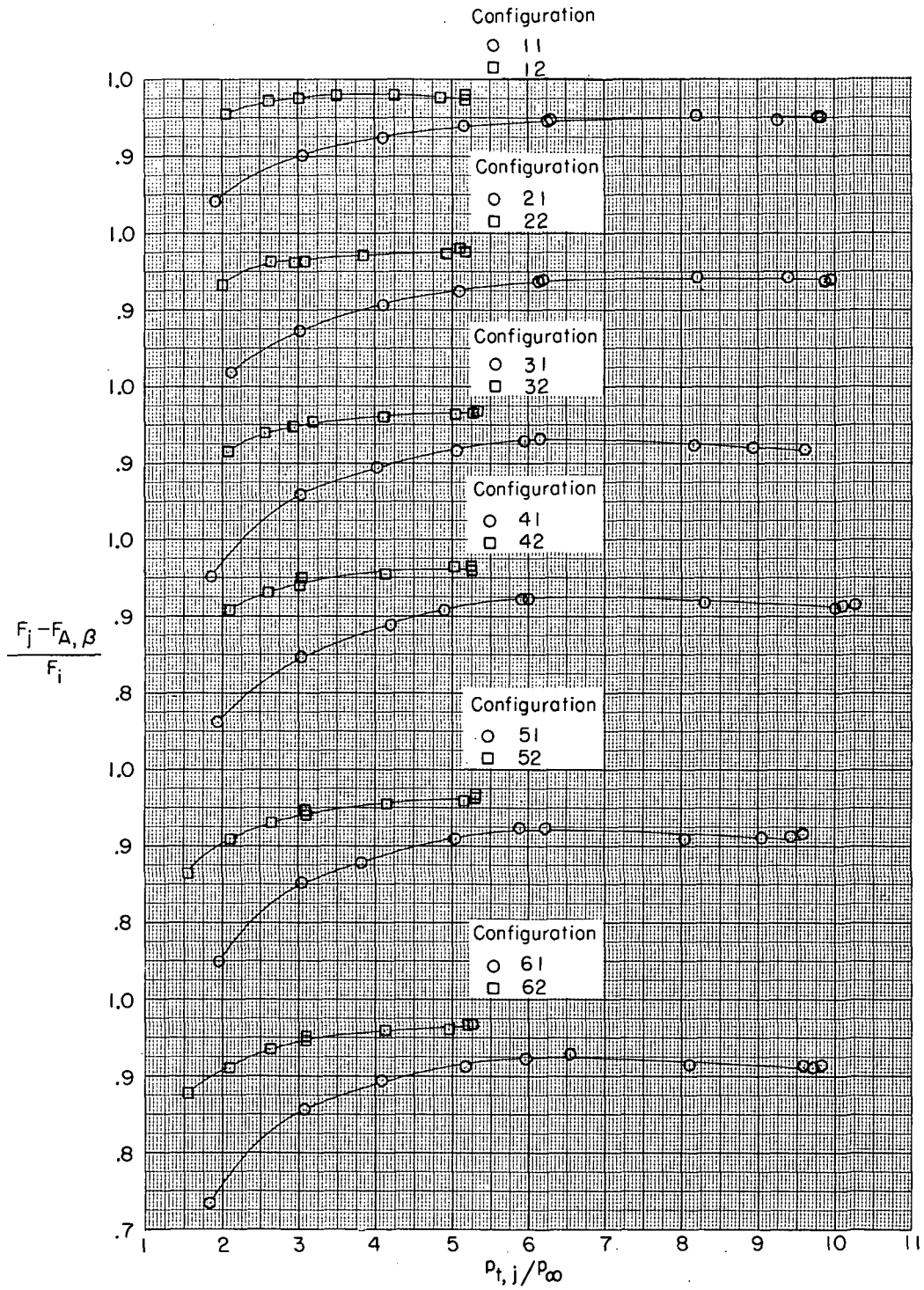

(d) M = 0.80.

Figure 13.- Continued.

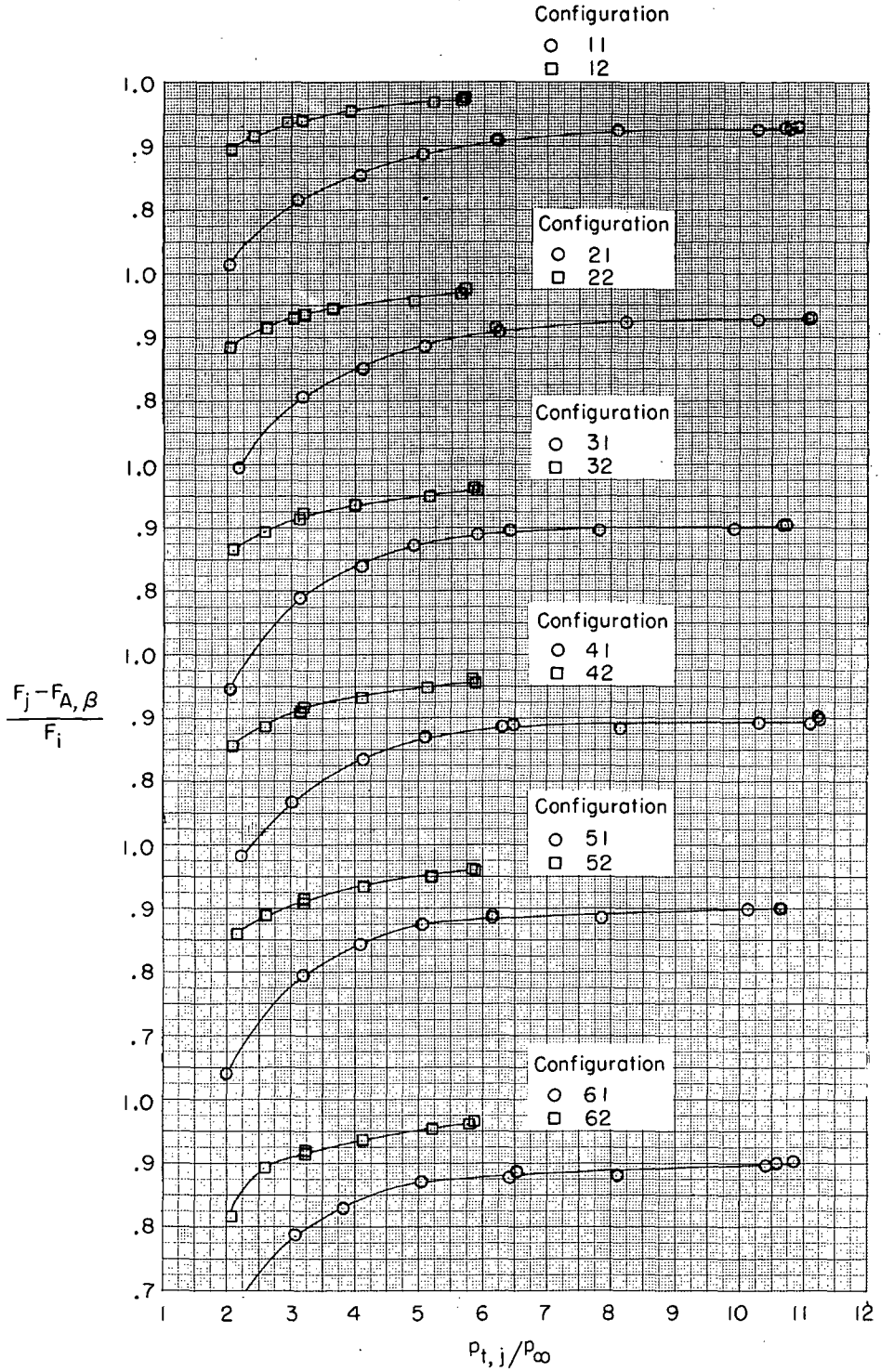

(e) M = 0.90.

Figure 13.- Continued.

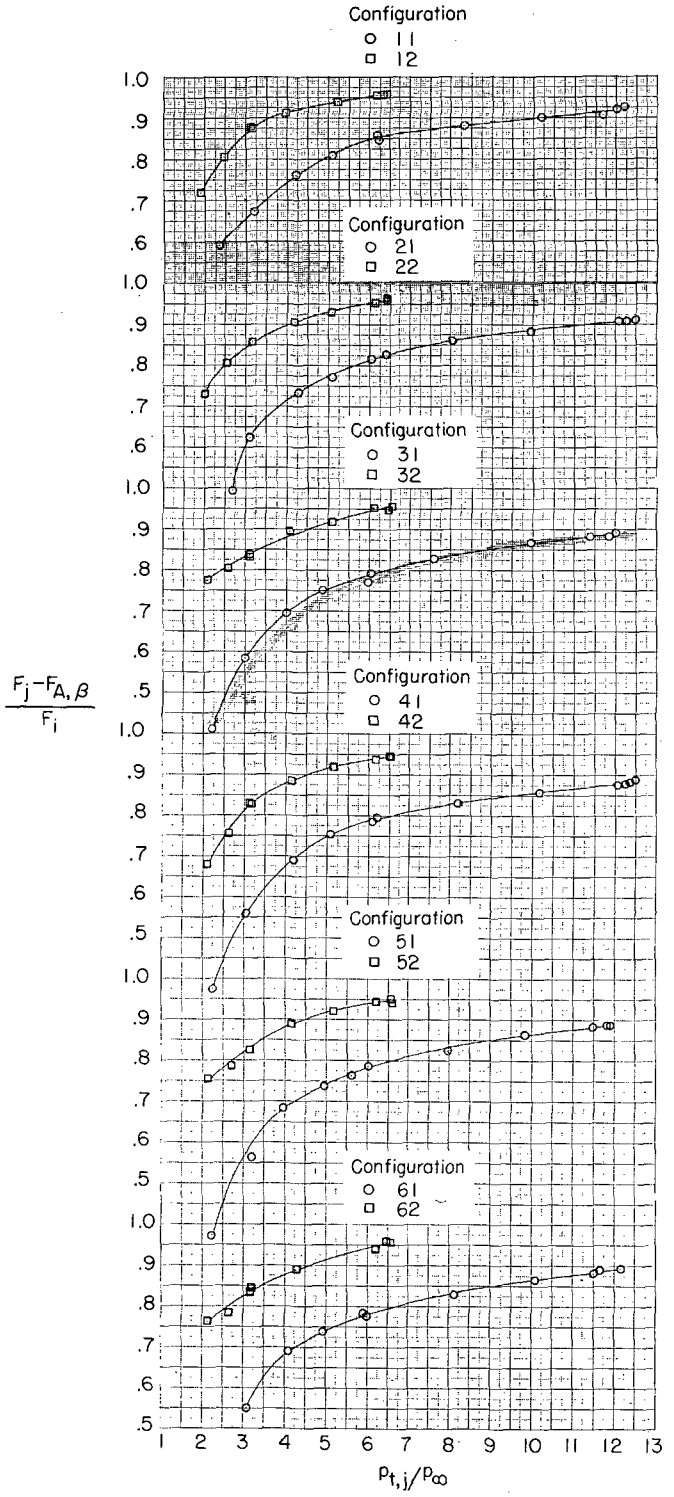

(f) M = 1.00.

Figure 13.- Continued.

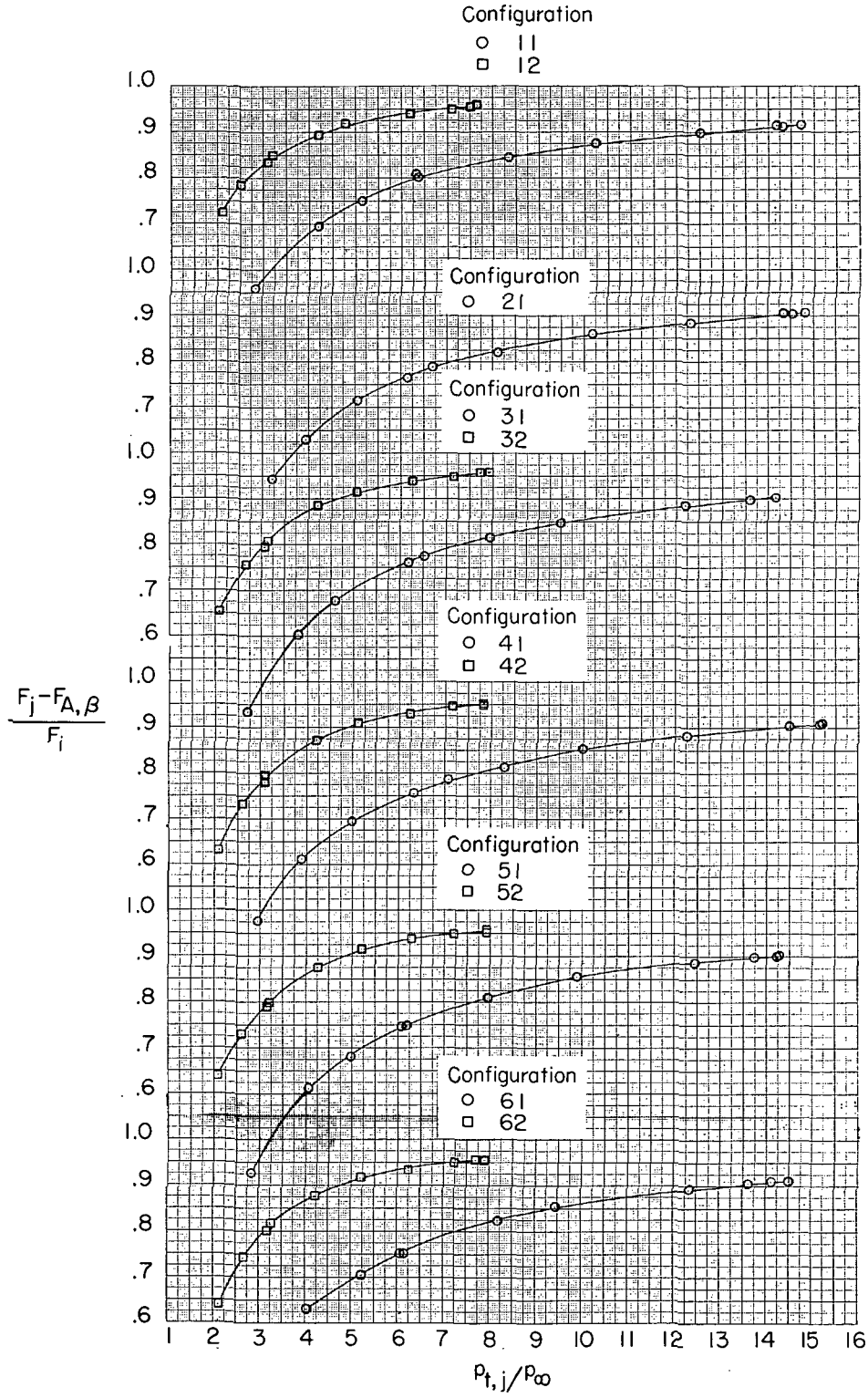

(g) M = 1.15.

Figure 13.- Continued.

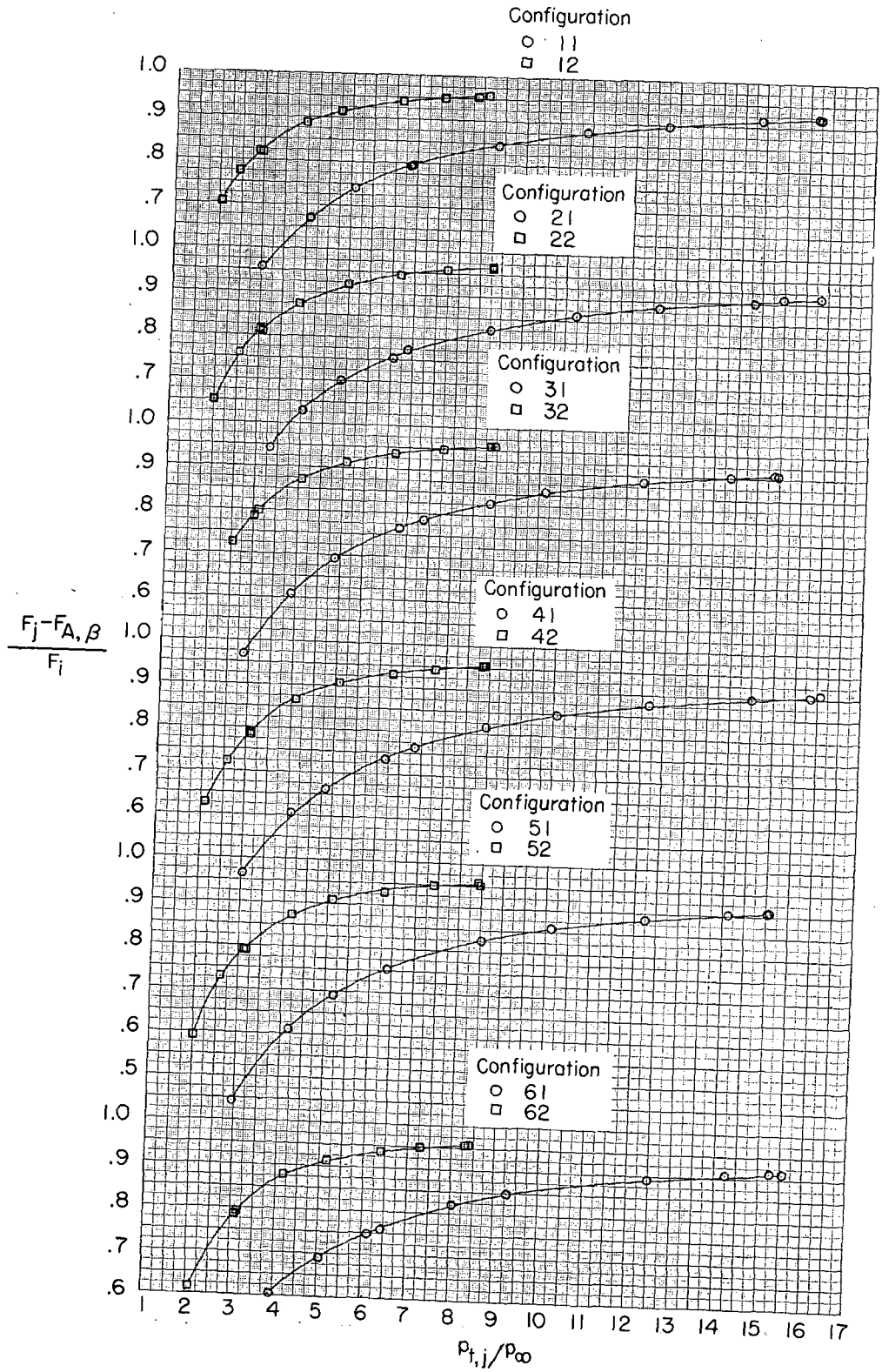

(h) M = 1.20.

Figure 13.- Continued.

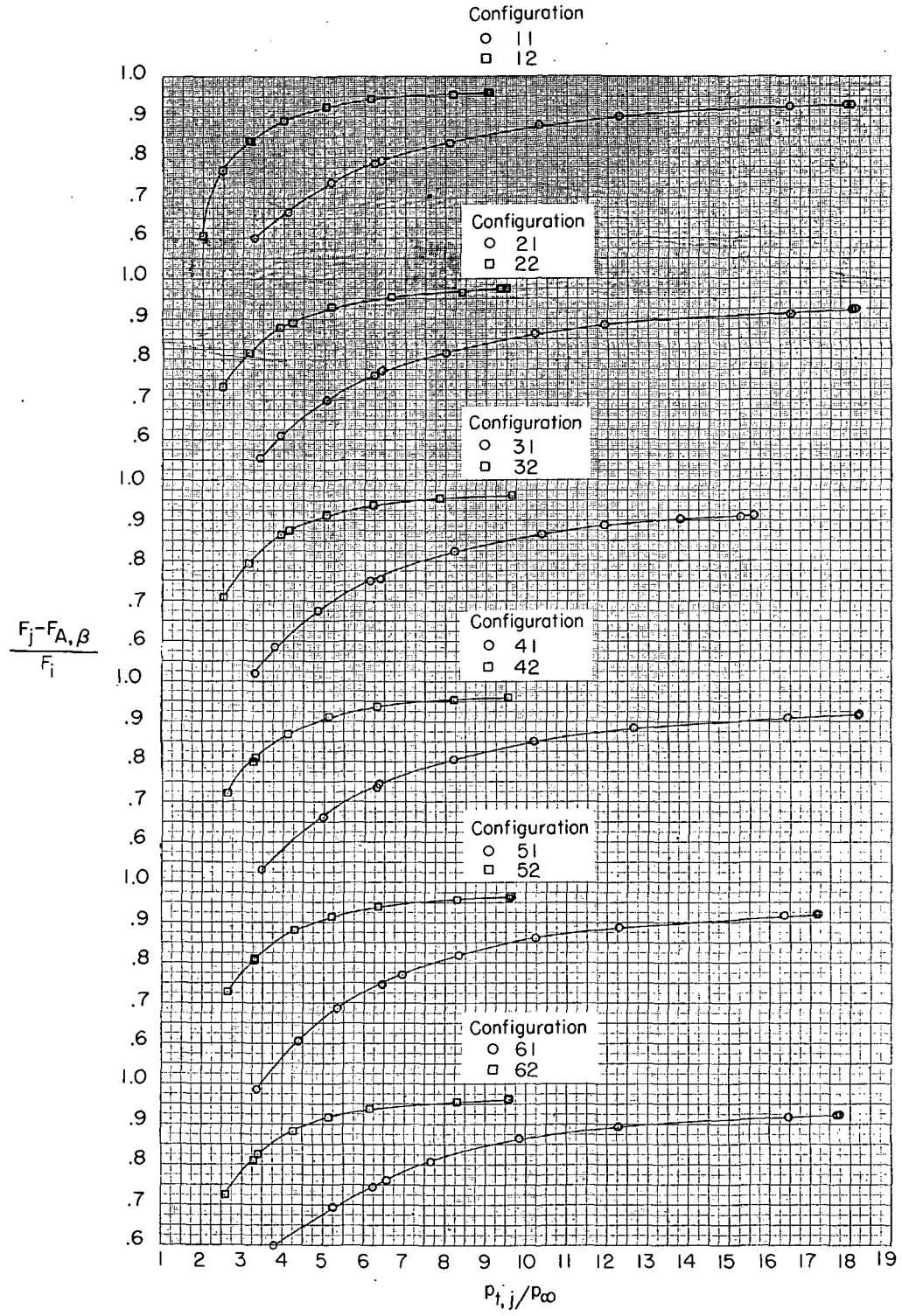

(i) M = 1.30.

Figure 13.- Continued.

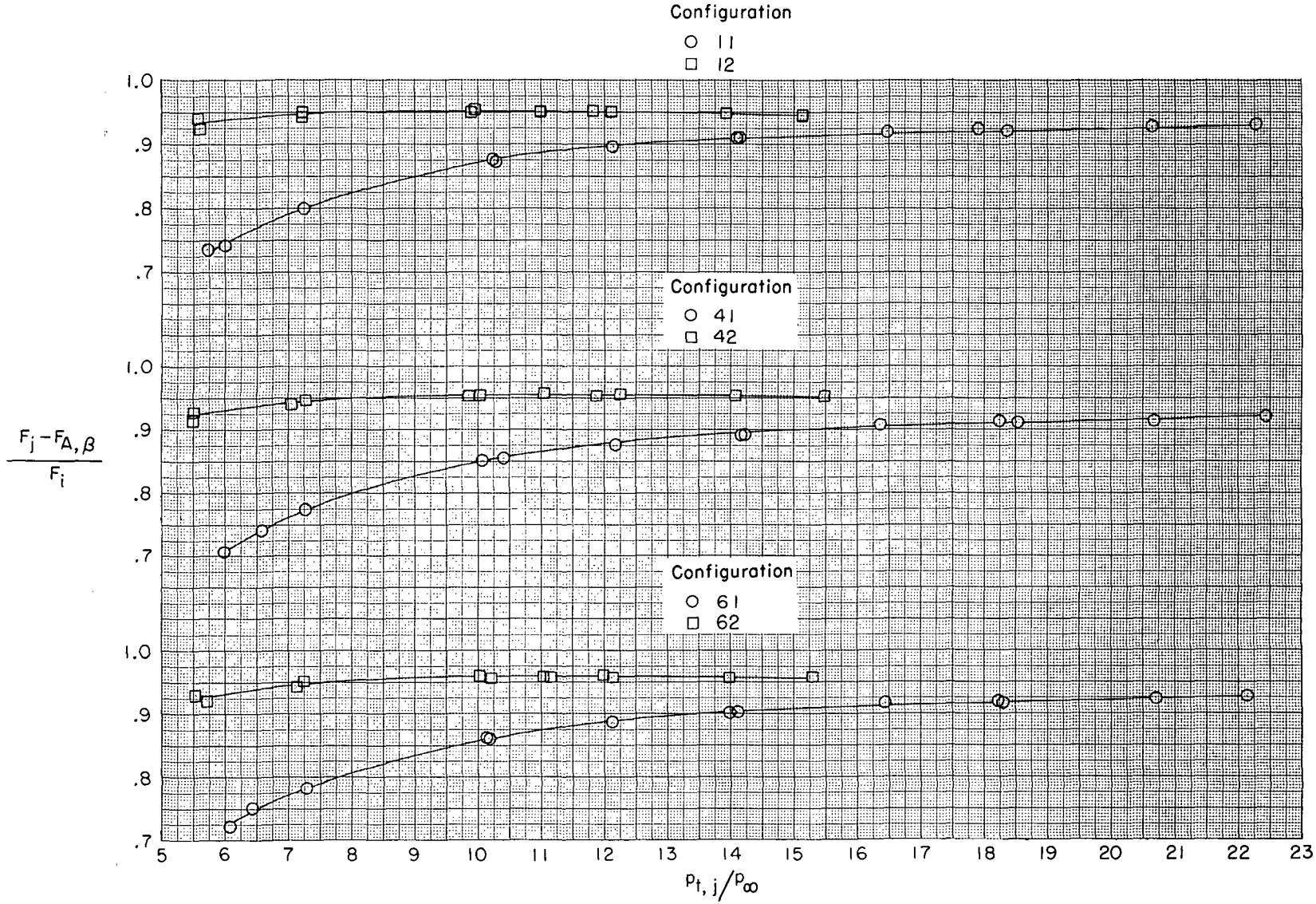

(j) M = 1.82.

Figure 13.- Concluded.

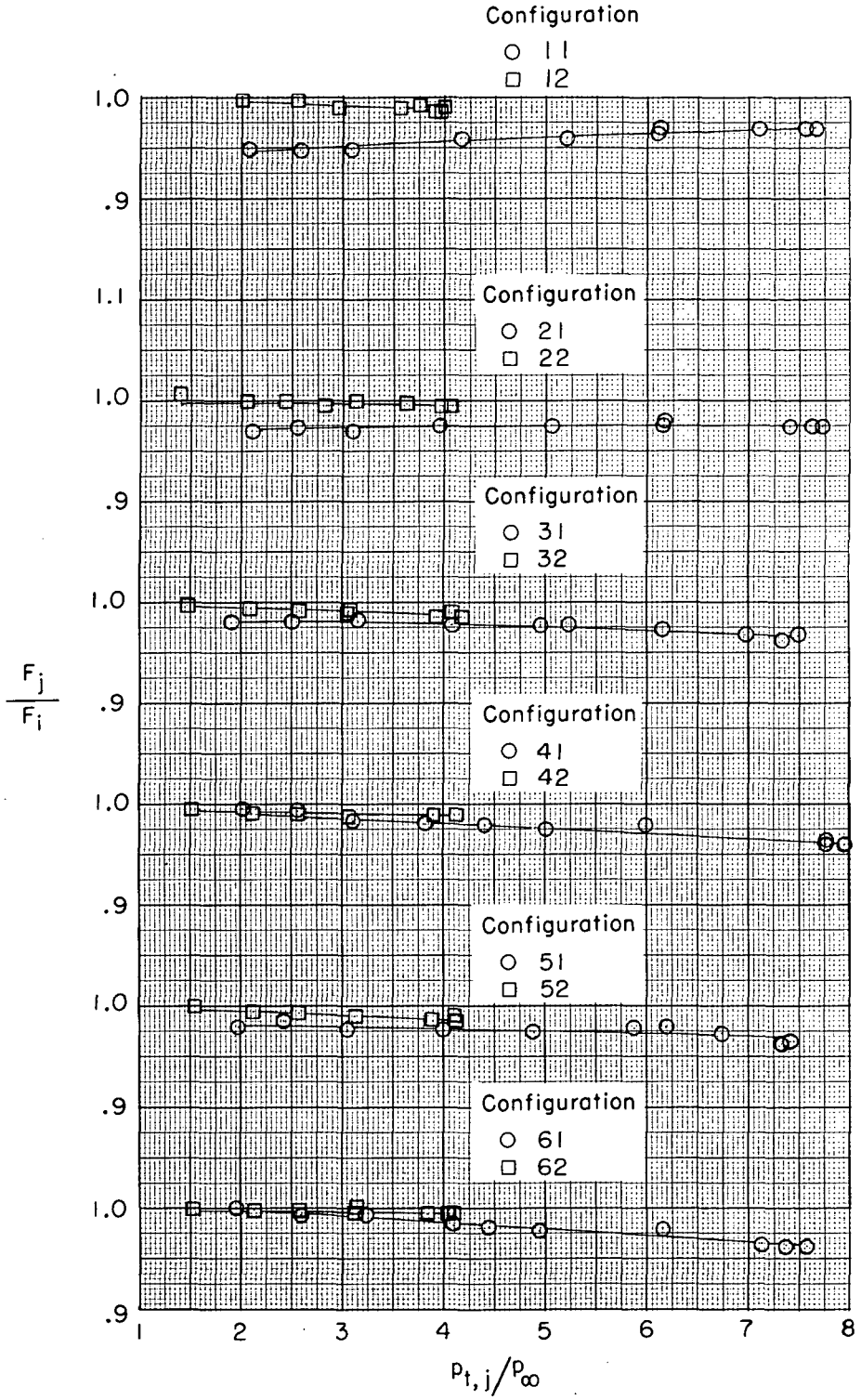

(a) M = 0.50.

Figure 14.- Variation of thrust ratio with jet total-pressure ratio for various configurations.

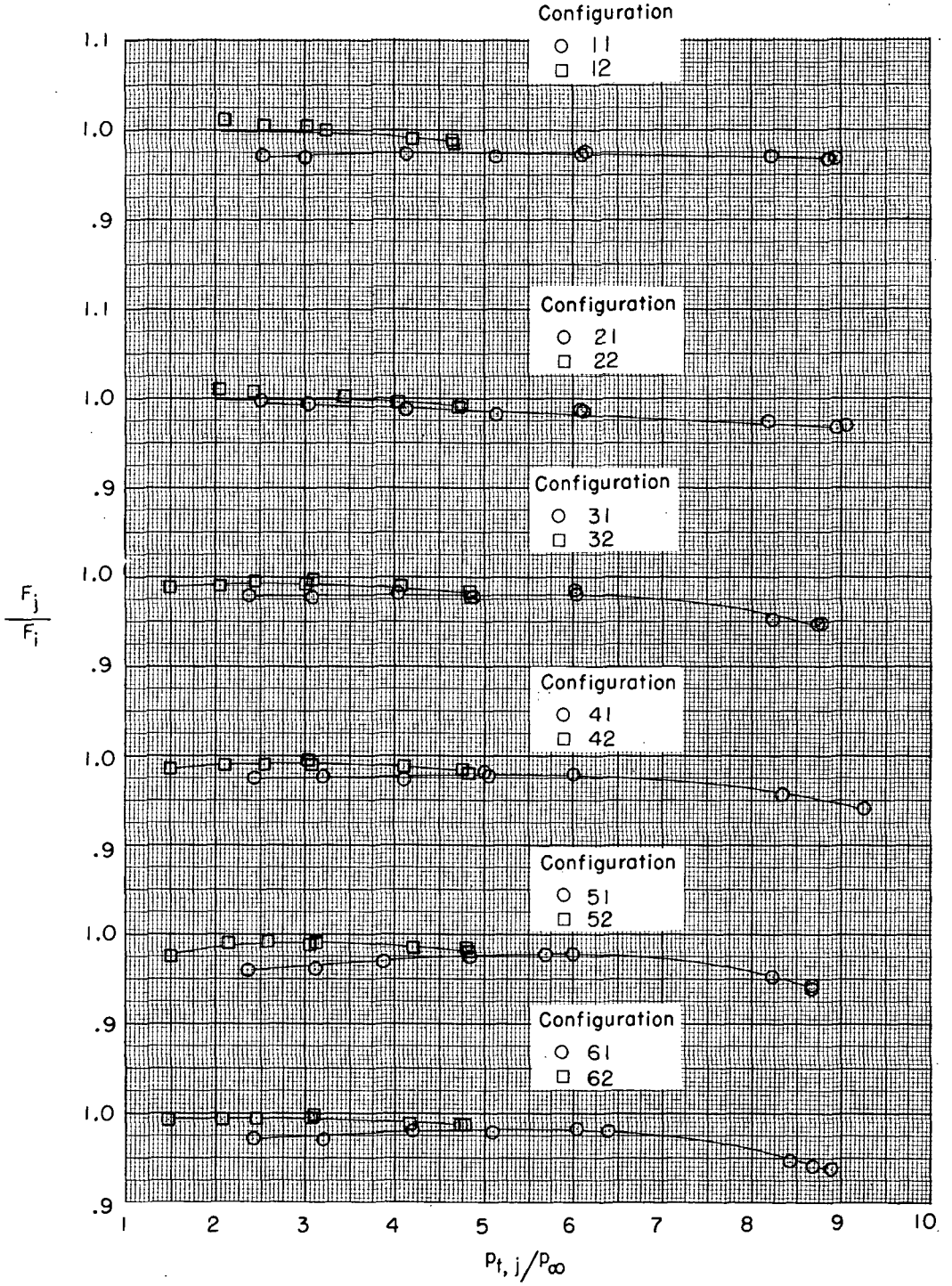

(b) M = 0.70.

Figure 14.- Continued.

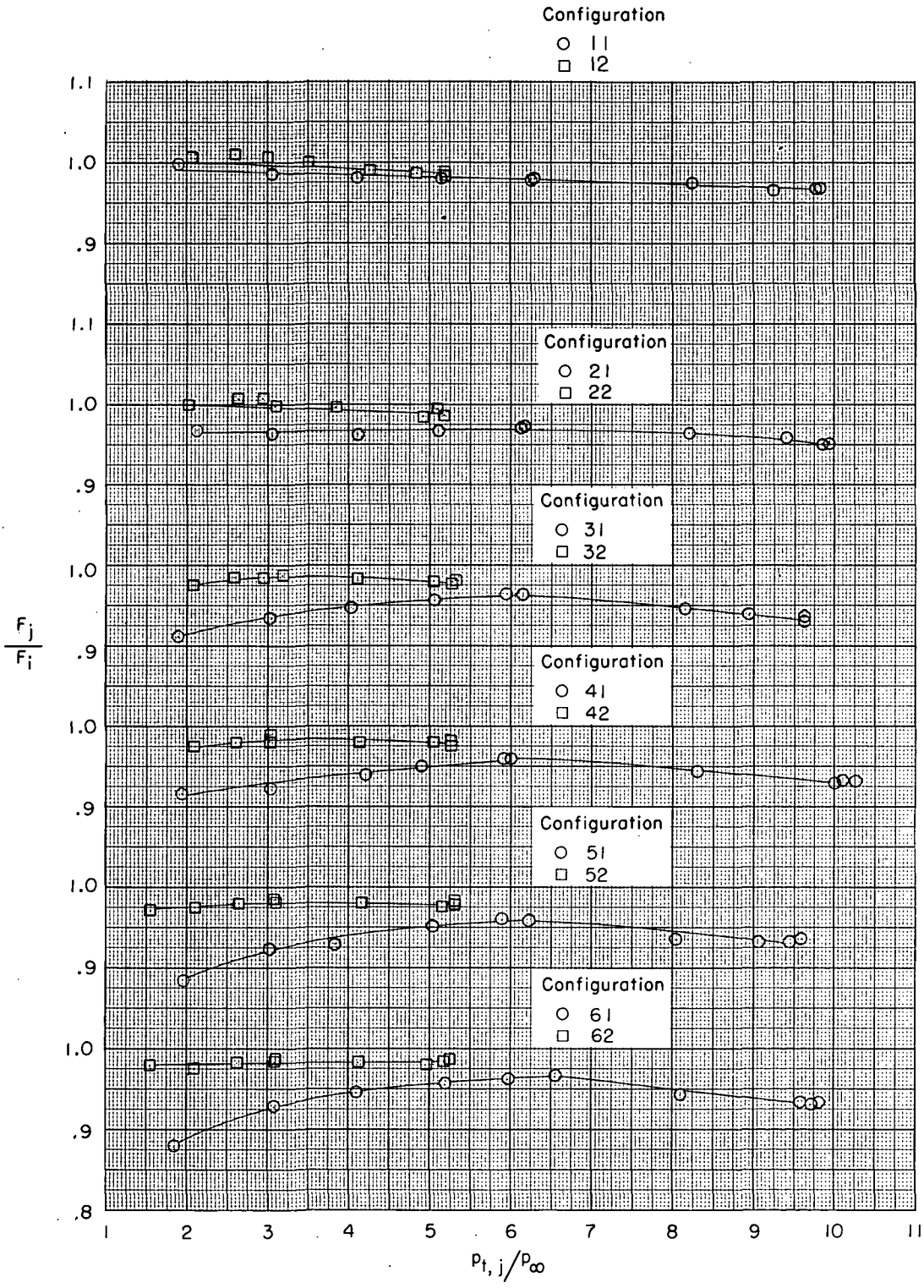

(c) M = 0.80.

Figure 14.- Continued.

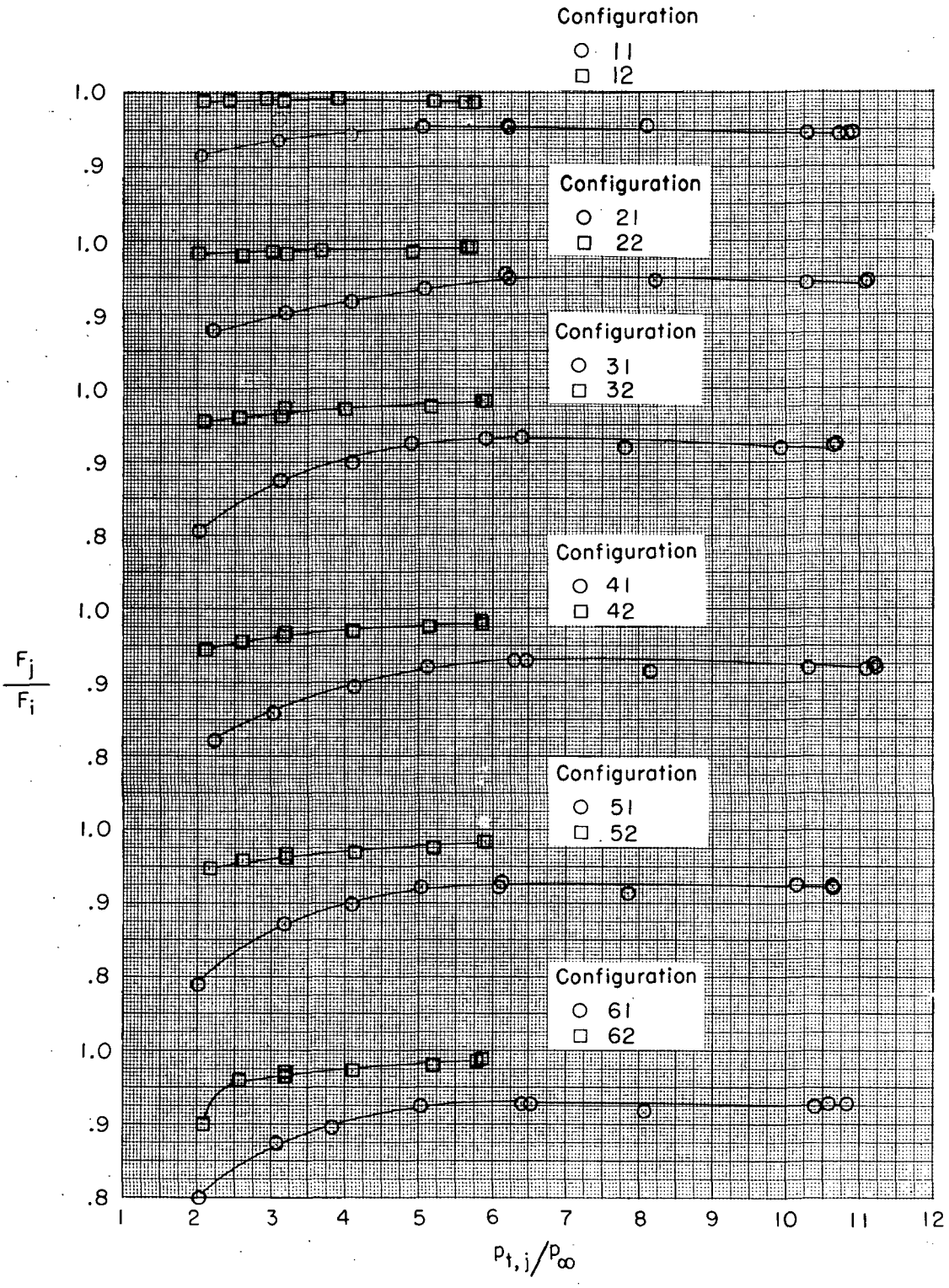

(d) M = 0.90.

Figure 14.- Continued.

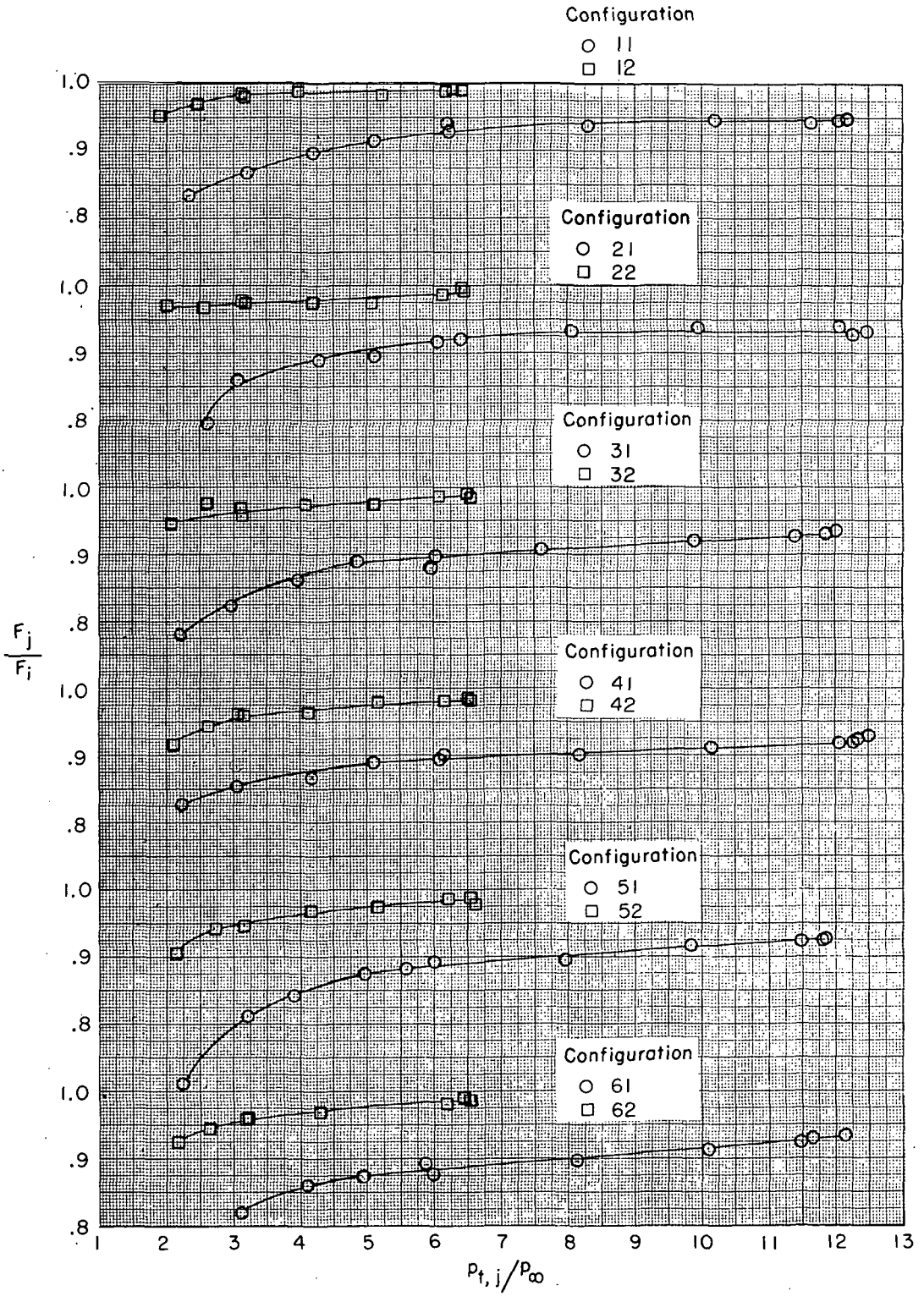

(e) M = 1.00.

Figure 14.- Continued.

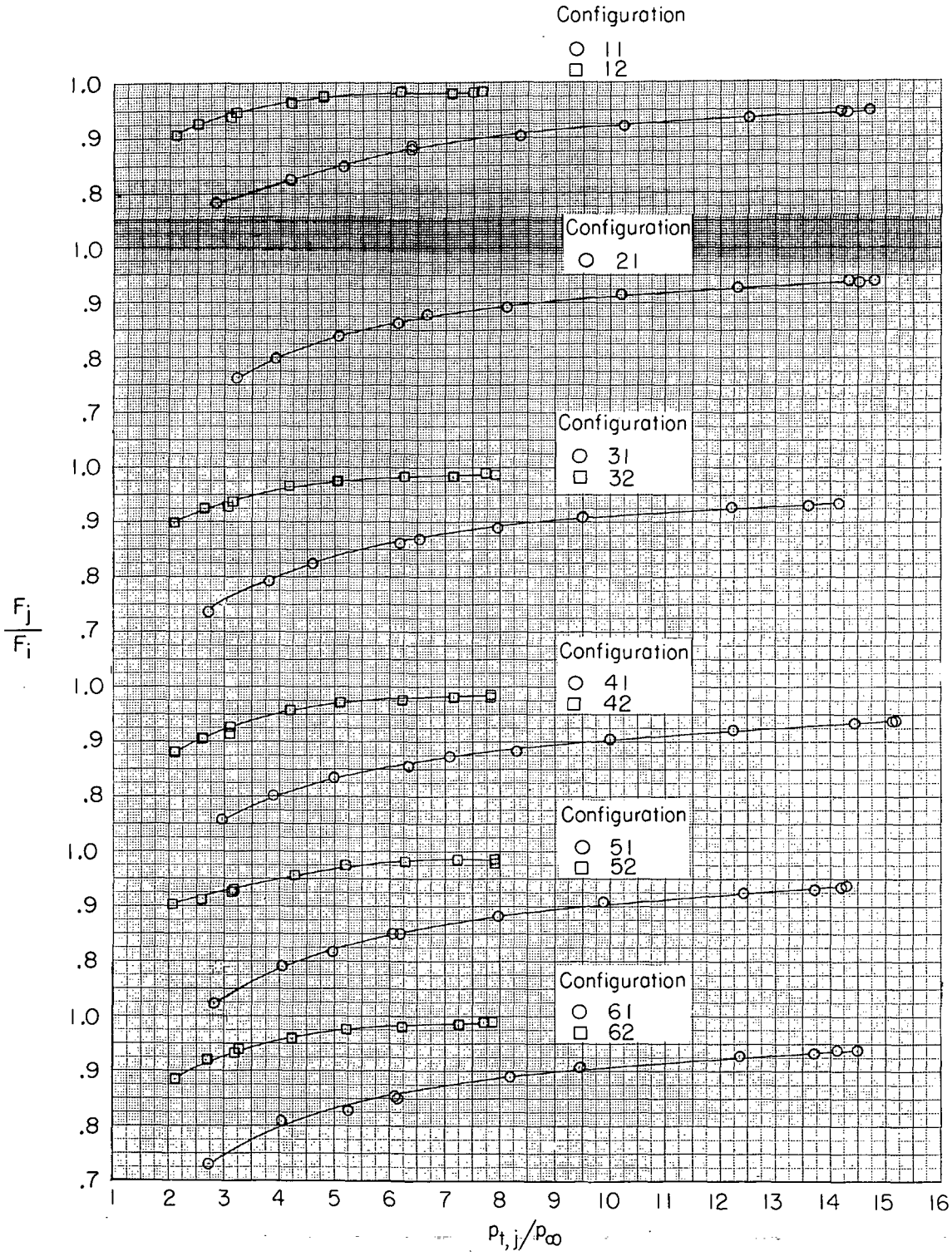

(f) M = 1.15.

Figure 14.- Continued.

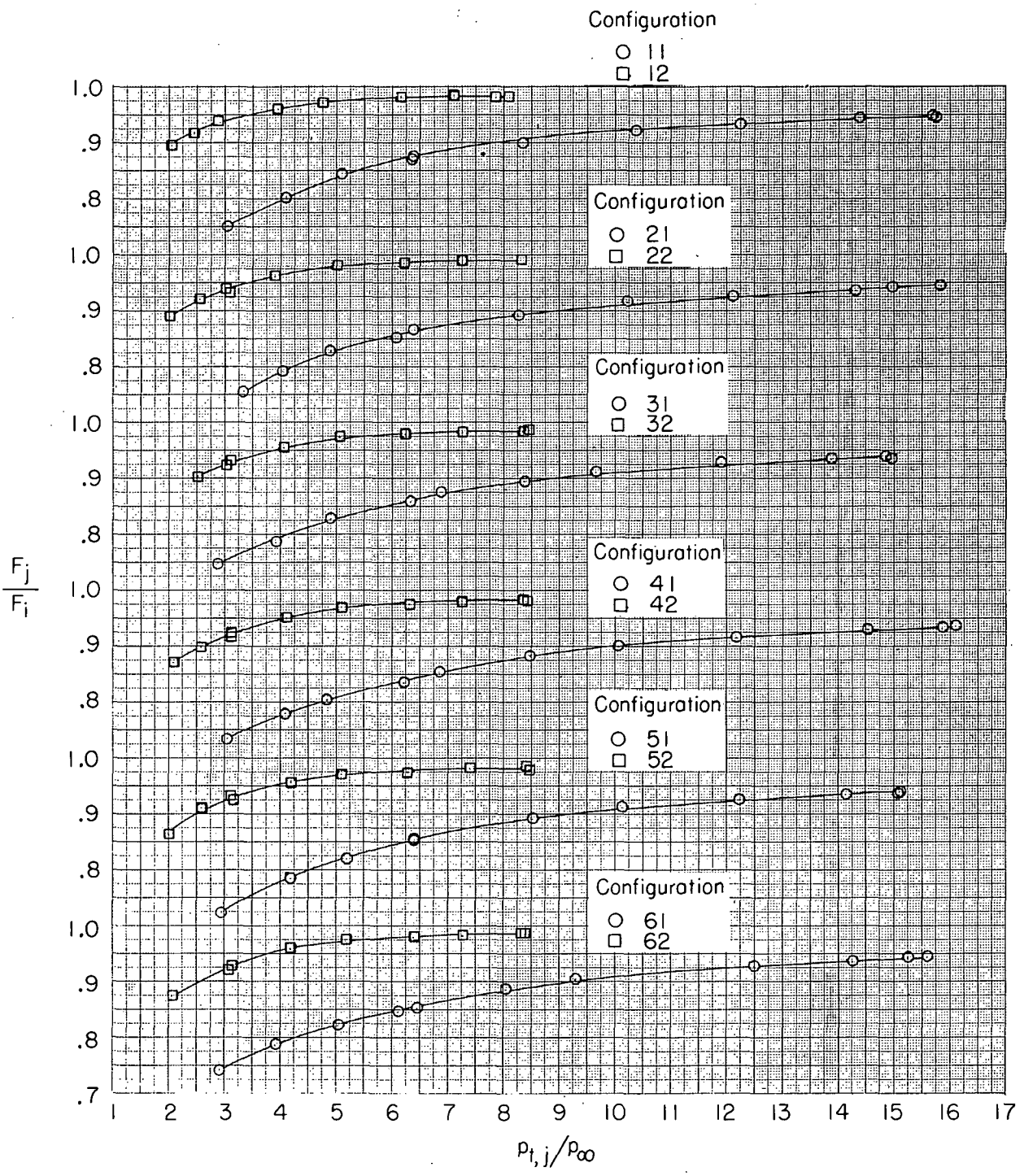

(g) M = 1.20.

Figure 14.- Continued.

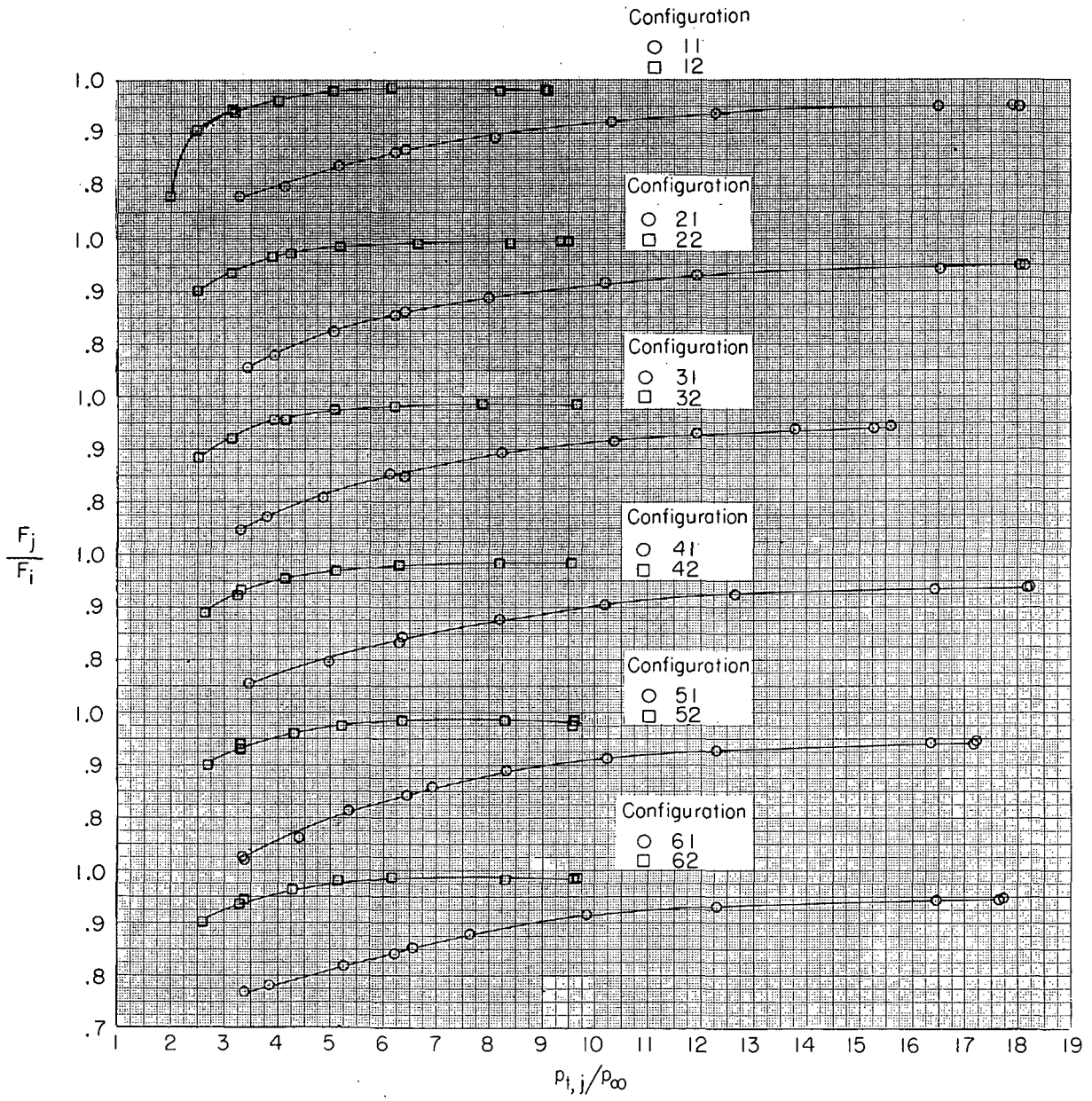

(h) M = 1.30.

Figure 14.- Continued.

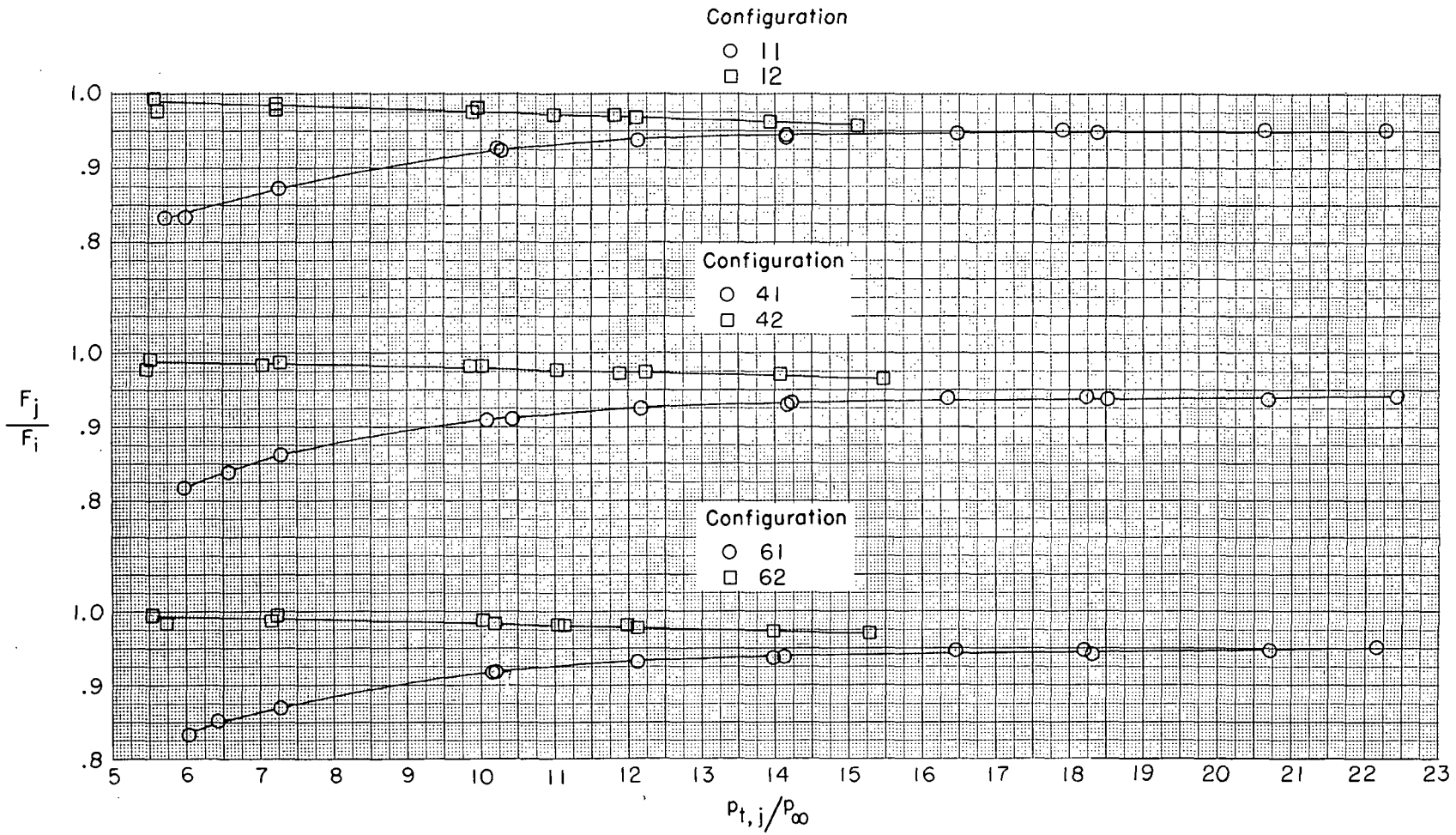

(i) M = 1.82.

Figure 14.- Concluded.

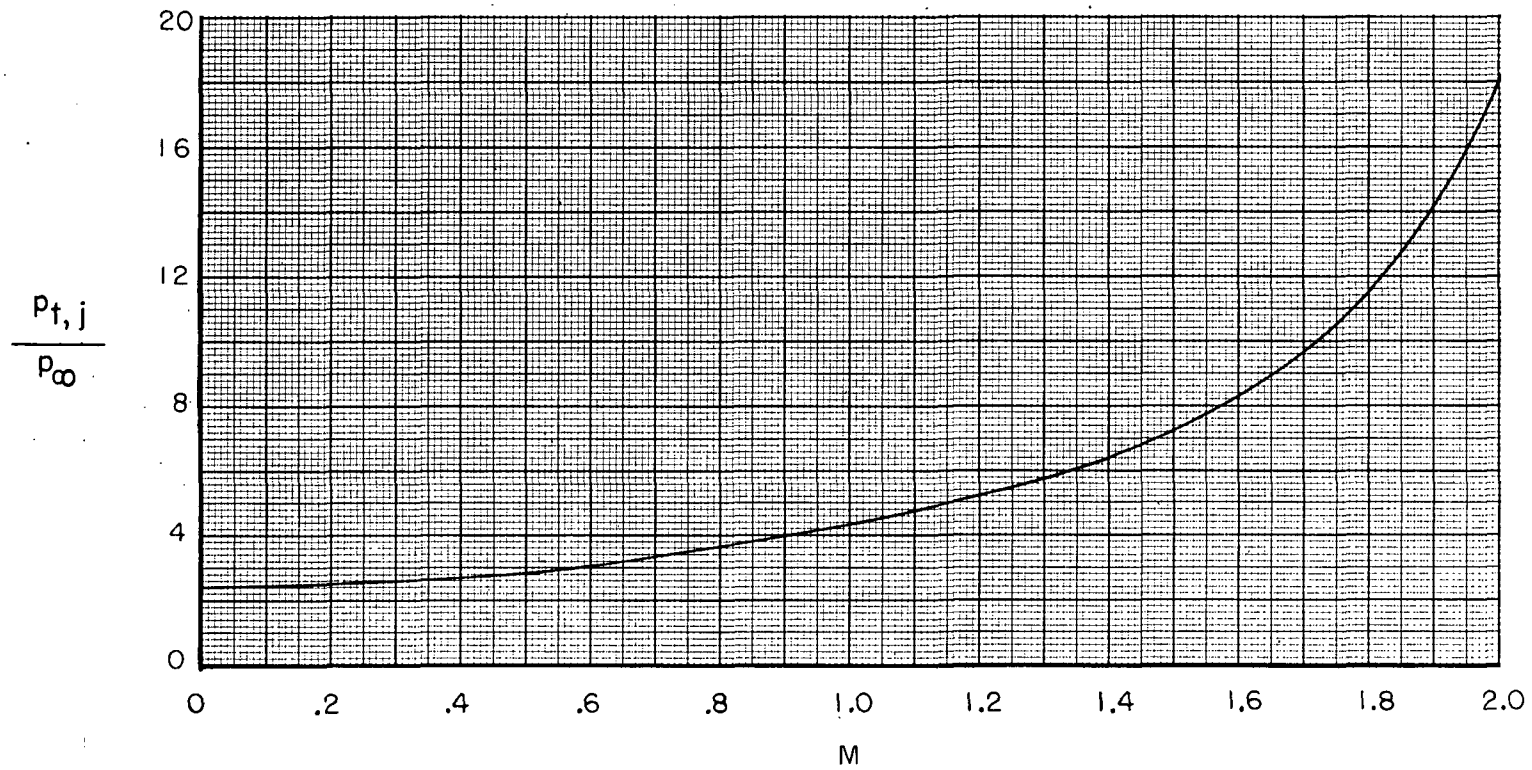

Figure 15.- Estimated schedule of variation of jet total-pressure ratio with Mach number for a typical turbojet engine.

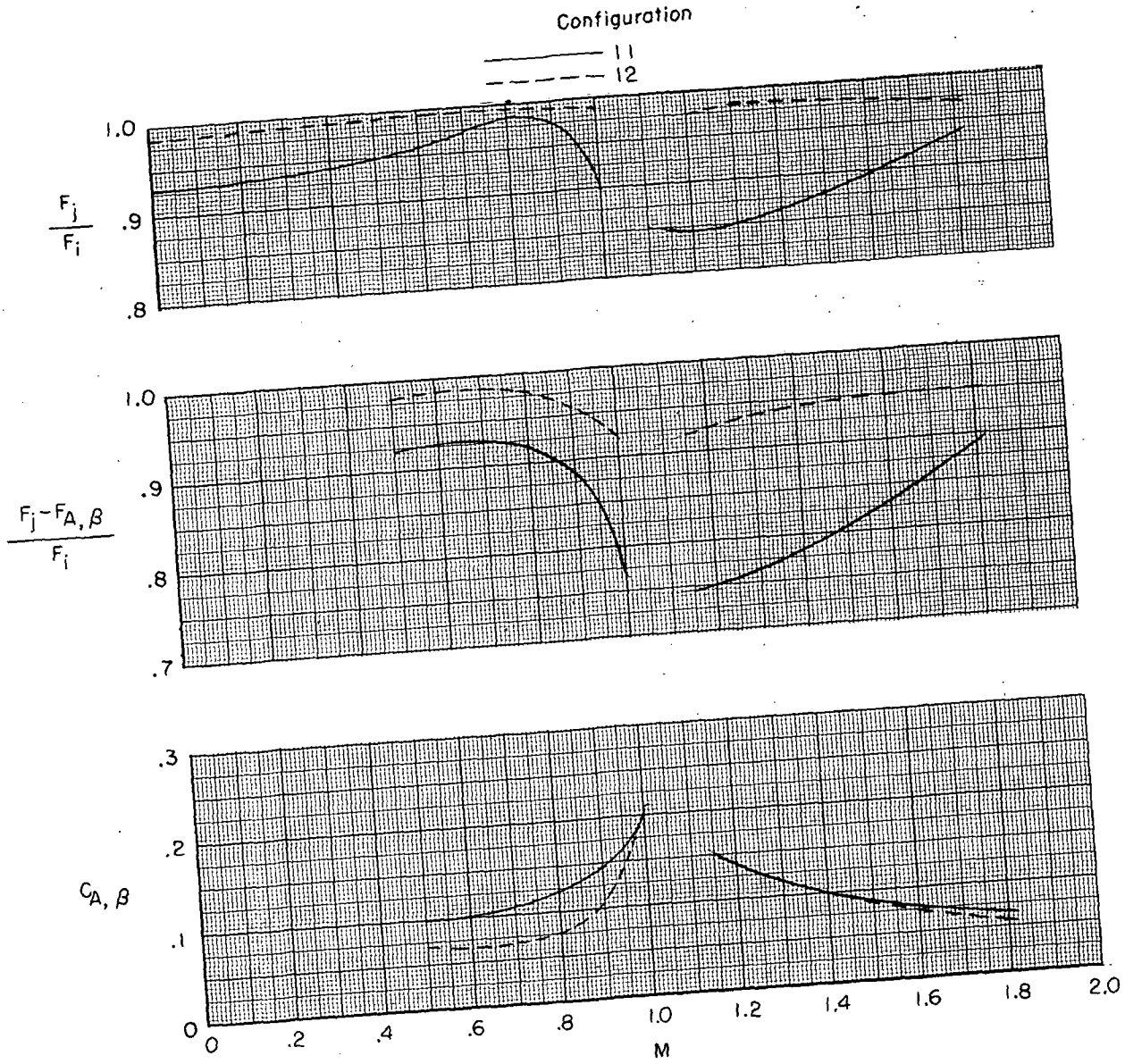

(a) Configurations 11 and 12.

Figure 16.- Variation of performance characteristics with Mach number for jet total-pressure ratio schedule.

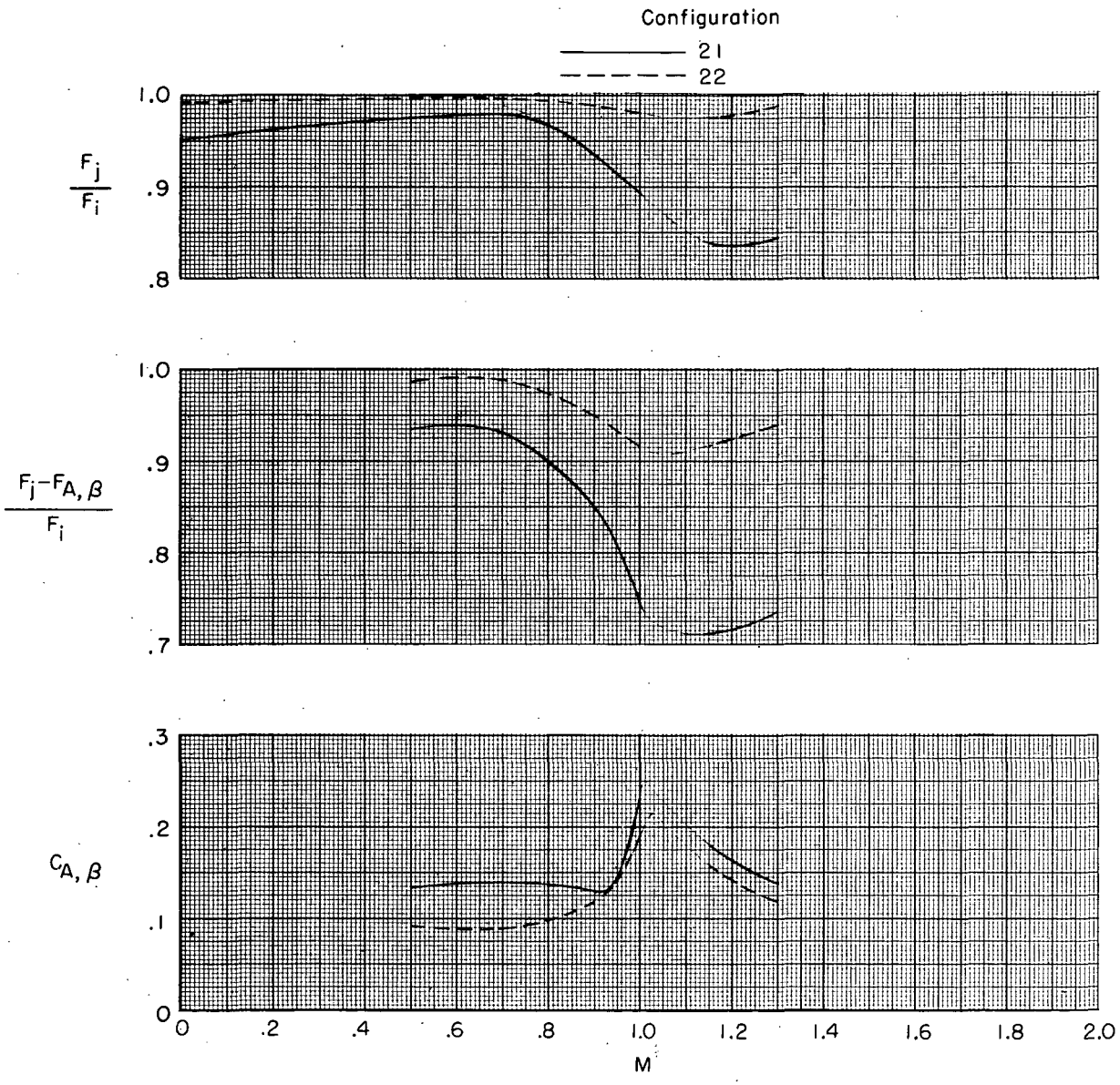

(b) Configurations 21 and 22.

Figure 16.- Continued.

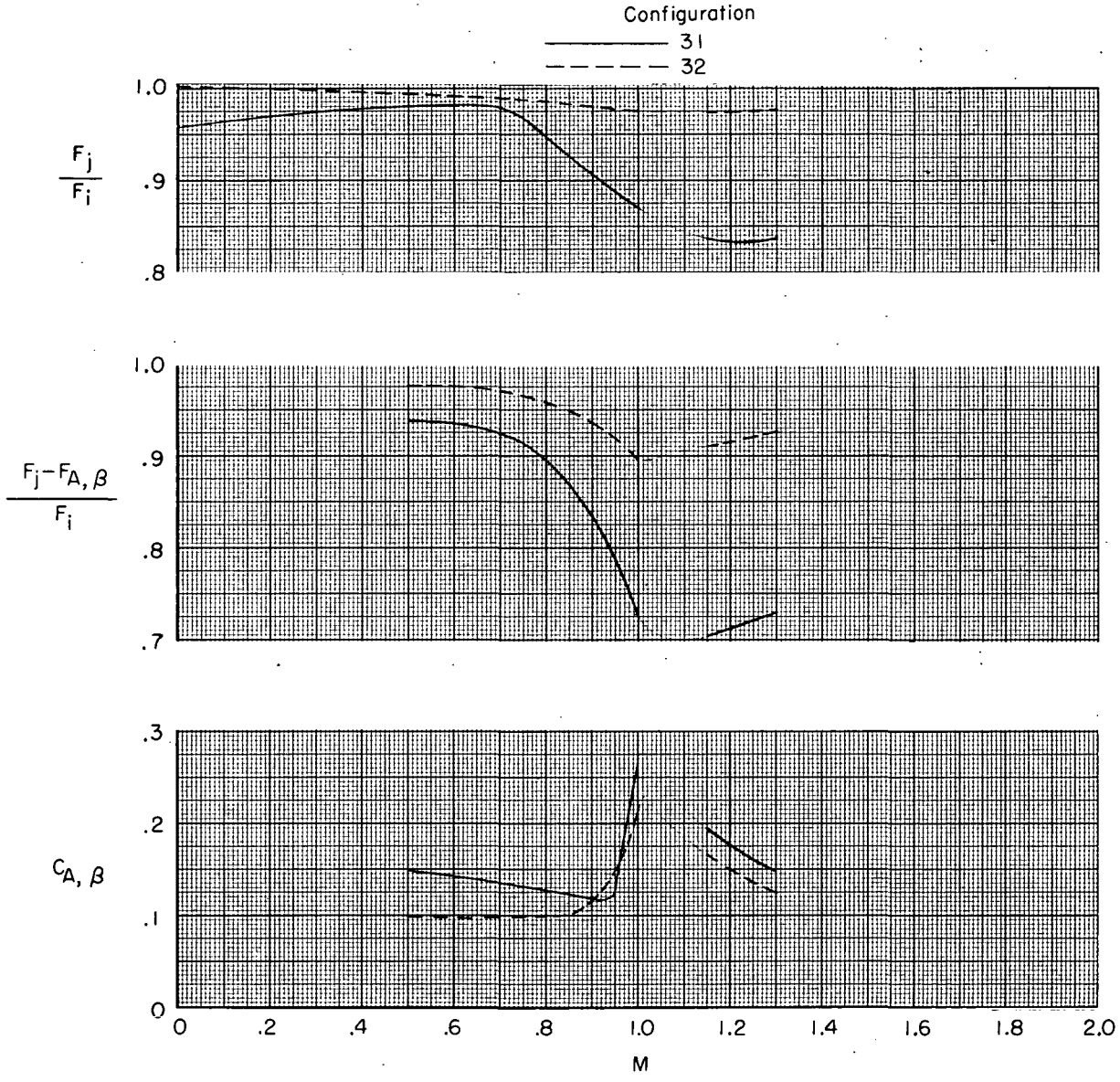

(c) Configurations 31 and 32.

Figure 16.- Continued.

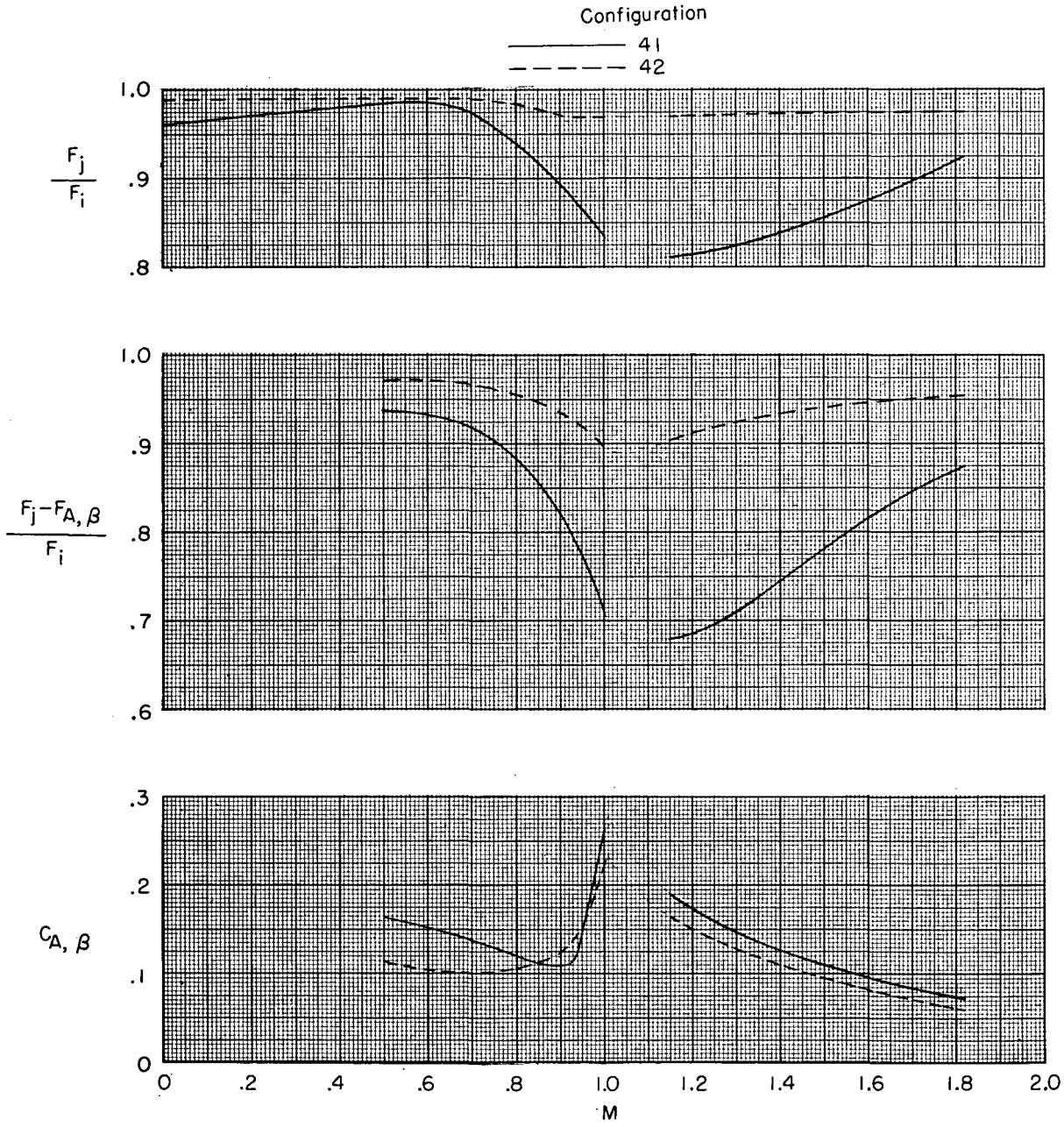

(d) Configurations 41 and 42.

Figure 16.- Continued.

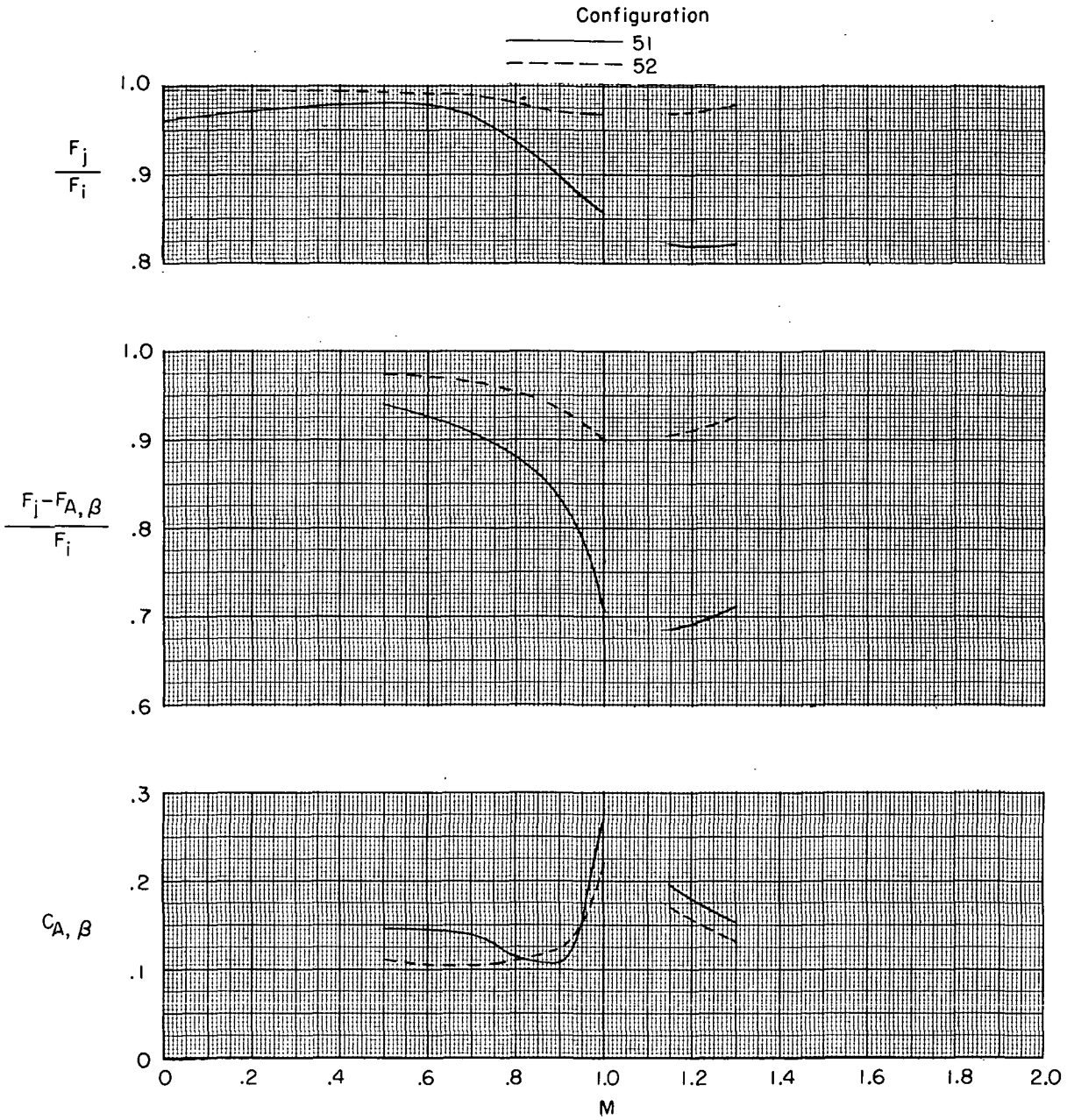

(e) Configurations 51 and 52.

Figure 16.- Continued.

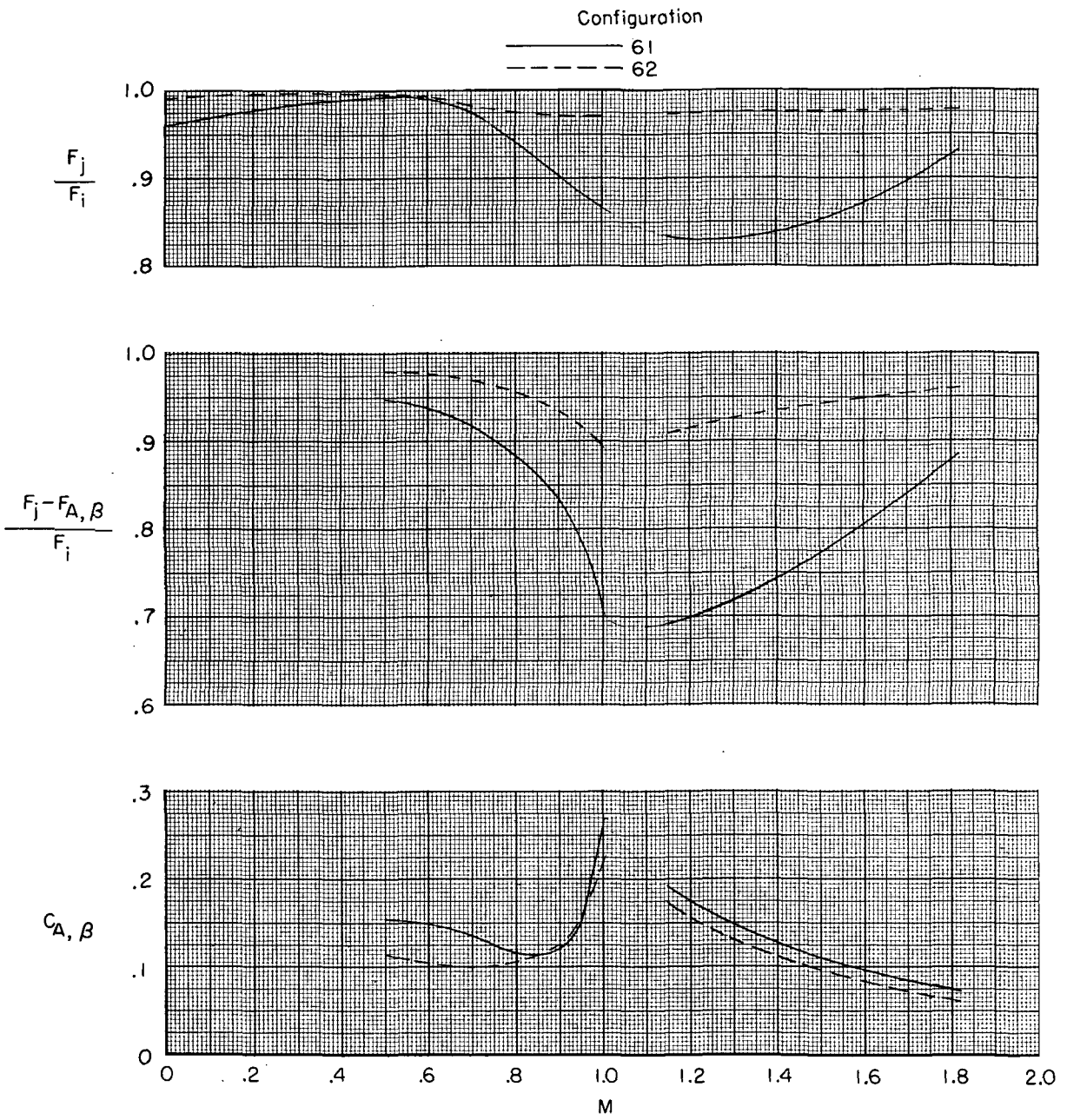

(f) Configurations 61 and 62.

Figure 16.- Concluded.

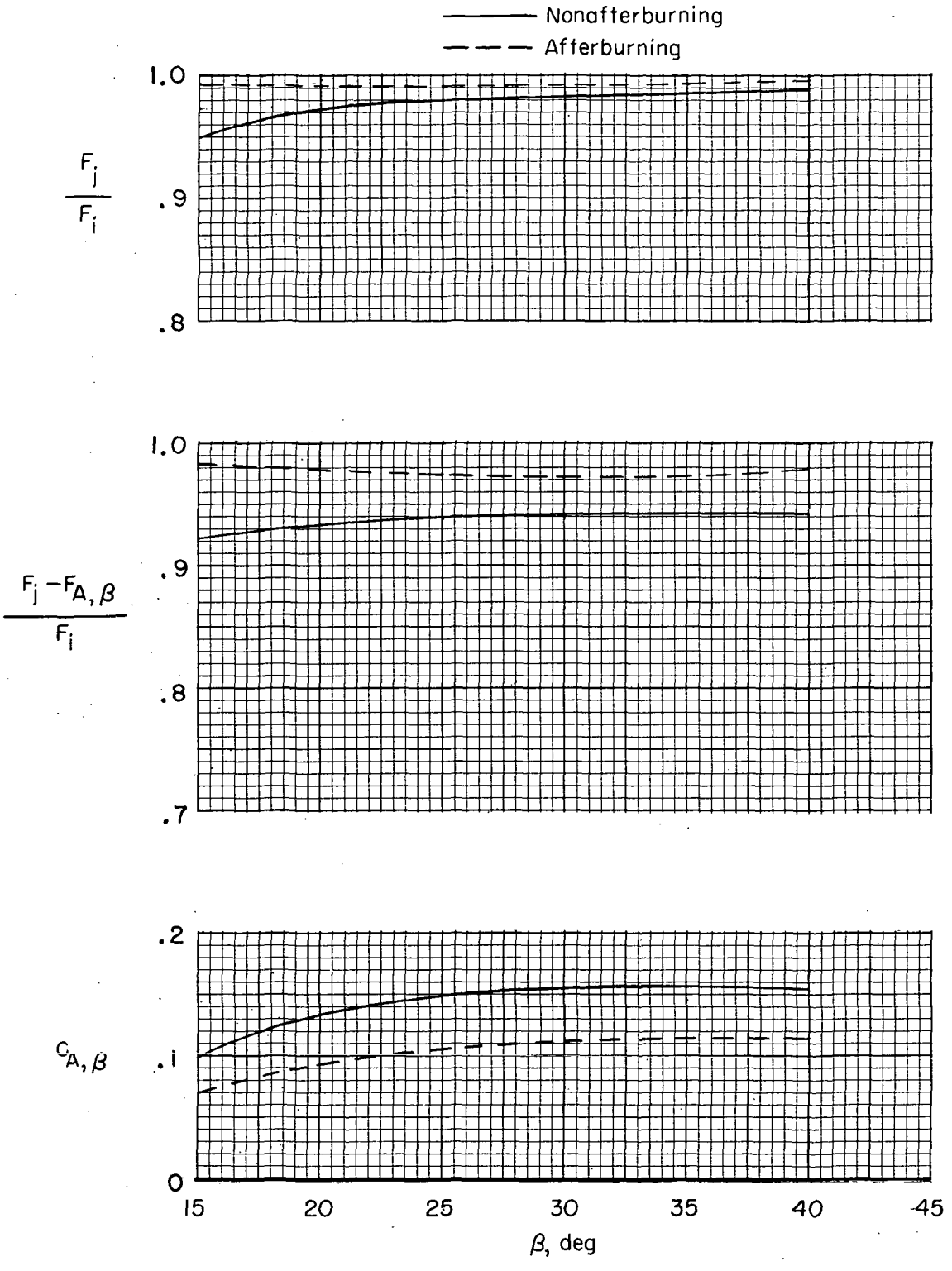

(a) M = 0.50.

Figure 17.- Effect of nozzle lip angle on performance for several Mach numbers.

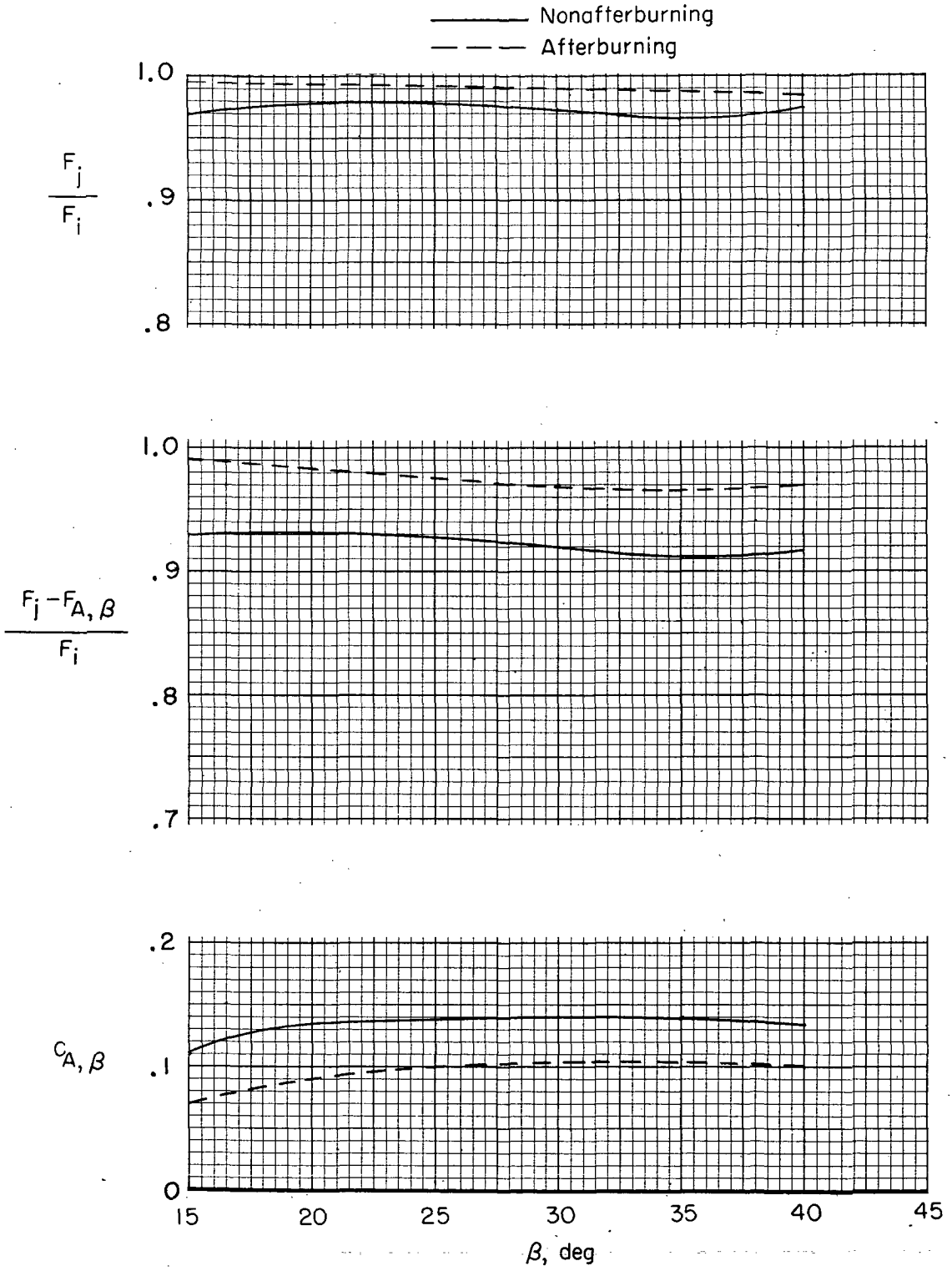

(b) M = 0.70.

Figure 17.- Continued.

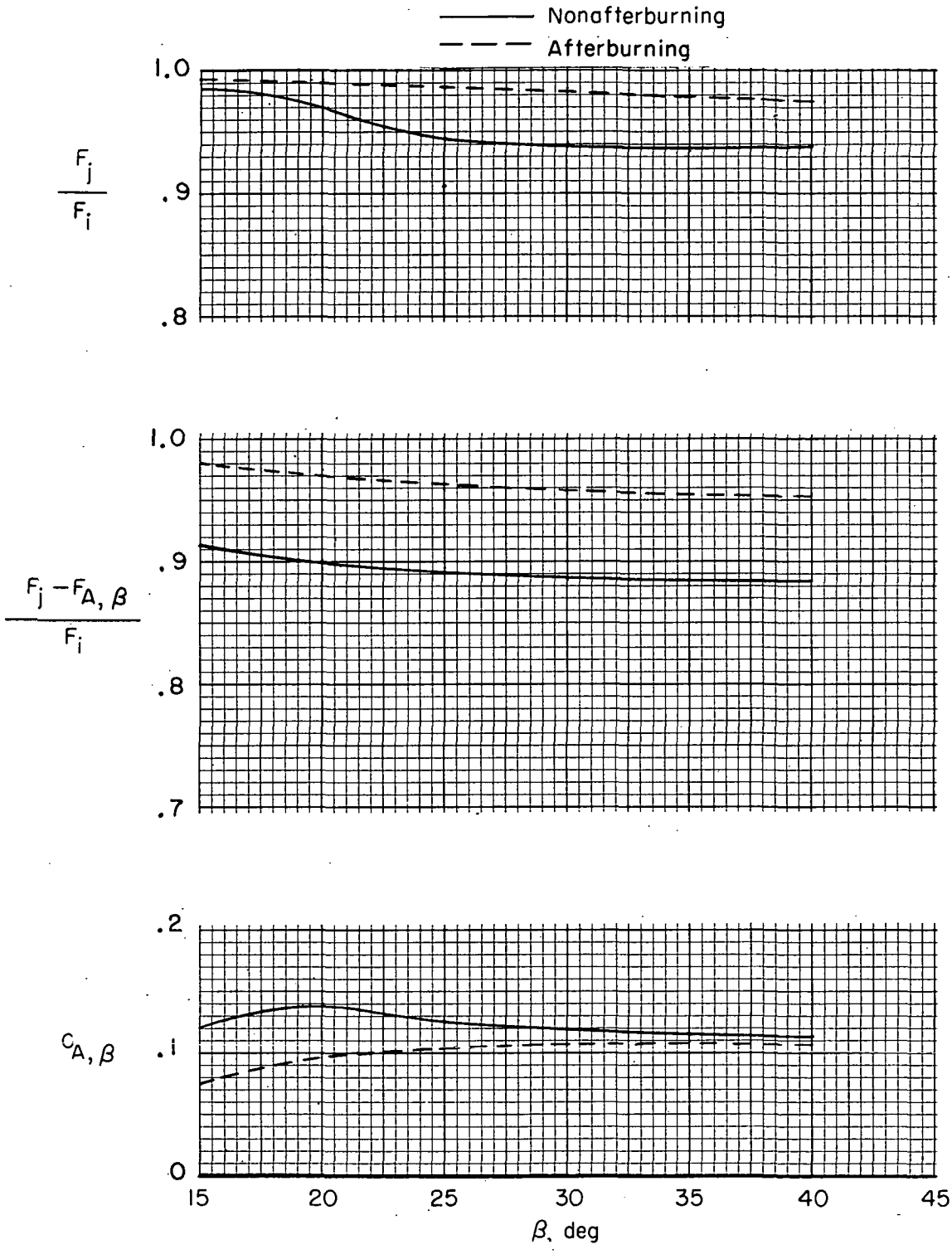

(c) M = 0.80.

Figure 17.- Continued.

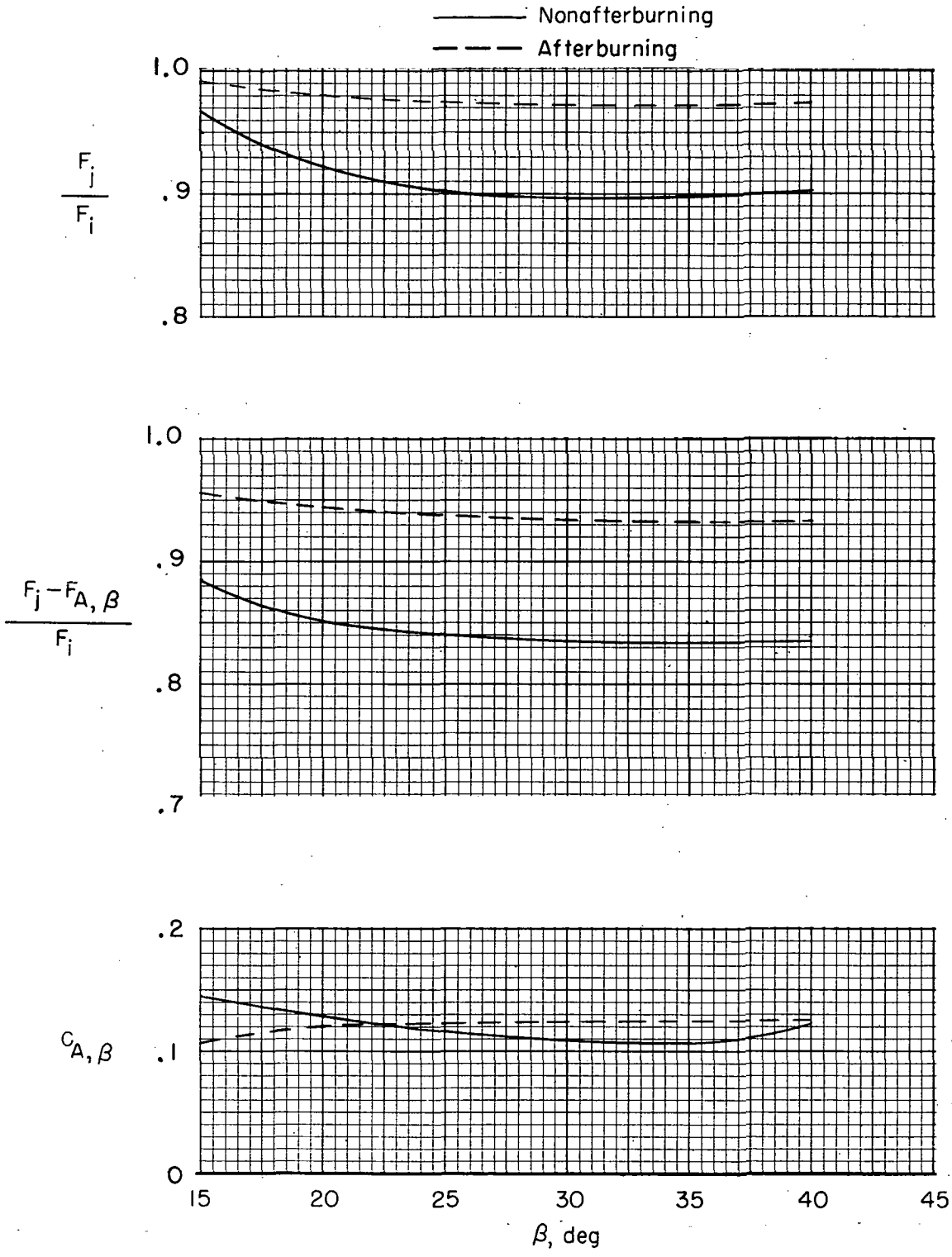

(d) M = 0.90.

Figure 17.- Continued.

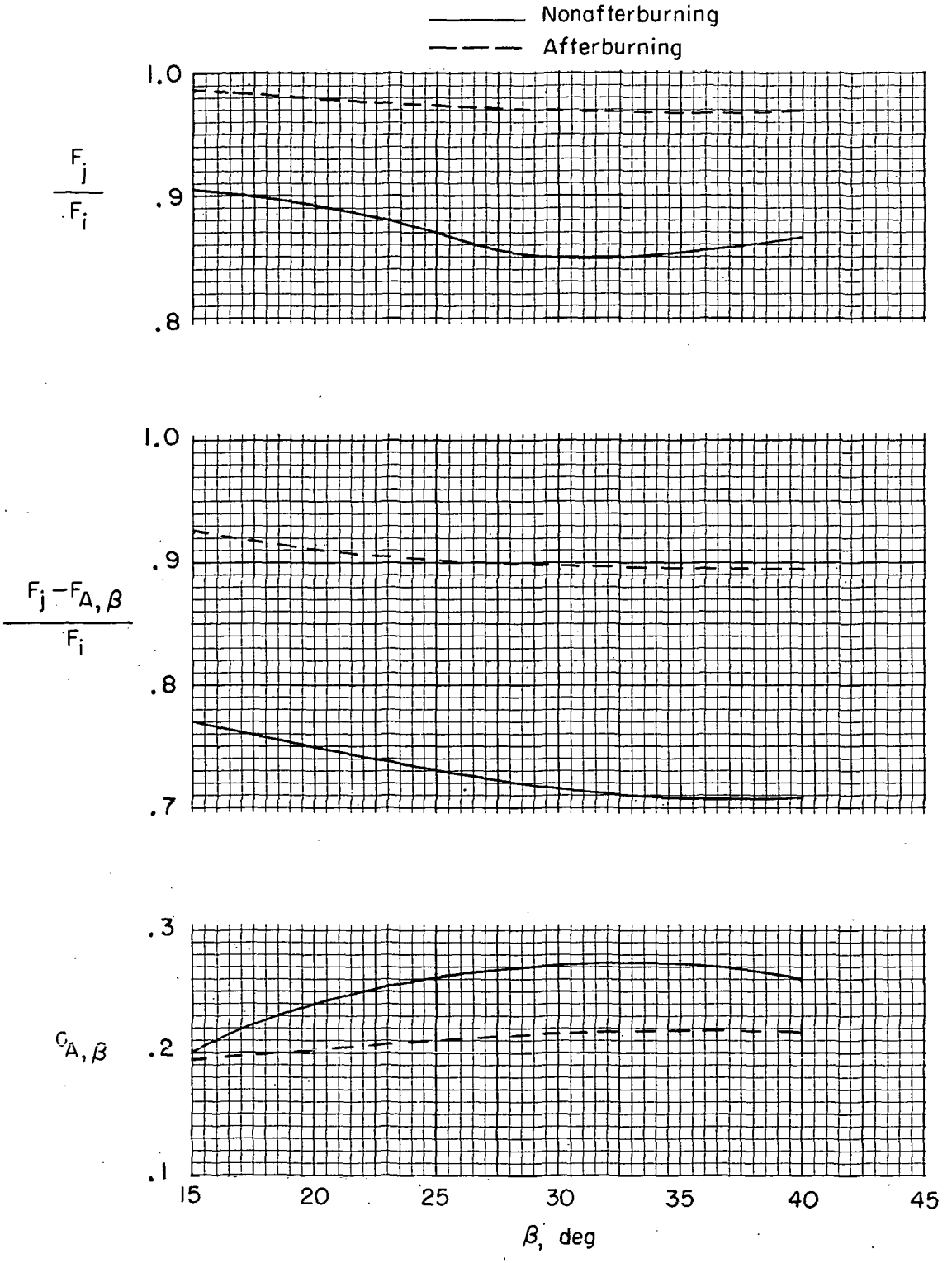

(e) M = 1.00.

Figure 17.- Continued.

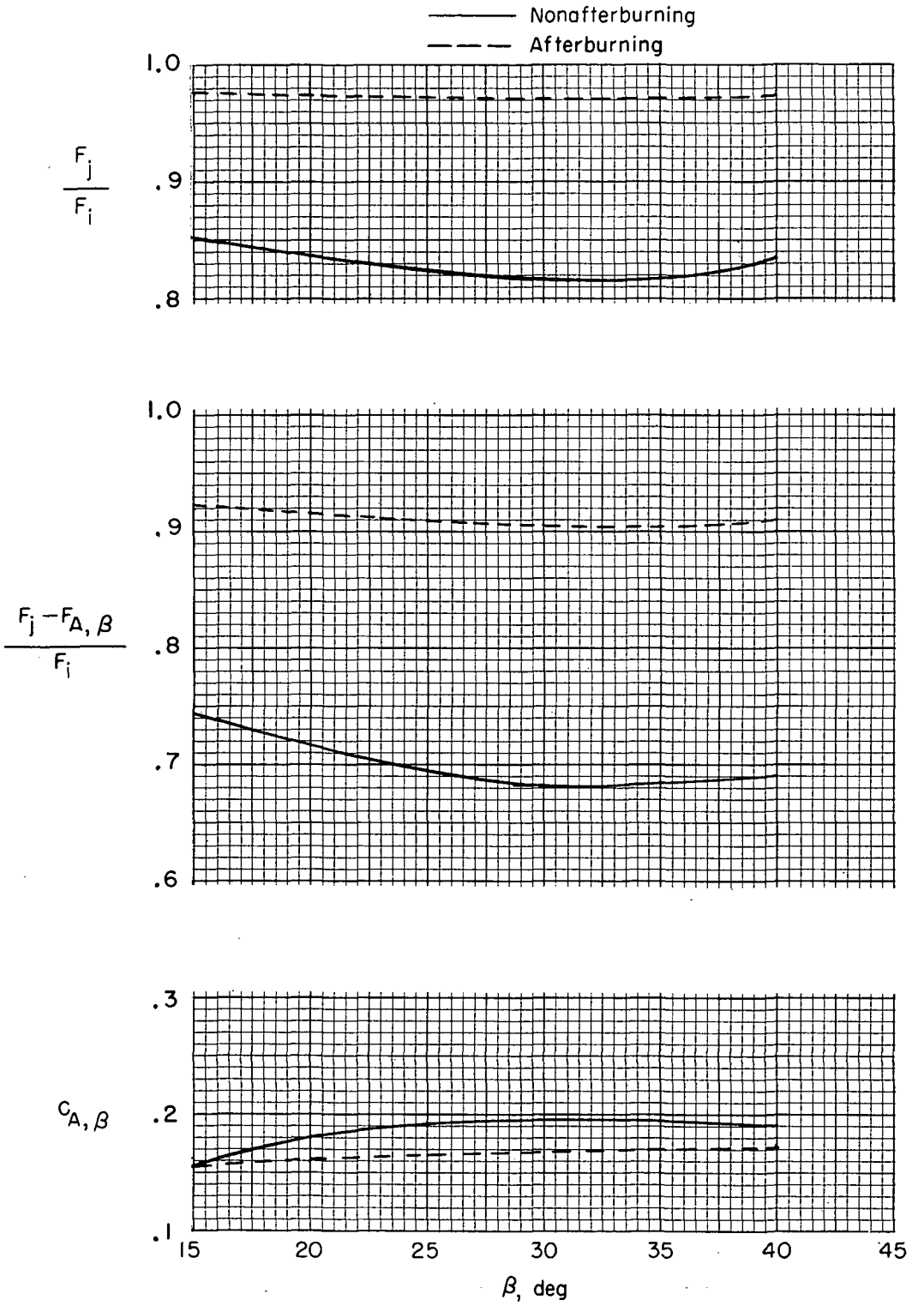

(f) M = 1.15.

Figure 17.- Continued.

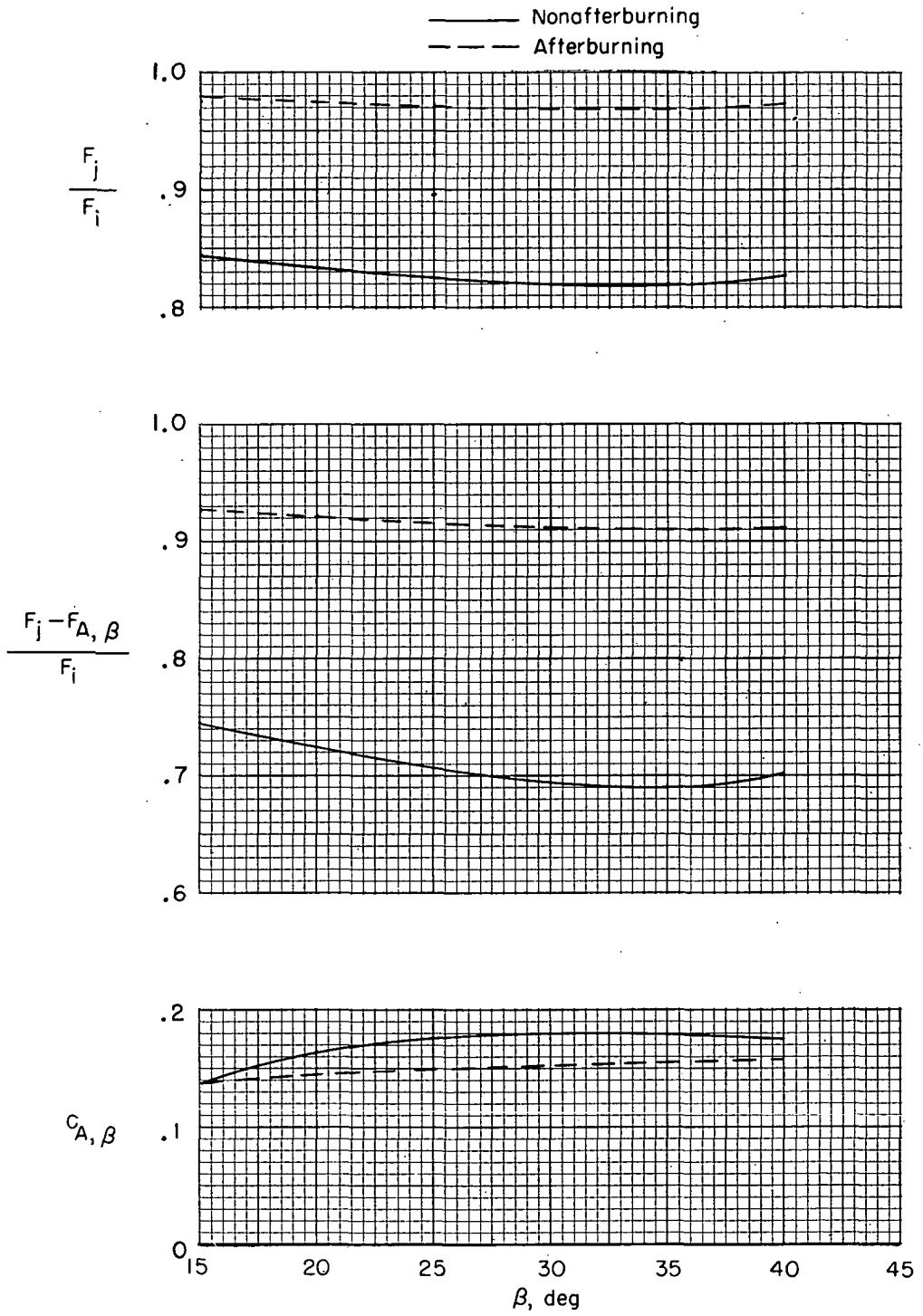

(g) M = 1.20.

Figure 17.- Continued.

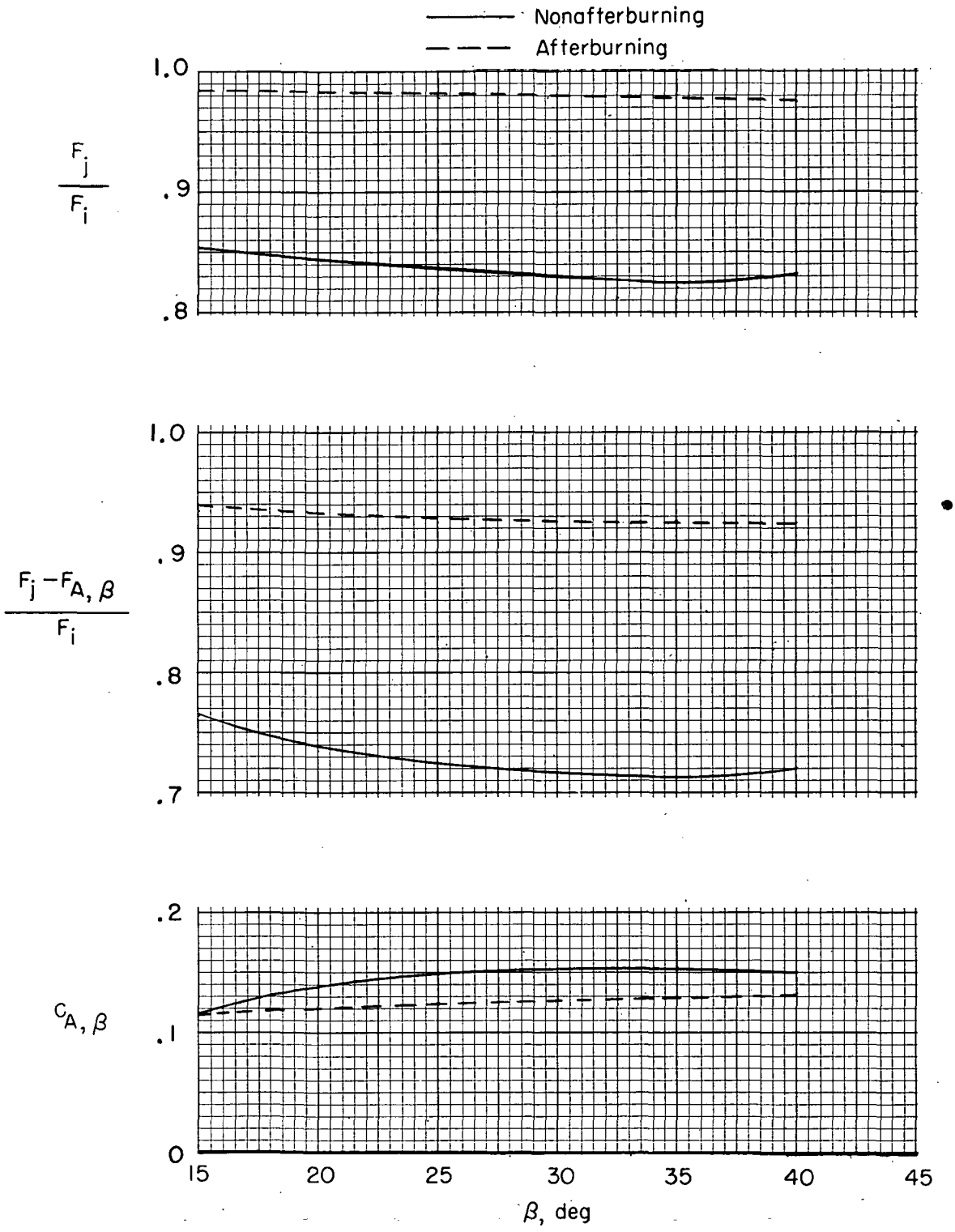

(h) M = 1.30.

Figure 17.- Continued.

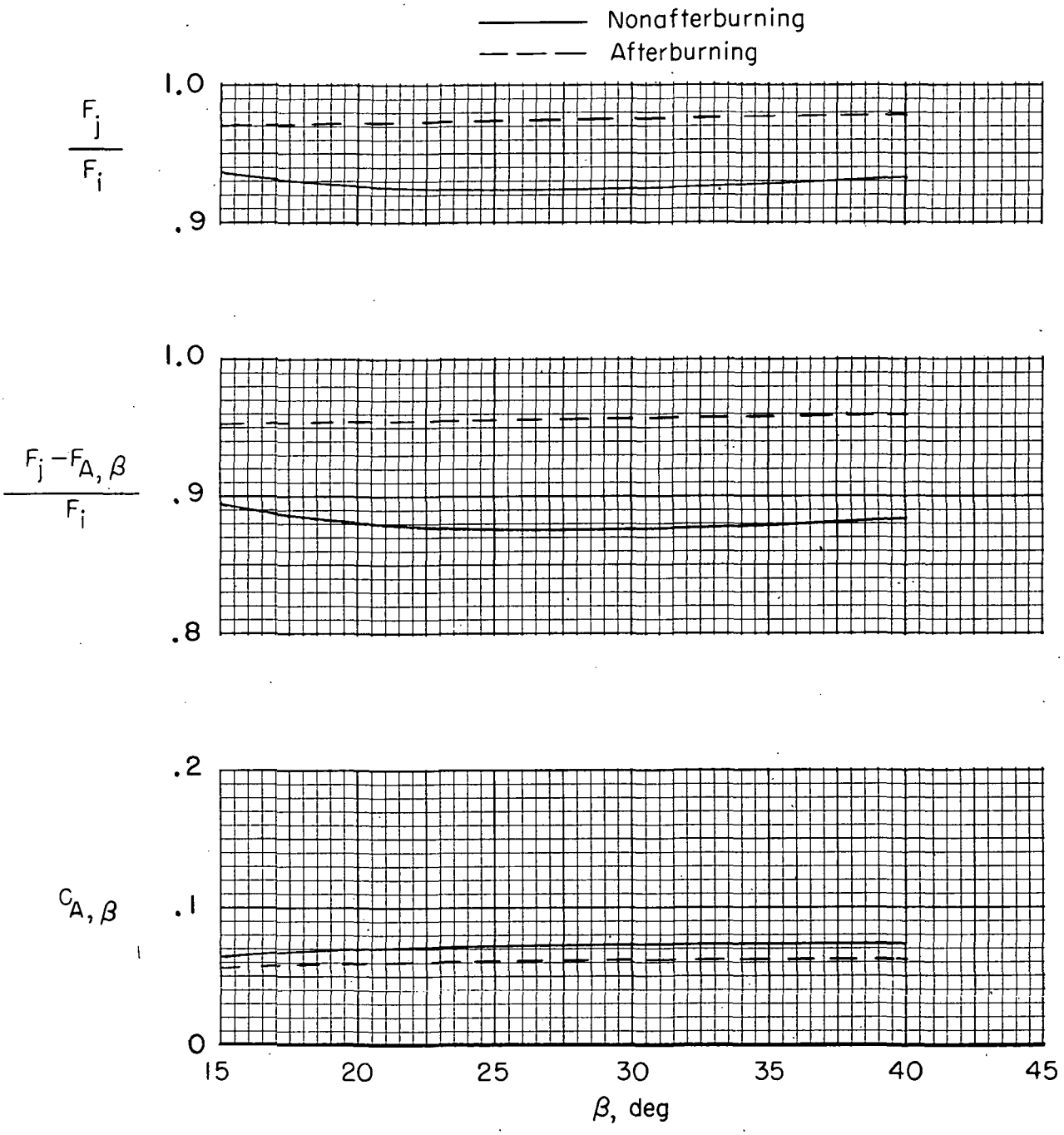

(i) M = 1.82.

Figure 17.- Concluded.

NATIONAL AERONAUTICS AND SPACE ADMINISTRATION
WASHINGTON, D.C. 20546

OFFICIAL BUSINESS
PENALTY FOR PRIVATE USE $300

SPECIAL FOURTH-CLASS RATE BOOK

POSTAGE AND FEES PAID
NATIONAL AERONAUTICS AND SPACE ADMINISTRATION
451

U.S.MAIL

POSTMASTER: If Undeliverable (Section 158 Postal Manual) Do Not Return

"The aeronautical and space activities of the United States shall be conducted so as to contribute . . . to the expansion of human knowledge of phenomena in the atmosphere and space. The Administration shall provide for the widest practicable and appropriate dissemination of information concerning its activities and the results thereof."

—NATIONAL AERONAUTICS AND SPACE ACT OF 1958

NASA SCIENTIFIC AND TECHNICAL PUBLICATIONS

TECHNICAL REPORTS: Scientific and technical information considered important, complete, and a lasting contribution to existing knowledge.

TECHNICAL NOTES: Information less broad in scope but nevertheless of importance as a contribution to existing knowledge.

TECHNICAL MEMORANDUMS: Information receiving limited distribution because of preliminary data, security classification, or other reasons. Also includes conference proceedings with either limited or unlimited distribution.

CONTRACTOR REPORTS: Scientific and technical information generated under a NASA contract or grant and considered an important contribution to existing knowledge.

TECHNICAL TRANSLATIONS: Information published in a foreign language considered to merit NASA distribution in English.

SPECIAL PUBLICATIONS: Information derived from or of value to NASA activities. Publications include final reports of major projects, monographs, data compilations, handbooks, sourcebooks, and special bibliographies.

TECHNOLOGY UTILIZATION PUBLICATIONS: Information on technology used by NASA that may be of particular interest in commercial and other non-aerospace applications. Publications include Tech Briefs, Technology Utilization Reports and Technology Surveys.

Details on the availability of these publications may be obtained from:

SCIENTIFIC AND TECHNICAL INFORMATION OFFICE

NATIONAL AERONAUTICS AND SPACE ADMINISTRATION

Washington, D.C. 20546